The Pennsylvania State University

The Graduate School

Intercollege Graduate Degree Program in Plant Biology

QUERYING PLANT CELL WALL MATRIX ORGANIZATION WITH CLICK CHEMISTRY

A Dissertation in

Plant Biology

by

Daniel D. McClosky

Submitted in Partial Fulfillment
of the Requirements
for the Degree of

Doctor of Philosophy

May 2019

The dissertation of Daniel D. McClosky was reviewed and approved* by the following:

Charles T. Anderson
Associate Professor of Biology
Dissertation Advisor
Chair of Committee

Daniel J. Cosgrove
Eberly Professor of Biology

Gabriele Monshausen
Associate Professor of Biology

William Hancock
Professor, Chair of the Intercollege Graduate Program in Bioengineering

Teh-Hui Kao
Distinguished Professor of Biochemistry and Molecular Biology
Head of the Intercollege Graduate Degree Program in Plant Biology

*Signatures are on file in the Graduate School

ABSTRACT

Plant cells accomplish growth through the controlled deformation of their walls in response to internal turgor. This control is exerted only indirectly by the protoplast: it synthesizes an extracellular matrix, and it is the biomechanical properties of the resulting wall that directly determine the shape, size, and strength of the resulting cell. The ordered synthesis of paracrystalline cellulose microfibrils, major load-bearing components of the wall, occurs at the cell surface, but the remainder of the polysaccharides in the wall are synthesized intracellularly and must be delivered to the wall. Recent research highlights underappreciated roles for both pectins and hemicelluloses in determining wall mechanical properties, through interactions with cellulose microfibrils; the ordered delivery of these matrix polysaccharides thus may have important consequences for emergent physical properties of the wall, and by extension, overall plant form. To directly observe and study matrix polysaccharide delivery to the growing wall, we have employed a metabolic labeling technique. This has revealed (1) subcellular heterogeneity in the deposition patterning of different matrix polysaccharides, and (2) clues as to the drivers of this patterning.

The roles of matrix polysaccharides in establishing cell wall mechanical properties are becoming more well-supported in recent years, but how they are delivered and organized into the growing wall remains unclear. Expanding on a metabolic labeling approach, we observed that in some cell types of the model plant, *Arabidopsis thaliana*, newly-synthesized matrix assumes a non-random organization in developing primary walls. In our approach, this resulted in fluorescent features on the μm scale. In primary root epidermal cells, subcellular regions destined to transition to tip-growing root hairs differentially accumulated a glucose analog, showing that particular chemical reporters can highlight regions of differential accumulation of special matrix polysaccharides, in this case, callose. Experiments with a different chemical reporter modeled on fucose that is incorporated with striated patterns of deposition into the walls of differentiating root epidermal cells, revealed that it is the cellulose microfibril array that drives the organization of recently-deposited matrix, not underlying cortical microtubules, which exert a more indirect effect on matrix patterning. However, microtubules do appear to play some role in orchestrating matrix deposition, since metabolic labeling revealed defects in matrix polysaccharide deposition in a series of mutants in a common genetic pathway involving the kinesin, Fragile Fiber1 (FRA1).

In summary, I demonstrate an expansion of the metabolic labeling toolkit in Arabidopsis, and an extension of the method to address fundamental questions of wall matrix organization and delivery, including a dissection of the differential influences of the cytoskeleton, the pre-existing cellulose microfibril array, and a kinesin. This work reveals new aspects of the assembly of plant cell walls, which can serve as renewable sources of fuel, food, and fiber.

TABLE OF CONTENTS

LIST OF FIGURES

LIST OF TABLES

ACKNOWLEDGEMENTS

This dissertation is the product of my efforts, but behind those efforts are many others. First, I acknowledge my advisor, Dr. Charles T. Anderson. He counseled me through both difficult setbacks and exciting advances, and modeled patience and insight through it all.

I am thankful for my committee members, Dr. Daniel Cosgrove, Dr. Gabriele Monshausen, and Dr. William Hancock. They made time for many committee meetings, offering great insight and reviewing progress on multiple projects. I would like to thank Dr. Gong Chen, who also served on my committee for the bulk of my time at Penn State, and whose expertise in bioorganic synthesis made much of my research possible.

I owe thanks to the Anderson lab, including Dr. Chaowen Xiao, Dr. Peter Dowd, Dr. Deborah Petrik, Yue Rui, Will Barnes, Melissa Ishler, Yintong Chen, and Thomas McCarthy. I owe especial thanks to Dr. Bo Wang for both his synthetic expertise and comradery.

Last but not least, I would like to thank Yuwei Li, my parents, Stan and Wendy McClosky, and my friends, for providing me with both tangible and emotional support through my studies.

This work was supported by the Center for Lignocellulose Structure and Formation, an Energy Frontier Research Center funded by the U.S. Department of Energy, Office of Science, Basic Energy Sciences (grant no. DE–SC0001090).

Chapter 1

Introduction

1.1 Study System: The Seedling Root of Arabidopsis

Arabidopsis thaliana, a model plant species with abundant genetic resources available, well-established cytological protocols, and an extensive history of physico-chemical investigations of the structural biology and biochemistry of its cell walls, will be the model organism for this dissertation[1]. It is important to note, however, that a major advantage of metabolic labeling with click chemistry is its applicability to any organism, not just model species[2]. Therefore, the translation of knowledge learned from studying Arabidopsis primary cell walls should be portable to other species; verification of the trends and principles shown here should be rapid in other systems.

More specifically, the organ under examination will be the root tip. Root tips are optimal for metabolic labeling studies because they are regions of rapid cell proliferation, dramatic cell expansion, high permeability, and low levels of native pigmentation and autofluorescence. Epidermal cells are the most amenable living cell type to microscopy in this region. They comprise an outer layer, one cell thick, that surrounds the root cortex. Their development can be summarized in three spatial stages. From the root tip towards the shoot, these zones are division, elongation, and differentiation[3, 4]. In the division zone, cells lay down cell plates, which mature into cell walls, separating the mother cell into two daughter cells. The cell plate is laid down anticlinally, leaving the daughter cells in the same cell layer as the mother cell. The first of these divisions yields a root-tip resident cell that remains a part of the root apical meristem, and a new

cell destined for later expansion and further division. In this region, axial cell expansion occurs, but to a minimal degree, maintaining roughly equally-sized cells. Radial expansion also occurs, resulting in a widening of the root organ. Shootward from this zone lies the “elongation zone”, where cells undergo extreme turgor-driven elongation, resulting in visco-elastic deformation through a process of regulated creep, which is a mode of mechanical deformation [5]. Moving shootward, in the next zone, “differentiation”, this expansion terminates, and alternating epidermal cell files visually differentiate into trichoblast-containing and atrichoblast-containing cell files. Trichoblasts are defined by their capacity to produce root hairs, which are long extensions of the cell into the surrounding media. At the basal region of a trichoblast, a nascent root hair first bulges and then protrudes cylindrically, increasing the root surface area. Growth of the root hair follows a syndrome, tip-growth, than differs from the diffuse growth pattern of most other plant cells, but is analogous to pollen tube growth[6].

While the term “differentiation zone” refers to the emergence of the most obvious physical difference between trichoblasts and atrichoblasts (root hair formation), cell identity is actually established as early as the meristematic zone, by positional information[7]. Trichoblast files are located above clefts between cortical cells; atrichoblast files contact a single cortical cell row[8]. This early establishment of cell identity first becomes macroscopically apparent when small differences in cell length appear in the division zone[4]. Trichoblast files contain cells that are consistently shorter than their neighboring atrichoblast cells. To avoid bulging or otherwise warping the overall shape of the root tip as a consequence of differential cell expansion, the plant must tightly coordinate cell division and cell elongation in this zone. Perhaps to accommodate radial expansion of the overall root organ, trichoblast cells in the division zone undergo occasional lateral division, giving rise to a double-file of trichoblast cells. While this is rare enough that most trichoblast cell files neighbor atrichoblast cell files on either side, some micrographs in this work may capture adjacent trichoblast cell files. This is the origin of such an

arrangement. Rapid cell elongation occurs in both cell identities, however, invisibly, ploidy levels begin to diverge between cell identities at this stage. The relatively longer atrichoblast cells begin endoreduplication cycles later than trichoblast cell files, and after elongation ceases, will have undergone fewer total cycles[9]. The two cell identities are also metabolically divergent during rapid elongation; for example, in cross-section trichoblasts are revealed to be densely cytoplasmic, while atrichoblasts are highly vacuolated[10].

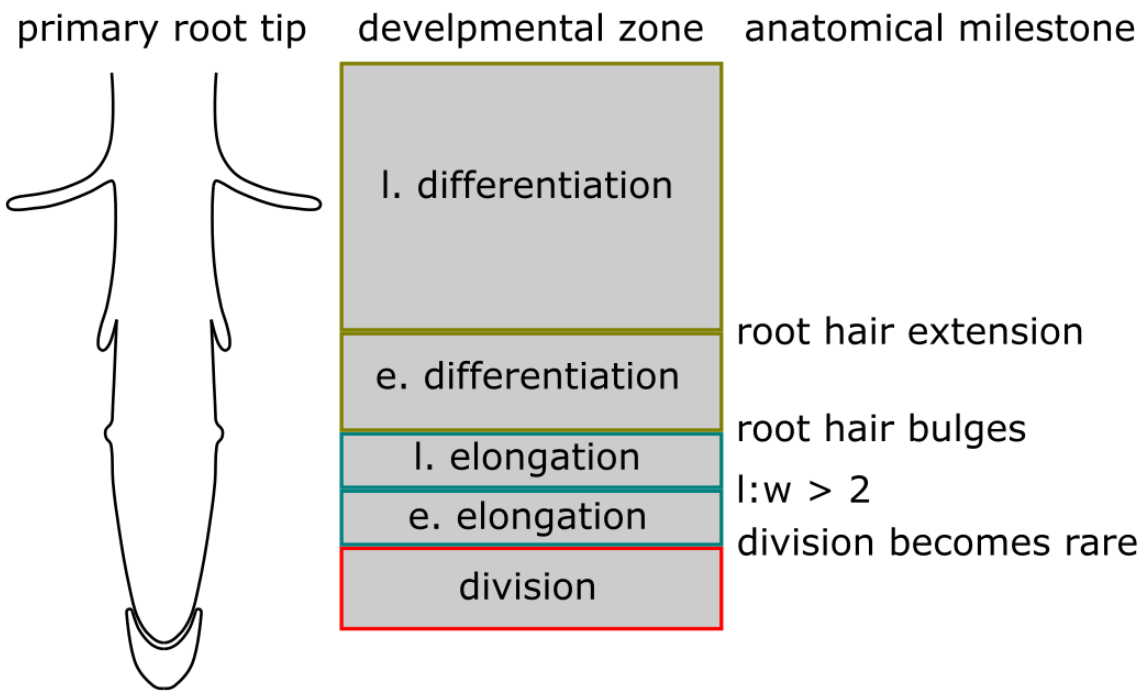

Figure 1-1. Delineation of Arabidopsis root tip developmental zones. Anatomical milestones used in this study to delineate root developmental zones. Modified from [12].

For the purposes of this study, I will pragmatically distinguish an “early differentiation zone”, where root hair bulges are first evident, and a “late differentiation zone” where root hairs have expanded to the degree that they have a clearly definable cylindrical shaft. I will also subdivide the elongation zone, somewhat arbitrarily, into “early elongation” and “late elongation”

zones, where early elongation zone cells are <2 times as long as wide (but new cell divisions are rare or absent) and late elongation zone cells are >2 times as long as wide. This roughly corresponds to the "distal elongation zone"[11] of kinematic studies (i.e. the "transition zone" of [12]), and the "fast elongation zone" of [12], respectively. These sub-categories are introduced for convenience and rapid communication of cell location and developmental progress, and are not meant to represent discrete changes in development. Rather, they serve as milestones of development in the context of a specific study system: Arabidopsis seedling roots growing in liquid culture after 4-5 d vertical growth on solid media.

1.2 The Primary Cell Wall

Plant cell walls are composite structures, dominated by polysaccharides, water, and proteins[13]. Plant cell expansion, a fundamental process underlying plant growth, is ultimately driven by the turgor pressure of the protoplast, but the direction, speed and shape of expansion is dictated by the properties of the primary wall[5, 14]. The wall that is assembled and deformed during this process is called the primary cell wall, to distinguish it from the secondary wall, which is laid down after cell growth has ceased, if at all. Axial growth occurs according to two syndromes, diffuse and tip-growth. In diffuse axial growth, the walls yield symmetrically, promoting elongation of the entire cell. In tip-growth, at least in the context of expanding root hairs, only the distal-most region of a subcellular region expands. It must be initiated from a subregion of an existing wall. In both cases, controlled mechanical deformation of the wall results in its expansion, and new wall material must be added to the growing wall to maintain wall thickness. This process is dynamic and ultimately coordinated by the cell, resulting in specific plant cell shapes, but this control is exerted through their walls' anisotropic yielding.

The most obvious source of anisotropy in wall organization is the (1,4)-beta-glucan, cellulose. Cellulose glucan chains coalesce rapidly after their synthesis at the plasma membrane to form para-crystalline cellulose microfibrils (CMFs)[15]. Neutron and X-ray scattering data, along with solid-state NMR analyses support spatial models where CMFs contain 18 or 24 glucan chains, arranged in a hexagonal cross-section, with two parallel hydrophobic faces and four hydrophilic faces[16-19]. However, thicker fibrillar structures have been observed with atomic force microscopy and electron microscopy (e.g. [20],[21]). Even in the range of resolutions allowed by visible light microscopy, fibrillar features may be observed in the wall[22]. These larger structures are likely bundles of multiple CMFs, which are thought to form after individual CMF synthesis, though the timing and coordination of bundling is not currently clear. Interactions both between CMFs and also between CMFs and other wall polysaccharides (hereafter, 'matrix polysaccharides') are important for determining wall deformation mechanics, and by extension, cell shape[23, 24].

CMFs are organized in stacked lamellae[15], where fibrils within a single lamella assume a single prevailing orientation. In the outer periclinal walls of root epidermal cells, the net cellulose orientation seems to transition from transverse to the growth axis at the innermost lamellae to more-longitudinal at the outermost lamellae[25]. However, in some tissues neighboring lamellae may have very different prevailing CMF orientations; successive neighboring lamellae of onion scale epidermal walls have been shown by atomic force microscropy (AFM) investigation to differ in orientation[20]. The other major glycans of primary cell walls were long thought to be more-or-less isotropically organized in the wall, present either as tethers between CMFs (disorganized, except where adsorbed onto cellulose microfibrils) [26], or as components of a hydrated gel between the CMFs and their cross-tethers[27].

While cellulose appears to be the only crystalline component of the primary cell wall, there are other polysaccharides in plant cell walls that have (1,4)-beta-linked backbones with an

equatorial configuration. These are known as hemicelluloses[28]. In the primary walls of most plants, the major hemicellulose present is xyloglucan, a (1,4)-beta-linked glucan with xylose-containing side-chains that are (1,6)-alpha-linked to many of the glucose residues. Other hemicelluloses include variously substituted xylans and mannans. Xyloglucan side-chains in Arabidopsis include fucose, galactose, and xylose residues. Pectins are a more diverse class of polysaccharides, unified chemically by the presence of galacturonic acid-containing backbones[29]. Homogalacturonan (HG) has a (1,4)-alpha-linked galacturonic acid backbone. The degree to which its carboxyl moieties are methyl-esterified is thought to be a major determinant of wall mechanical properties[30, 31]. Rhamnogalacturonan-I is characterized by its backbone of a repeating disaccharide unit, [,2)-alpha-L-rhamnose (1,4)-alpha-D-galacturonic acid(1,], the rhamnose residues of which are frequently decorated with neutral sugar side-chains, including galacatans, arabinans, and arabinogalactans. Fucose has also been observed to link, in some cases, to RG-I galactan[32]. While HG and RG-I have variable structures, the third pectic component, RG-II, appears to have a highly-conserved structure, composed of 12 different glycosyl residues, among them, L-fucose and L-galactose. These are organized into six side-chains, which branch from a (1,4)-alpha-linked galacturonic acid backbone[33]. While often considered distinct polysaccharides, the above classes of pectins may, in the wall, be covalently linked[29]. This is exemplified by the discovery of the APAP1 proteoglycan, which features covalent linkages between peptide, RG-I, HG, and arabinoxylan components[34]. Even cellulose has recently been suggested to be covalently bound to matrix wall components; there is only indirect evidence of such a linkage, however[35]. The primary walls of commelinoid monocots have a matrix glycan composition that differs markedly from those of other angiosperms[36]. While xyloglucans and pectins are also present in these structures, they are much reduced in quantity, replaced by variously substituted and cross-linked xylans[37]. This distinction is

important because this group of plants includes the grasses, which are major targets for the development of cellulosic biofuel feedstocks.

The importance of non-covalent interactions between cellulose and pectic domains for controlling wall mechanics is becoming more clear. Most of these clues have come thanks to revolutionary advances in the solid-state NMR study of the plant cell wall[38]. These experiments have revealed and characterized multiple subdomains of pectin that vary in motility as well as chemical composition[39]. Some of these domains appear to have strong intermolecular interactions with cellulose microfibrils[40]. These intermolecular interactions help explain, for example, the growth phenotypes of plants with altered pectin molecular weight due to altered polygalacturonase activity[41]. Pectin-cellulose interactions have also been observed and emphasized in *in vitro* polymer studies[42] of artificial and semi-artificial polymer composites[43]. However, the extent to which these composites recapitulate interactions in the plant cell wall, which is far more complex, remains uncertain.

1.3 Molecular probes for plant cell walls

Models of the primary cell wall are often drawn such that the matrix is disperse; only the hemicelluloses directly interact with cellulose microfibrils (e.g. [13]). However, sub-micron scale heterogeneity in matrix component distribution does exist, for example as revealed by monoclonal antibody and carbohydrate-binding module (CBM) labeling [44]. These probes offer specific detection of polysaccharides, but their large size can limit their ability to permeate to the real sites of their antigens[45]. Other polysaccharides can also mask the antigenic polysaccharide's epitope[46], though this masking phenomenon itself can be informative[47]. An approach, analogous to tagging proteins with intrinsically fluorescent proteins, that could image polysaccharides directly would be more ideal. Autoradiography of walls that have incorporated

salvaged ^{14}C radiolabeled monosaccharides can reveal the distribution of those polysaccharides[48, 49]. However, this is not amenable to live cell imaging. Plants also have a great diversity of enzymatic activities capable of interconverting various monosaccharides (rev. in [50]), which can limit the specificity of the label.

Another, emergent approach for tracking polysaccharides takes advantage of orthogonal chemical reactions to directly couple sugars to a fluorophore. Orthogonal chemical reactions are those that are so selective that the relevant functional groups react with one another and not with other groups present in the reaction milieu. Orthogonality is an important characteristic of the versatile Cu(I)-catalyzed azide-alkyne cycloaddition, popularly known as a 'click' reaction [51, 52]. Modification of this reaction by the use of either Cu(I)-chelating ligands[53] or a ring-strained internal alkyne group[54] can make this orthogonal reaction "biorthogonal," that is, specific enough to distinguish unique reactivity and mild enough to avoid toxicity in living organisms. While native sugars lack either required functional group, sugar salvage pathway and other biosynthetic enzymes appear to tolerate some azido- or ethynyl- functionalized monosaccharides (hereafter, "click sugars" (rev. in[2]). In a typical experiment, a click sugar is introduced to living cells, which internalize it and incorporate it into a native polysaccharide. The native polysaccharide, which now contains either an azido or ethynyl functional group, can be click-labeled with a small fluorescent dye molecule that has the complementary functionality.

A growing number of successfully incorporated and labeled click sugars have been used in a wide range of living systems. In bacteria and vertebrates, the microscale distribution of varied monosaccharides such as N-acetylneuraminic acid, N-acetylgalactosamine, N-acetylglucosamine, fucose[2, 55], and 3-deoxy-D-manno-octulosonic acid (Kdo)[56] has been investigated using clickable analogs. In plants, the first demonstration of an incorporated and tracked click-sugar, as a metabolic tracer for the cell wall, used fucose alkyne (FucAl)[22]. There is indirect evidence that the alkynyl reporter is incorporated into the RG-I component of pectin.

This was surprising, because fucose itself has only rarely been shown to be a component of RG-I domains[32], and because xyloglucan was thought to be the major site of any salvaged fucose based on the fact that approximately 50% of all primary wall fucose is a part of XyG[57]. However, analysis of click-labeling in *xxt1 xxt2*, an Arabidopsis mutant lacking any functional expression of the xylosyltransferases required to decorate the glucan backbone of XyG, showed no quantitative difference in FucAl incorporation intensity ([22], this work). This leaves RG-II as potential target of FucAl incorporation. This interpretation was ruled out by [22], based on size exclusion chromatographic analysis. Briefly, alcohol-insoluble residue was prepared from plants that were treated with FucAl, and then click-reacted with a compatible fluorophore. The residue was then treated with polygalacturonase and pectin methylesterase, which should have degraded most of the pectin present, freeing intact RG-II molecules to be extracted, which should then elute in the included fractions collected after separation via size-exclusion chromatography. However, fluorescence was only detected in the void volume fractions recovered from the column, which was interpreted to mean that the fluorescence was associated with a high molecular weight macromolecule, not RG-II. Given similar labeling patterns and kinetics with KDO-azide[58], which is thought to label RG-II, perhaps this interpretation should be revisited. It is odd, for example, that no positive evidence of RG-II elution in the included-volume was shown, labeled fluorescently or not. If the pectin degradation step was not complete enough, for example, then RG-II would have remained covalently linked to HG pectic domains, eluting with them in the void volume.

Successful incorporation of click sugars is probably dependent on substrate promiscuity by the sugar salvaging set of biochemical pathways[50]. Salvage pathways recycle free monosaccharides to NDP-activated forms, which are the substrates of polysaccharide-synthesizing glycosyltransferases. For example, the UDP pyrophosphorylase SLOPPY in Arabidopsis can accept a wide variety of sugar-1-phosphates (Glc-1-P, Gal-1-P, Xyl-1-P, Ara-1-

P, and GalA-1-P) and convert them in the presence of UTP to their corresponding UDP-sugars[59]. Since the discovery that FucAl labels nascent pectin, other click-compatible chemical reporters have seen use in planta, making visible the most recently synthesized lignin [29, 30][60], N-linked glycans, and even putative novel auxin-binding sites[31]. Azido-modified sugars have also been found to be incorporated into Arabidopsis cell walls, though, with the exception of a Kdo analog that ultimately labels RG-II[32], they apparently must be applied at relatively higher concentrations than FucAl[33]. Azido-modified reporters are attractive because they are compatible with a ring-strained-catalyzed cyclooctyne ligation reaction that avoids the toxic Cu(I) catalyst[34].

1.4 Dissertation Outline

Building on the work described above, my dissertation work started with attempts to answer the following questions:

1. If we expand the toolbox of available click sugars to fluorescently label other cell wall matrix polysaccharides, will their distributions differ from those of FucAl and Kdo-azide? Chapter 2 will introduce the synthesis and screening of a number of new click-functionalized sugar chemical reporters. I then characterize the novel incorporation pattern of 6dAG, a new click sugar that may report on the location of callose synthesis.

2. Can alkynyl sugars be used for live cell imaging experiments, despite the traditional hurdle of copper toxicity? In Chapter 3 I adapt a ligand-protection strategy from the field of bioconjugation[61] to preserve plant cell viability during the click labeling reaction between an alkynyl reporter and an azido-functionalized fluorescent probe. This enables the co-visualization of the cortical microtubule array underlying a wall with patterned matrix deposition, which prompts my further investigation into the cell's regulatory mechanism underlying such patterns.

The role of the cortical microtubule cytoskeleton in regulating cell wall properties is then investigated from another perspective in Chapter 4. Here, I use metabolic labeling to help clarify a confusing wall-associated phenotype for a mutant with a lesion in a kinesin-encoding gene. Finally, Chapter 5 looks forward to the future applications of bio-orthogonal labeling in the study of plant cell walls.

1.5 References

1. Somerville, C. and M. Koornneef, *A fortunate choice: the history of Arabidopsis as a model plant.* Nat Rev Genet, 2002. **3**(11): p. 883-9.
2. Laughlin, S.T. and C.R. Bertozzi, *Imaging the glycome.* Proceedings of the National Academy of Sciences of the United States of America, 2009. **106**(1): p. 12-17.
3. Petricka, J.J., C.M. Winter, and P.N. Benfey, *Control of Arabidopsis root development.* Annu Rev Plant Biol, 2012. **63**: p. 563-90.
4. Scheres, B., P. Benfey, and L. Dolan, *Root development.* Arabidopsis Book, 2002. **1**: p. e0101.
5. Cosgrove, D.J., *Growth of the plant cell wall.* Nat Rev Mol Cell Biol, 2005. **6**(11): p. 850-61.
6. Rounds, C.M. and M. Bezanilla, *Growth mechanisms in tip-growing plant cells.* Annu Rev Plant Biol, 2013. **64**: p. 243-65.
7. Berger, F., et al., *Positional information in root epidermis is defined during embryogenesis and acts in domains with strict boundaries.* Curr Biol, 1998. **8**(8): p. 421-30.
8. Galway, M.E., et al., *The TTG gene is required to specify epidermal cell fate and cell patterning in the Arabidopsis root.* Dev Biol, 1994. **166**(2): p. 740-54.
9. Bhosale, R., et al., *A Spatiotemporal DNA Endoploidy Map of the Arabidopsis Root Reveals Roles for the Endocycle in Root Development and Stress Adaptation.* Plant Cell, 2018. **30**(10): p. 2330-2351.
10. Dolan, L., et al., *Cellular-Organization of the Arabidopsis-Thaliana Root.* Development, 1993. **119**(1): p. 71-84.
11. Ishikawa, H. and M.L. Evans, *Specialized zones of development in roots.* Plant Physiol, 1995. **109**: p. 725-7.
12. Verbelen, J.P., et al., *The Root Apex of Arabidopsis thaliana Consists of Four Distinct Zones of Growth Activities: Meristematic Zone, Transition Zone, Fast Elongation Zone and Growth Terminating Zone.* Plant Signal Behav, 2006. **1**(6): p. 296-304.
13. Somerville, C., et al., *Toward a systems approach to understanding plant-cell walls.* Science, 2004. **306**(5705): p. 2206-2211.
14. Wolf, S., K. Hematy, and H. Hofte, *Growth control and cell wall signaling in plants.* Annu Rev Plant Biol, 2012. **63**: p. 381-407.
15. Polko, J.K. and J.J. Kieber, *The Regulation of Cellulose Biosynthesis in Plants.* Plant Cell, 2019. **31**(2): p. 282-296.

16. Fernandes, A.N., et al., *Nanostructure of cellulose microfibrils in spruce wood.* Proc Natl Acad Sci U S A, 2011. **108**(47): p. E1195-203.
17. Thomas, L.H., et al., *Structure of cellulose microfibrils in primary cell walls from collenchyma.* Plant Physiol, 2013. **161**(1): p. 465-76.
18. Jarvis, M.C., *Structure of native cellulose microfibrils, the starting point for nanocellulose manufacture.* Philos Trans A Math Phys Eng Sci, 2018. **376**(2112).
19. Newman, R.H., S.J. Hill, and P.J. Harris, *Wide-angle x-ray scattering and solid-state nuclear magnetic resonance data combined to test models for cellulose microfibrils in mung bean cell walls.* Plant Physiol, 2013. **163**(4): p. 1558-67.
20. Zhang, T., Y. Zheng, and D.J. Cosgrove, *Spatial organization of cellulose microfibrils and matrix polysaccharides in primary plant cell walls as imaged by multichannel atomic force microscopy.* Plant J, 2016. **85**(2): p. 179-92.
21. Sugimoto, K., R.E. Williamson, and G.O. Wasteneys, *New Techniques Enable Comparative Analysis of Microtubule Orientation, Wall Texture, and Growth Rate in Intact Roots of Arabidopsis.* Plant Physiology, 2000. **124**: p. 1493-1506.
22. Anderson, C.T., I.S. Wallace, and C.R. Somerville, *Metabolic click-labeling with a fucose analog reveals pectin delivery, architecture, and dynamics in Arabidopsis cell walls.* Proc Natl Acad Sci U S A, 2012. **109**(4): p. 1329-34.
23. Park, Y.B. and D.J. Cosgrove, *Xyloglucan and its interactions with other components of the growing cell wall.* Plant Cell Physiol, 2015. **56**(2): p. 180-94.
24. Cosgrove, D.J., *Re-constructing our models of cellulose and primary cell wall assembly.* Curr Opin Plant Biol, 2014. **22**: p. 122-131.
25. Anderson, C.T., et al., *Real-Time Imaging of Cellulose Reorientation during Cell Wall Expansion in Arabidopsis Roots.* Plant Physiology, 2010. **152**(2): p. 787-796.
26. Keegstra, K., et al., *The Structure of Plant Cell Walls: III. A Model of the Walls of Suspension-cultured Sycamore Cells Based on the Interconnections of the Macromolecular Components.* Plant Physiol, 1973. **51**(1): p. 188-97.
27. Carpita, N.C. and D.M. Gibeaut, *Structural models of primary cell walls in flowering plants: consistency of molecular structure with the physical properties of the walls during growth.* Plant J, 1993. **3**(1): p. 1-30.
28. Scheller, H.V. and P. Ulvskov, *Hemicelluloses.* Annu Rev Plant Biol, 2010. **61**: p. 263-89.
29. Atmodjo, M.A., Z. Hao, and D. Mohnen, *Evolving views of pectin biosynthesis.* Annu Rev Plant Biol, 2013. **64**: p. 747-79.
30. Braybrook, S.A., H. Hofte, and A. Peaucelle, *Probing the mechanical contributions of the pectin matrix: insights for cell growth.* Plant Signal Behav, 2012. **7**(8): p. 1037-41.
31. Peaucelle, A., et al., *Pectin-induced changes in cell wall mechanics underlie organ initiation in Arabidopsis.* Curr Biol, 2011. **21**(20): p. 1720-6.
32. Nakamura, A., et al., *Analysis of structural components and molecular construction of soybean soluble polysaccharides by stepwise enzymatic degradation.* Biosci Biotechnol Biochem, 2001. **65**(10): p. 2249-58.
33. Ndeh, D., et al., *Complex pectin metabolism by gut bacteria reveals novel catalytic functions.* Nature, 2017. **544**(7648): p. 65-70.
34. Tan, L., et al., *An Arabidopsis cell wall proteoglycan consists of pectin and arabinoxylan covalently linked to an arabinogalactan protein.* Plant Cell, 2013. **25**(1): p. 270-87.
35. Broxterman, S.E. and H.A. Schols, *Interactions between pectin and cellulose in primary plant cell walls.* Carbohydr Polym, 2018. **192**: p. 263-272.
36. Vogel, J., *Unique aspects of the grass cell wall.* Curr Opin Plant Biol, 2008. **11**(3): p. 301-7.

37. Hatfield, R.D., D.M. Rancour, and J.M. Marita, *Grass Cell Walls: A Story of Cross-Linking.* Front Plant Sci, 2016. **7**: p. 2056.
38. Dick-Perez, M., et al., *Structure and Interactions of Plant Cell-Wall Polysaccharides by Two- and Three-Dimensional Magic-Angle-Spinning Solid-State NMR.* Biochemistry, 2011. **50**(6): p. 989-1000.
39. Wang, T. and M. Hong, *Solid-state NMR investigations of cellulose structure and interactions with matrix polysaccharides in plant primary cell walls.* Journal of Experimental Botany, 2016. **67**(2): p. 503-514.
40. Wang, T., O. Zabotina, and M. Hong, *Pectin-cellulose interactions in the Arabidopsis primary cell wall from two-dimensional magic-angle-spinning solid-state nuclear magnetic resonance.* Biochemistry, 2012. **51**(49): p. 9846-56.
41. Phyo, P., et al., *Effects of Pectin Molecular Weight Changes on the Structure, Dynamics, and Polysaccharide Interactions of Primary Cell Walls of Arabidopsis thaliana: Insights from Solid-State NMR.* Biomacromolecules, 2017. **18**(9): p. 2937-2950.
42. Zykwinska, A.W., et al., *Evidence for in vitro binding of pectin side chains to cellulose.* Plant Physiol, 2005. **139**(1): p. 397-407.
43. Lopez-Sanchez, P., et al., *Cellulose-pectin composite hydrogels: Intermolecular interactions and material properties depend on order of assembly.* Carbohydrate Polymers, 2017. **162**: p. 71-81.
44. Lee, K.J.D., S.E. Marcus, and J.P. Knox, *Cell Wall Biology: Perspectives from Cell Wall Imaging.* Molecular Plant, 2011. **4**(2): p. 212-219.
45. Rydahl, M.G., et al., *Report on the Current Inventory of the Toolbox for Plant Cell Wall Analysis: Proteinaceous and Small Molecular Probes.* Front Plant Sci, 2018. **9**: p. 581.
46. Marcus, S.E., et al., *Pectic homogalacturonan masks abundant sets of xyloglucan epitopes in plant cell walls.* Bmc Plant Biology, 2008. **8**.
47. Marcus, S.E., et al., *Restricted access of proteins to mannan polysaccharides in intact plant cell walls.* Plant J, 2010. **64**(2): p. 191-203.
48. Gibeaut, D.M. and N.C. Carpita, *Tracing cell wall biogenesis in intact cells and plants.* Plant Physiology, 1991. **97**: p. 551-561.
49. Roberts, R.M. and V.S. Butt, *Incorporation of 14C-L-arabinose into polysaccharides of maize root-tips.* Planta, 1970. **94**: p. 175-183.
50. Bar-Peled, M. and M.A. O'Neill, *Plant nucleotide sugar formation, interconversion, and salvage by sugar recycling.* Annu Rev Plant Biol, 2011. **62**: p. 127-55.
51. Rostovtsev, V.V., et al., *A stepwise huisgen cycloaddition process: copper(I)-catalyzed regioselective "ligation" of azides and terminal alkynes.* Angew Chem Int Ed Engl, 2002. **41**(14): p. 2596-9.
52. Tornoe, C.W., C. Christensen, and M. Meldal, *Peptidotriazoles on solid phase: [1,2,3]-triazoles by regiospecific copper(i)-catalyzed 1,3-dipolar cycloadditions of terminal alkynes to azides.* J Org Chem, 2002. **67**(9): p. 3057-64.
53. Chan, J., S.C. Dodani, and C.J. Chang, *Reaction-based small-molecule fluorescent probes for chemoselective bioimaging.* Nat Chem, 2012. **4**(12): p. 973-84.
54. Agard, N.J., J.A. Prescher, and C.R. Bertozzi, *A strain-promoted [3 + 2] azide-alkyne cycloaddition for covalent modification of biomolecules in living systems.* J Am Chem Soc, 2004. **126**(46): p. 15046-7.
55. Rabuka, D., et al., *A chemical reporter strategy to probe glycoprotein fucosylation.* J Am Chem Soc, 2006. **128**(37): p. 12078-9.
56. Dumont, A., et al., *Click-mediated labeling of bacterial membranes through metabolic modification of the lipopolysaccharide inner core.* Angew Chem Int Ed Engl, 2012. **51**(13): p. 3143-6.

57. Vanzin, G.F., et al., *The mur2 mutant of Arabidopsis thaliana lacks fucosylated xyloglucan because of a lesion in fucosyltransferase AtFUT1.* Proc Natl Acad Sci U S A, 2002. **99**(5): p. 3340-5.
58. Dumont, M., et al., *Plant cell wall imaging by metabolic click-mediated labelling of rhamnogalacturonan II using azido 3-deoxy-D-manno-oct-2-ulosonic acid.* Plant J, 2016. **85**(3): p. 437-47.
59. Kotake, T., et al., *UDP-sugar pyrophosphorylase with broad substrate specificity toward various monosaccharide 1-phosphates from pea sprouts.* J Biol Chem, 2004. **279**(44): p. 45728-36.
60. Simon, C., et al., *Visualizing Lignification Dynamics in Plants with Click Chemistry: Dual Labeling is BLISS!* J Vis Exp, 2018(131).
61. Hong, V., et al., *Analysis and optimization of copper-catalyzed azide-alkyne cycloaddition for bioconjugation.* Angew Chem Int Ed Engl, 2009. **48**(52): p. 9879-83.

Chapter 2

The click-compatible sugar 6-deoxy-alkynyl glucose metabolically incorporates into Arabidopsis root hair tips and arrests their growth

2.1 Abstract

Plant cell walls are dynamic structures whose polysaccharide components are rearranged and recycled during growth and morphogenesis. Covalent fluorescent tagging of these polysaccharides following a metabolic labeling approach can help elucidate these changes. Herein reported are the synthesis and seedling-incorporation of a plant polysaccharide chemical reporter, 6-deoxy-alkynyl glucose (6dAG), that is modeled on D-glucose. This compound was selected by screening a small library of novel ethynyl-functionalized sugar analogs. Whereas fucose-alkyne, a previously reported chemical reporter for pectin, incorporates diffusely throughout growing cell walls, 6dAG incorporated specifically into root hair tips. This incorporation occurs in a time- and concentration-dependent manner. 6dAG exposure both induces and colocalizes with callose deposition in this tissue, and arrests both root hair and root growth. These results show that plants can incorporate an additional alkynyl-modified sugar analog into their metabolism, and into a discrete subcellular location.

Permissions for Published Work

Chapter 2 includes part of one publication:

Daniel D. McClosky, Bo Wang, Gong Chen, and Charles T. Anderson. (2016) The click-compatible sugar 6-deoxy-alkynyl glucose metabolically incorporates into *Arabidopsis* root hair tips and arrests their growth. ***Phytochemistry***, Vol. 123: 16-24, doi:

http://dx.doi.org/10.1016/j.phytochem.2016.01.007

www.sciencedirect.com/journal/phytochemistry © 2016 Elsevier Ltd.

Elsevier permissions:

Used here in accordance with Elsevier Permission Guidelines:

"Can I include/use my article in my thesis/dissertation?

Yes. Authors can include their articles in full or in part in a thesis or dissertation for non-commercial purposes."

https://www.elsevier.com/about/policies/copyright/permissions

Accessed 2/9/2019

2.2 Author Contributions

D.D.M., B.W., G.C., and C.T.A designed experiments; D.D.M. and B.W. performed experiments; D.D.M. and B.W. analyzed results, D.D.M. and C.T.A. wrote the manuscript. Author of the Dissertation, D.D.M., designed experiments, performed research, and analyzed the data for all results reported besides the organic syntheses and chemical characterization of 6dAG, which were performed by B.W.

2.3 Introduction

The primary walls of plant cells are dynamic extracellular structures that enable tissue growth and determine cellular and organismal morphology[1]. They are composed of carbohydrate polymers that interact with one another to form strong, flexible networks that are reorganized during cell growth[2-4]. Many of these carbohydrate polymers contain glucose monomers: for example, cellulose, the main load-bearing component of the plant cell wall, is composed of β-1,4-linked glucan chains that coalesce to form partially crystalline microfibrils with high tensile strength[5]. Xyloglucan, the most abundant hemicellulose in the primary walls of many eudicot plant species, contains a backbone of β-1,4-linked glucose monomers that is decorated with neutral sugar sidechains, whereas the linear polymer, mixed-linkage glucan, contains β-1,4- and β-1,3-linked glucose subunits. Callose, a specialized cell wall polymer that is produced during new cell wall formation and in response to external stimuli such as wounding and pathogen attack, is composed of linear β-1,3-linked glucan chains[6, 7]. Although candidate glycosyltransferases for all of these polymers have been identified at the genetic level, many details of where and when these polymers are synthesized, delivered to the cell wall, and modified during cellular development and expansion are unknown[8, 9]. Since cell wall carbohydrates embody much of the biomass produced by plants via photosynthesis, improved knowledge of their dynamics will be useful for the sustainable production of food, materials, and renewable bioenergy.

The ability to specifically label newly synthesized carbohydrate polymers with fluorescent tags is an effective method for following their life histories in living organisms. However, because carbohydrate polymers cannot be tagged genetically in the same way that proteins can be tagged with fluorescent markers such as GFP, they must be labeled by other means. One such approach is metabolic labeling, in which sugar analogs act as chemical

reporters, becoming incorporated into natural polymers before being covalently linked to fluorescent probes using, for example, a copper-catalyzed cyclization reaction (a subset of "click reactions") [10, 11]. This method has been used to investigate the details of glycan synthesis and metabolism across diverse biological taxa[12, 13]. For example, a click chemistry-based approach to label nascent pectins in root epidermal cell walls of the model plant Arabidopsis thaliana (L.) Heynh. was previously adopted using the click-compatible fucose analog fucose-alkyne. This study found that fucose-alkyne-containing pectins are initially delivered to discrete locations across the cell surface that likely represent sites of exocytic vesicle fusion and that fucose alkyne-containing pectins become reorganized into linear fibrillar arrangements as cell elongation progresses and they age in the cell wall[14].

In addition to their reorganization during diffuse growth, cell wall components are also reorganized during the transition to tip growth in the same cell. This transition in wall properties occurs in some Arabidopsis root epidermal cells. At a certain point along the root developmental gradient, two distinct cell files become visible, trichoblasts and atrichoblasts, which are distinguishable by the presence of root hair bulges in the former. These files typically alternate along the circumference of the root; their identity is determined by the arrangement of cortex cells below[15]. Root hair bulges of trichoblasts are regions of distinct wall biochemistry and mechanics where a subregion of the outer wall changes growth schemes. Unlike the diffuse expansion that had occurred during primary cell expansion, these bulges expand by tip growth, the polarized addition of new wall material to elongate the growing tip[16].

Diversifying the click chemistry-based approach to enable the metabolic labeling of cellulose, hemicelluloses, and/or callose would allow for the study of how these polymers change in abundance and distribution over developmental time in any plant species of interest. Although azido-linked analogs for several monosaccharides that are commonly found in cell walls are commercially available, and azido 3-deoxy-D-manno-oct-2-ulosonic acid (KDO-azide) was

recently reported to incorporate into pectic rhamnogalacturonan-II[17], it was previously found that fucose-azide is not efficiently incorporated into plant cell walls as compared to fucose-alkyne[14]. Thus, there is a need to expand the toolbox of click-compatible analogs of monosaccharides, such as glucose, galactose, xylose, rhamnose, and arabinose, that are present in cell wall carbohydrates. In this work, the synthesis of one such analog, 6-deoxy-alkynyl glucose (6dAG), and its use in metabolic labeling experiments in Arabidopsis roots, is reported. This compound is incorporated into Arabidopsis root epidermal cells in a metabolism-, time-, and concentration-dependent manner, but unexpectedly, 6dAG incorporation results in specific labeling of a subcellular structure, the root hair bulge, and inhibits root hair growth, suggesting that it might be incorporated into a novel cell wall component that affects cell wall expansion in root hairs.

2.4 Results and Discussion

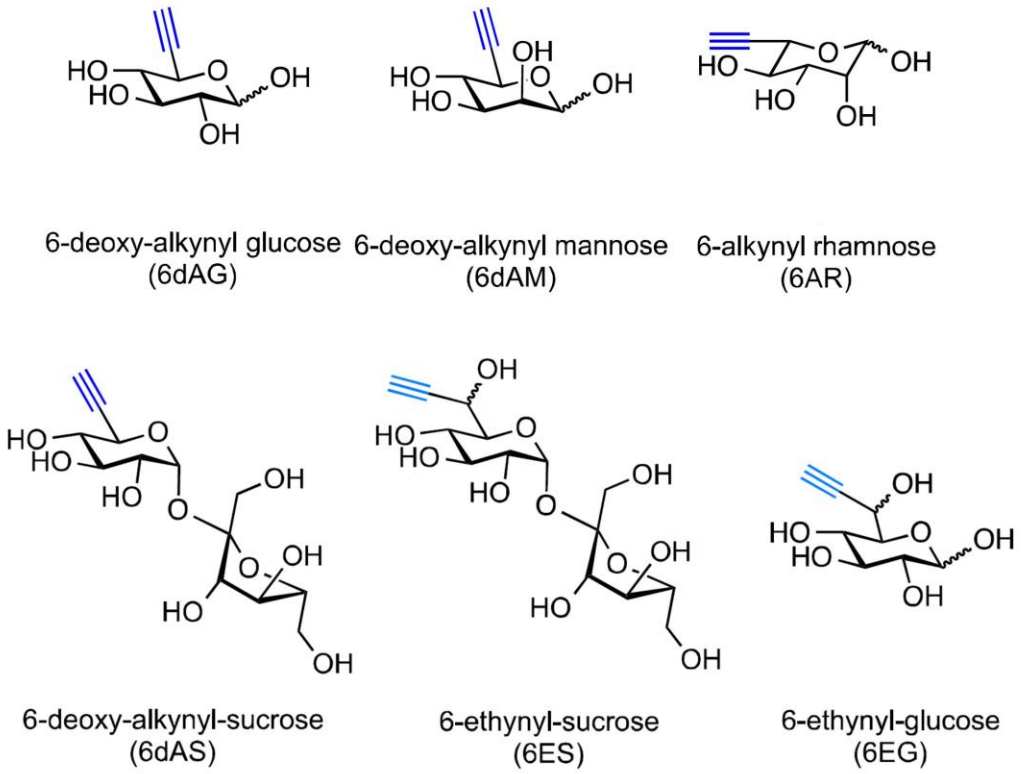

Figure 2-1: Structures of novel alkyne-functionalized sugar analogs for click-labeling experiments.

2.4.1 Development and screening of a small library of alkynyl sugar analogs

To expand the number of click-compatible sugar analogs beyond fucose-alkyne and KDO-azide, we designed and synthesized analogs to three other sugars that are present in plant cell walls: glucose, rhamnose, and mannose (Figure 2-1, reproduced from[18]). Four of these analogs have alkynyl groups in place of 6-OH groups on the native sugar; these are '6-deoxy-alkynyl' ('6dA') analogs in our nomenclature. We also produced two analogs in which an ethynyl group is incorporated at the C6 position of the sugar, and the 6-OH group remains. We term these

‘6-ethynyl’ (‘6E’) analogs. Neither analog type is directly parallel in design to fucose-alkyne where the alkynyl moiety is in place of a methyl group (fucose is a naturally-occurring 6-deoxy-sugar). Synthesis of the 6dA analogs followed a general strategy of (1) differential protection of hydroxy groups, followed by (2) oxidation of the C6-hydroxy group to the corresponding aldehyde, then (3) Seyferth-Gilbert homologation[19, 20] of the aldehyde to the alkynyl moiety, and finally (4) deprotection and (5) peracetylation. The detailed synthetic scheme for 6dAG is given in the next section; synthesis of the other three 6dA analogs and the design and synthesis of the 6E analogs are given in [18].

Next, each of these analogs was assayed for incorporation into Arabidopsis root epidermal cell walls. The sugar analogs were introduced to the plants by incubating 4 d old seedlings it liquid MS media, at a concentration of 10 µM of the analog, for 24 h under constant light. These were then washed, click-labeled with 1 µM Alexa488-azide under catalysis by 1 mM Cu(I), then examined for wall-associated fluorescence in root tip developmental zones by spinning disk confocal microscopy. Additionally, commercially available azido-analogs of glucose (2-deoxy-2-azido-glucose (‘2dZG’ by analogy to ‘6dAG’) and 6-deoxy-6-azido-glucose) and galactose (2-deoxy-2-azido-galactose (‘2dZGal’ by analogy to ‘6dAG’) and 6-deoxy-6-azido-galactose) were screened similarly, except that these seedlings were treated with 1 µM Alexa488-alkyne in the click-labeling step. The results of the screen are given in Table 2-1; only 6dAG resulted in unambiguously wall-associated fluorescence.

Table 2-1: Screen of click-compatible sugar analogs for incorporation into expanding Arabidopsis root epidermal cell walls

NATIVE MONOSACCHARIDE	CLICK COMPATIBLE SUGAR-ANALOG	FLUORESCENT PROBE	FLUORESCENCE PATTERN
Fucose	FucAl $(OAc)_4$	Alexa488-Azide	Bright, wall-associated, evenly labels all outer periclinal walls
Galactose	2dZGal	Alexa488-Alkyne	No incorporation
	6dZGal	Alexa488-Alkyne	No incorporation
	6dZGal $(OAc)_4$	Alexa488-Alkyne	No incorporation
Mannose	6dAM $(OAc)_4$	Alexa488-Azide	No incorporation
Rhamnose	6dAR $(OAc)_4$	Alexa488-Azide	Dim, not wall-associated
Glucose	2dZG $(OAc)_4$	Alexa488-Alkyne	No incorporation
	6dZG $(OAc)_4$	Alexa488-Alkyne	No incorporation
	6dAG	Alexa488-Azide	Dim, wall-associated, differentially labels root hair bulges
	6dAG $(OAc)_4$	Alexa488-Azide	Bright, wall-associated, differentially labels root hair bulges
	6dAS $(OAc)_7$	Alexa488-Azide	No incorporation
	6ES $(OAc)_8$	Alexa488-Azide	No incorporation
	6EG $(OAc)_5$	Alexa488-Azide	No incorporation

2.4.2 Synthesis and design of 6-deoxy-alkynyl glucose

Synthesis of 6dAG started with commercially available D-glucose (Figure 2-2). To differentiate the C6-OH group from the other hydroxy groups, the C6-OH group was first protected with a *tert*-butyldimethylsilyl (TBS) group following a procedure similar to that reported[21], giving intermediate (2). The remaining hydroxy groups were protected by

methoxymethyl (MOM) groups, which can be easily deprotected under mild acidic conditions and survive the Seyferth–Gilbert homologation required to form the alkyne. The TBS group was removed with tetra-*n*-butylammonium fluoride (TBAF), giving key intermediate (3) in high yield. To form an alkyne at the C6-OH group, this carbon was oxidized by Dess–Martin oxidation to an aldehyde, and then the aldehyde was converted into alkyne (4) by reacting with diethyl diazomethylphosphonate[22]. Global deprotection under acidic conditions gave (5) in an excellent yield. Acetylation by acetic anhydride gave the corresponding per-*O*-acetylated derivative. In analogy to fucose-alkyne[14] and because of the acetate's greater utility for biological experiments, the acetate rather than "(5)" is hereafter referred to as "6dAG" for "6-deoxy-alkynyl glucose".

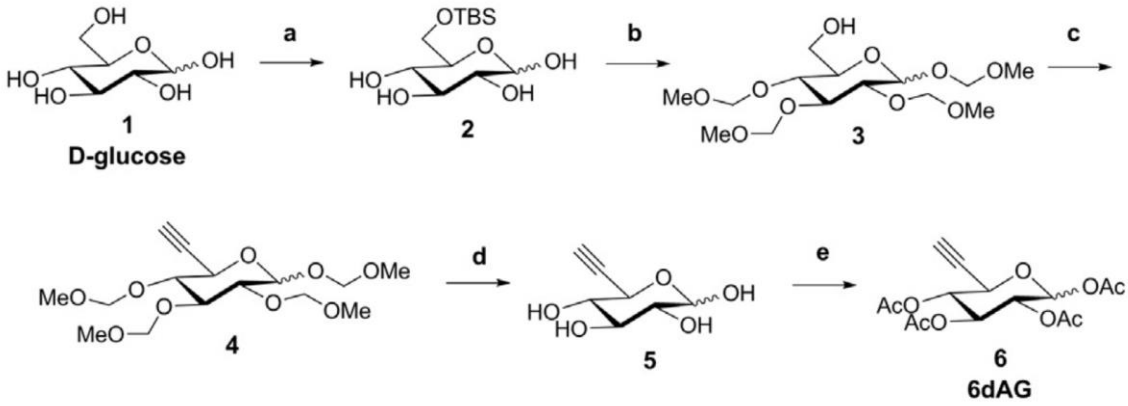

Figure 2-2: Synthesis scheme for 6-deoxy-alkynyl glucose. Reagents and conditions: (a) TBSCl, pyridine, overnight, 46%; (b) MOMCl, NaH, DMF, 2 h then TBAF, THF, 2 h, 82% over two steps; (c) DMP, DCM, 5 h then diethyl diazomethylphosphonate, NaH, THF, 0.5 h, 74% over two steps; (d) 0.1% H_2SO_4, 80 °C, overnight, 89%; (e) Ac_2O, pyridine, overnight, 88%.

2.4.3 Living Arabidopsis seedlings incorporate 6dAG into early differentiation zone epidermal cells

6dAG, was next tested as to whether it incorporated into Arabidopsis seedling roots, which have exposed cell walls and are specialized for nutrient absorption. Incorporated alkyne groups were labeled for detection with a click-reaction with azido-functionalized fluorophores. After incubating seedlings for 24 h in liquid media containing 10 μM 6dAG, followed by click-reacting with Alexa 594-azide, fluorescence was observed in the early differentiation zone of the root (Figure 2-3B). Of all the functional groups present in seedling tissue, only cell-incorporated alkyne groups should ligate to azido-functionalized fluorophores, since this reaction is highly selective[10]. Alexa 488-alkyne is structurally similar to Alexa 594-azide, but it lacks the azide group necessary for an orthogonal reaction with the alkyne group on 6dAG. After labeling seedlings incubated with 6dAG for 24 h with Alexa 488-alkyne, no significant fluorescence was observed (Figure 2-3A). To distinguish between two scenarios, one where active cellular metabolism is necessary for 6dAG incorporation, and another where 6dAG passively adsorbs onto external cell walls, whole seedlings were killed and fixed with 4% paraformaldehyde prior to incubation with 6dAG. When first incubated with 6dAG, then subjected to click-reaction, pre-fixed seedlings showed only faint autofluorescence at the root tip, indicating that they did not incorporate significant amounts of 6dAG (Figure 2-3E).

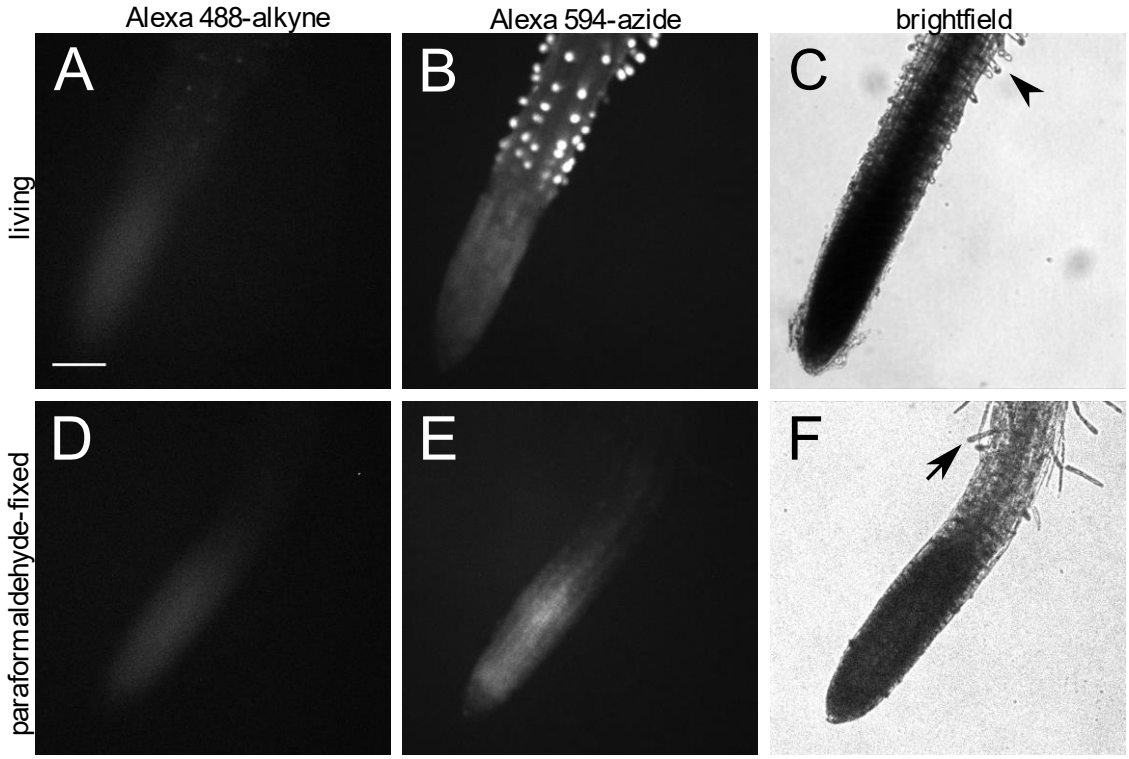

Figure 2-3: Arabidopsis seedlings metabolically incorporate exogenous 6-deoxy-alkynyl glucose. Representative maximum projections of z series of living (A–C) or paraformaldehyde-fixed (D–F) seedling root tips incubated with 10 µM 6dAG in liquid MS for 24 h, followed by click-reaction with Alexa 488-alkyne (A and D) and Alexa 594-azide (B and E). Brightness and contrast settings are identical for (A and D) and (B and E). Brightfield images of seedlings are shown in (C and F). Arrowhead and arrow indicate stunted and control root hairs, respectively. Scale bar = 100 µm. Images are representative fields of view from 3 independent experiments.

These data support the hypothesis that active metabolism is required for 6dAG incorporation into seedlings. Additionally, peracetylated 6dAG, which is more hydrophobic than its non-acetate counterpart, and should therefore be more membrane permeable, resulted in greater fluorescence after click-labeling compared to incubation with its non-acetylated counterpart (Figure 2-4), providing further evidence that the chemical reporter must be internalized prior to its incorporation. Likewise, when seedlings were incubated in liquid media lacking 6dAG prior to click-reaction, no Alexa 594-azide fluorescence was observed, indicating that exposure to fluorescent dyes alone does not result in dye binding. Only through the

combination of active metabolism, 6dAG exposure, and azido-functionalized fluorophore was bright fluorescence observed.

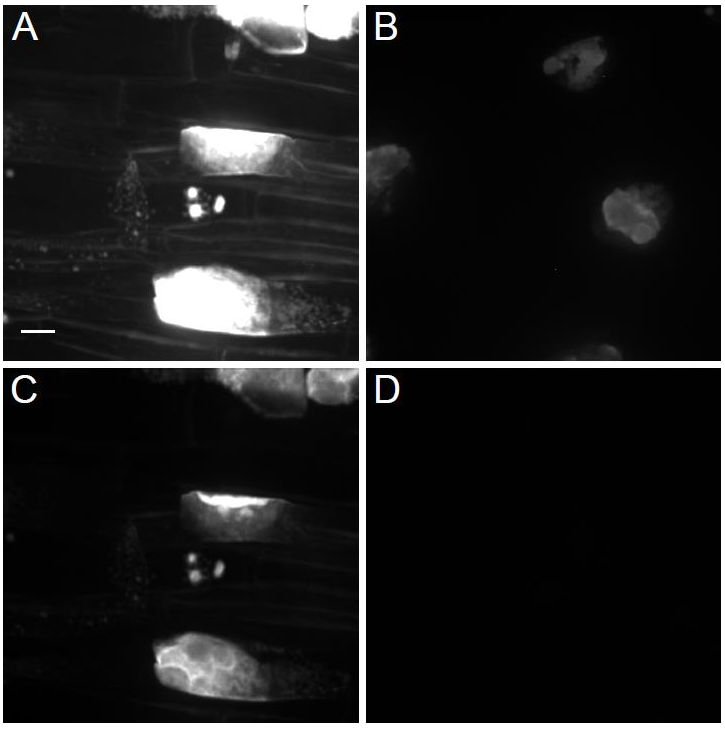

Figure 2-4: Acetylation enhances incorporation of 6dAG. Early differentiation zone root epidermal cells of: **(**A) Seedling treated with 10 μM 6dAG for 24 h, followed by click-reaction with Alexa 488-azide. (B) Seedling treated with 10 μM not-acetylated 6dAG for 24 h, followed by click-reaction with Alexa488-azide. (C) Same seedling as (A), but imaged with 100-fold less detector gain to achieve a properly exposed image. (D) Seedling treated with DMSO for 24 h, followed by click-reaction with Alexa 488-azide. Exposure settings, and brightness and contrast adjustments are identical for images A, B, and D. Scale bar = 10 μm.

.

Whether 6dAG is incorporated into cell walls or other cellular compartments was next examined. Click reaction conditions (1 h exposure to Cu(I)) result in cell membrane lysis in elongation zone cells in Arabidopsis seedling roots[14], probably due to Fenton reaction production of hydroxyl radicals, which damage membrane lipids[23]. After subjecting seedlings to click-reaction, it was found that the resulting fluorescence appeared at external cell borders and tips, and that brightfield-visible intracellular bodies exhibited Brownian motion. Without intact

membranes, this leaves the cell wall as the most likely compartment that could contain the labeled alkyne groups.

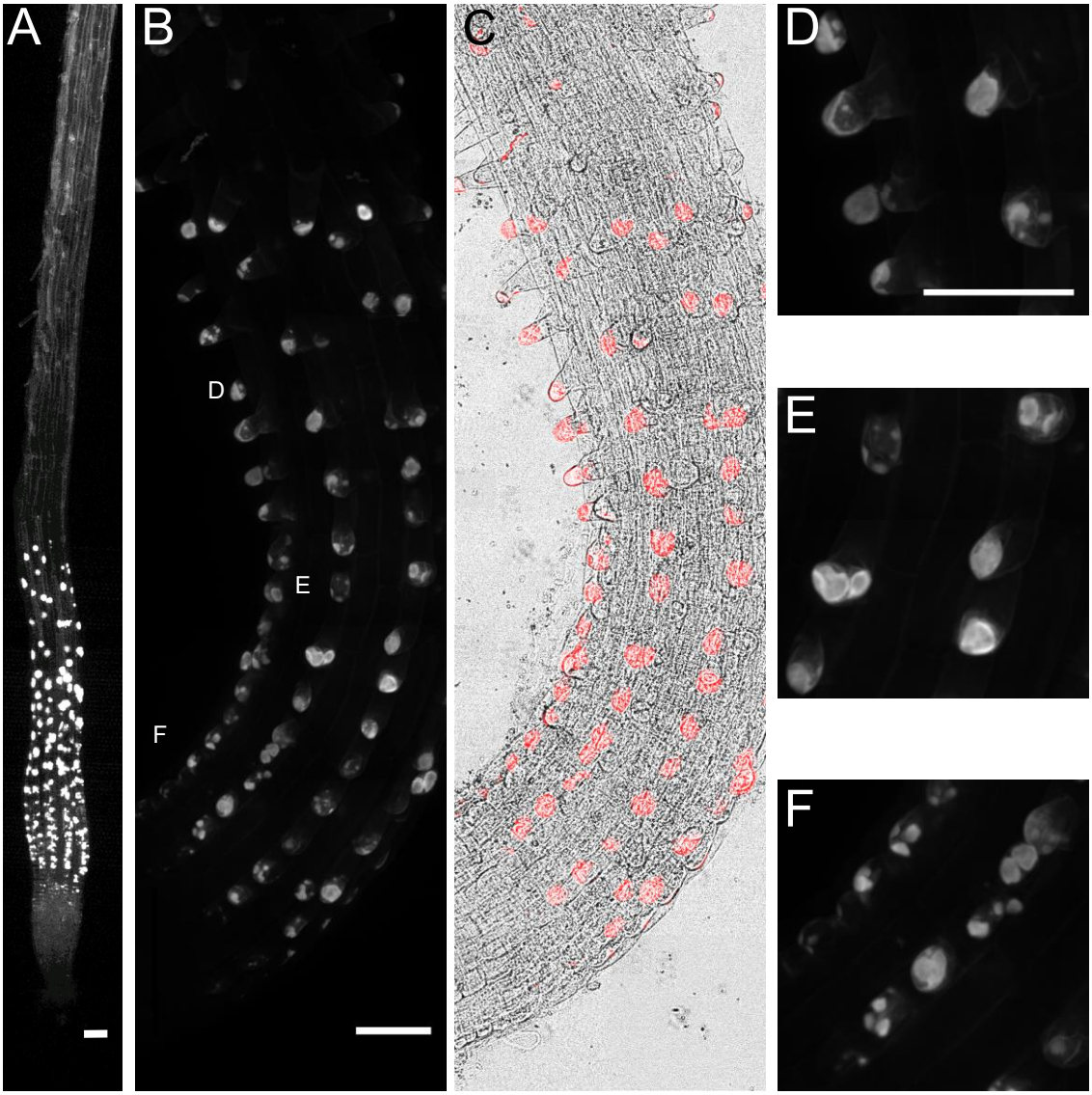

Figure 2-5: Arabidopsis seedlings incorporate 6-deoxy-alkynyl glucose into developing root hair bulges and tips in the early differentiation zone. (A) Low-magnification mosaic maximum projection of root tip of an Arabidopsis seedling incubated with 10 µM 6dAG in liquid MS for 24 h, followed by click-reaction with Alexa 594-azide. (B) Mosaic maximum projection of the early differentiation zone of an Arabidopsis root incubated with 10 µM 6dAG in liquid MS for 24 h, followed by click-reaction with Alexa 594-azide. Root tip is oriented to the lower left. (C) Overlay of Alexa 594-azide fluorescence (red) and brightfield. (D–F) Detail of older (D and E) and newly forming (F) root hair bulges labeled with Alexa 594-azide. Scale bars = 50 µm.

2.4.4 Seedlings incorporate 6dAG at the tips of growth-arrested root hairs

After establishing that Arabidopsis seedling roots incorporate 6dAG, the specific distribution of this chemical reporter along the developmental gradient embodied in these roots was next examined (Figure 2-5). Seedlings incorporate 6dAG at a specific developmental zone, namely, the early differentiation zone where root hair growth initiates (Figure 2-5A). 6dAG did not accumulate, however, in the more-rootward elongation and division zones (Figure 2-5A), nor did it accumulate in tissues with fully developed root hairs. Furthermore, 6dAG preferentially labeled trichoblasts over atrichoblasts within this zone, localizing to root hair bulges and emergent root hair tips (Figure 2-6). 6dAG patterning varied across this zone, clustering into distinct globules in some root hair bulges (Figure 2-5E) and appearing more uniform across the dome of other bulges (Figure 2-5C and D). This labeling pattern was accompanied by a reduction in root hair length (Figure 2-4C and 2-4F; arrows) that was dose-dependent (Figure 2-7A and 2-7B). It was also observed that continuous growth on 6dAG is toxic to Arabidopsis seedlings, as measured by a root elongation assay (Figure 2-7C and 2-7D). In both cases, addition of excess glucose did not ameliorate the toxic effect, though at intermediate concentrations of 6dAG (5 μM, 10 μM) excess glucose partially attenuated the effect on root elongation. Excess glucose resulted in longer roots in most treatments, but at these 6dAG concentrations the relative root length elongation due to excess glucose was more dramatic (Figure 2-7E).

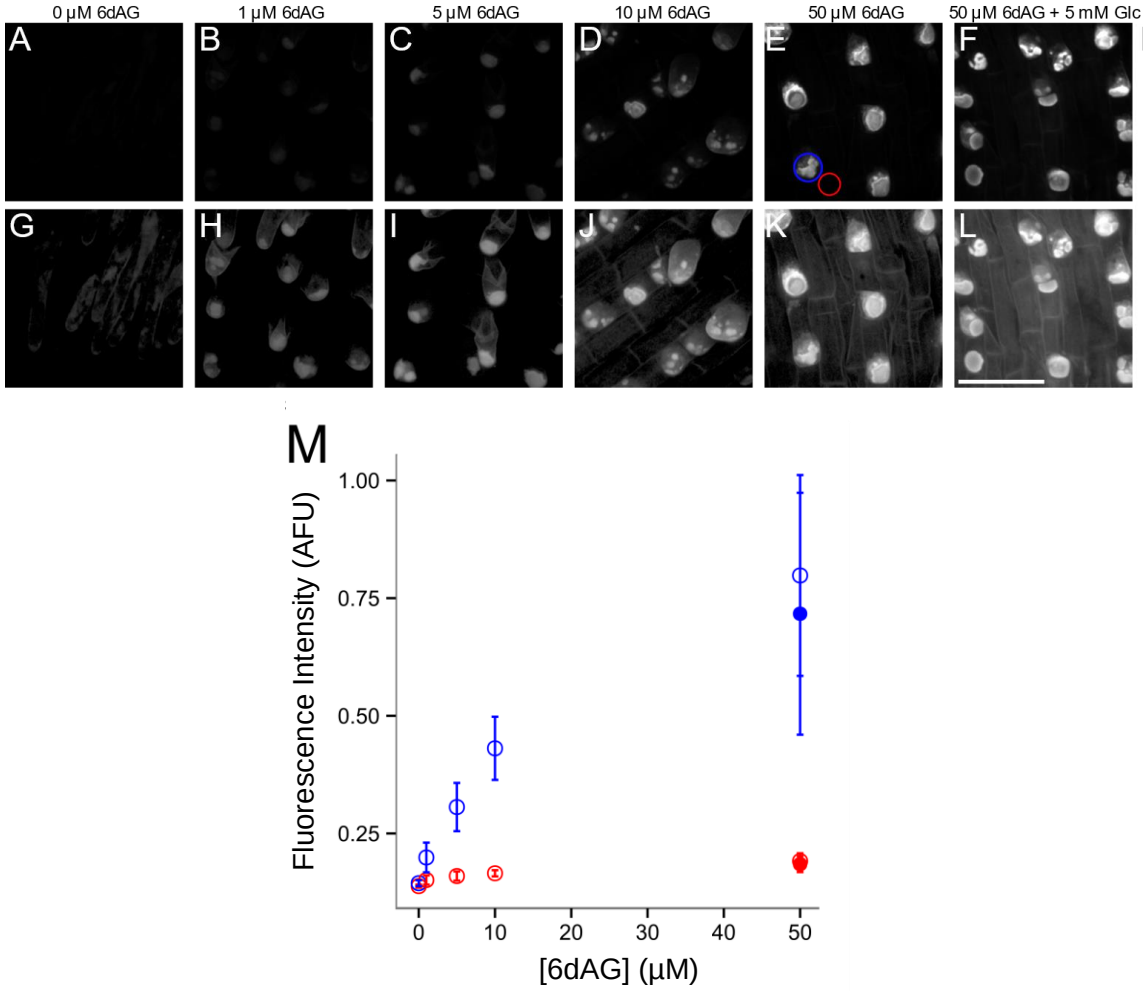

Figure 2-6: Fluorescence associated with 6-deoxy-alkynyl glucose incorporation is concentration-dependent. (A–F) Elongation-zone root epidermal cells after 24 h incubation with increasing concentrations (A = 0 µM; B = 1 µM; C = 5 µM; D = 10 µM; E = 50 µM) of 6dAG, followed by click-reaction with Alexa 488-azide. (F) Fluorescence after coincubation with 50 µM 6dAG and 5 mM glucose. Root tip is oriented to the lower left. Pixel intensities are depicted with equivalent brightness and contrast settings between images. (G–L) A–F with pixel intensities transformed with a gamma correction function ($\Gamma = 0.4$) to show greater detail in darker regions. Note extended root hairs in (G–I) and lack of root hair growth in (J–L). (M) Mean seedling fluorescence intensity for regions of interest at the rootward end of cells in trichoblast cell files (blue) and atrichoblast cell files (red). Open symbols denote incubation with 6dAG; filled symbols denote coincubation with 6dAG and 5 mM glucose. See (E) for example regions of interest. Error bars are ±95% CI, n = 15–17 seedlings per treatment. Scale bar = 50 µm.

2.4.5 6dAG incorporation is dose- and time-dependent

Next, the range of concentrations and exposure times that result in detectable incorporation of 6dAG was examined. In a 24 h endpoint titration experiment, incubation with concentrations of 6dAG as low as 1 µM resulted in detectable fluorescence, with increasing 6dAG concentration resulting in greater fluorescence until saturation near 50 µM (Figure 2-6). Fluorescence was also observed in atrichoblasts, although this fluorescence was saturated after exposure to greater than 5 µM 6dAG, and was much dimmer than trichoblast fluorescence (Figure 2-6M). Additionally, the time dependence of 6dAG incorporation was tested by exposing seedlings to 10 µM 6dAG for 2, 4, 6, 12, 18, and 24 h. If passive adsorption is the mechanism by which 6dAG was incorporated into seedlings, this would be expected to occur relatively quickly; however, seedlings required at least 6 h of exposure to 10 µM 6dAG before this reporter could be detected after click labeling, and 12 h before fluorescence was significantly higher than background fluorescence (Figure 2-7). These data further support the idea that metabolic activity is required for incorporation of 6dAG into seedlings. Long liquid-incubation time was not the cause of the fluorescence: seedlings exposed to DMSO for 24 h did not exhibit appreciable fluorescence, whereas seedlings exposed to 10 µM 6dAG for 24 h exhibited bright fluorescence in root hair tips (Figure 2-8D and E). These data indicate that 6dAG is incorporated into Arabidopsis roots in a concentration and time-dependent manner, with selective accumulation occurring in root hair tips.

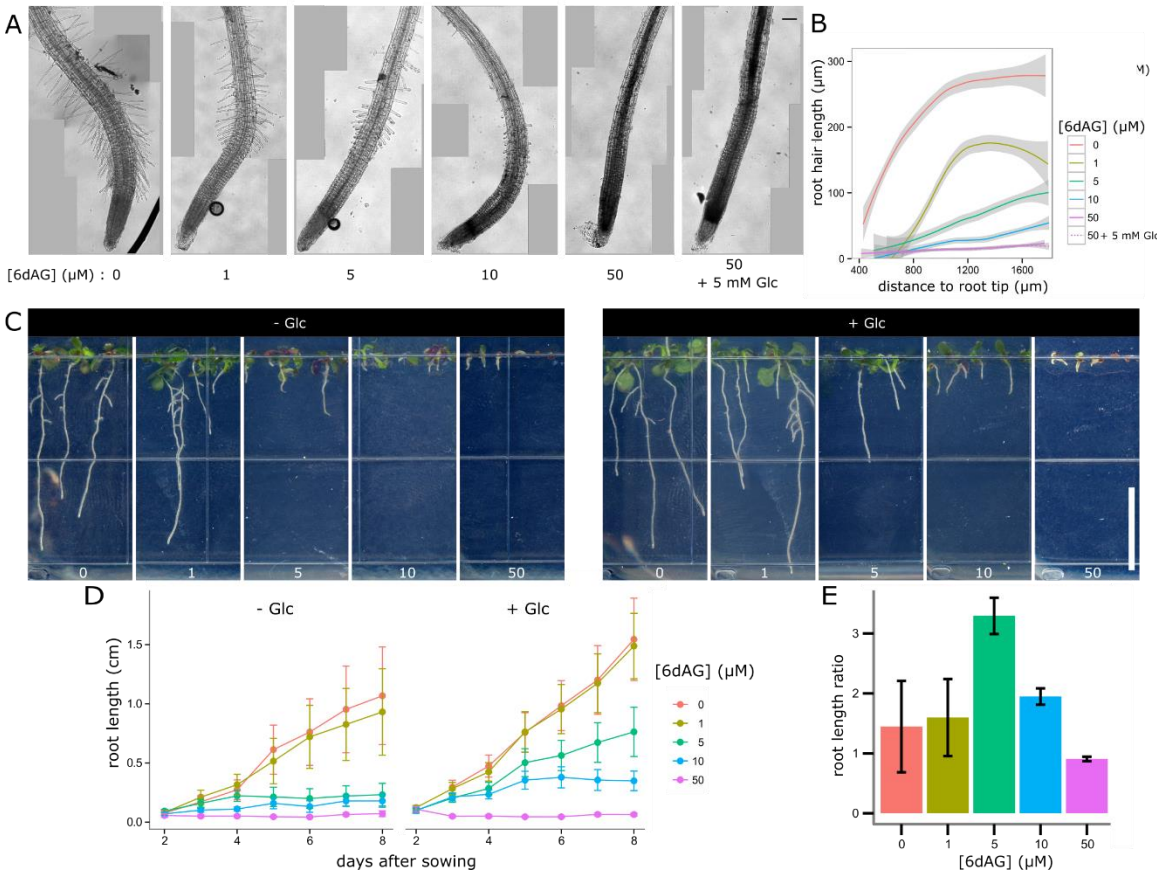

Figure 2-7: 6-deoxy-alkynyl glucose inhibits root and root hair elongation, regardless of the presence of excess glucose. (A) Representative brightfield mosaic images of primary roots from seedlings incubated in liquid MS containing varying [6dAG] and [glucose]. Scale bar = 100 μm. (B) Root hair lengths, plotted along their developmental gradient. Distances were measured from the root hair bases' nearest point on the root axis to the root tip, along the root axis. 16–73 root hair length measurements from each of 6–8 seedlings per [6dAG] exposure level were pooled by treatment, then fit with a Loess best-fit curve. Error shading = ± 95% CI. (C) Representative images of seedlings grown vertically for 8 d on agar containing varying [6dAG], with and without excess glucose (1 mM). Scale bar = 1 cm. (D) Primary root growth curves for vertically-grown seedlings on agar plates doped with 6dAG and/or excess glucose. One representative replicate of three experiments is shown. Error bars are ±95% CI; n = 20–36 seedlings per treatment. (E) Glucose enhancement of root elongation, reported as a ratio between lengths of primary roots grown with and without excess glucose. Error bars are ±95% CI.

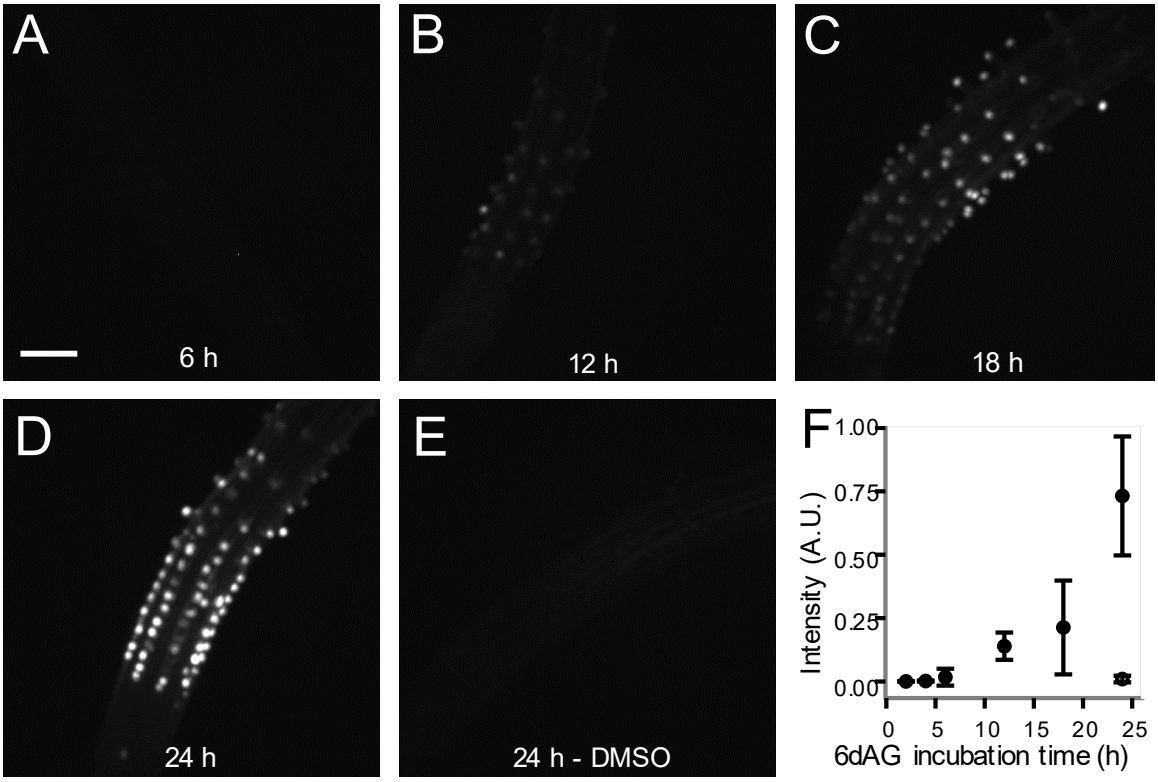

Figure 2-8: 6-Deoxy-alkynyl glucose incorporation is time-dependent. (A–D) Elongation-zone root epidermal cells exposed to 10 µM 6dAG for varying incubation time, followed by click-reaction with Alexa 594-azide. (E) Control seedling exposed to DMSO (6dAG solvent) for 24 h. Pixel intensities are depicted with equivalent brightness and contrast settings between images. (F) Summed fluorescence intensity for pixels above a thresholded value for images of seedlings with increasing 6dAG incubation time (filled symbols) or an equivalent volume of DMSO (open symbol). Note that for 2 h and 4 h incubations, fluorescence images are not shown. Error bars are ±95% CI, n = 9 seedlings per treatment. Scale bar = 100 µm.

2.4.6 6dAG incorporation sites colocalize with Sirofluor-stained β-1,3 glucans

6dAG-dependent fluorescence is associated specifically with the tips of growing root hairs, where cell walls are rapidly synthesized. This suggests that 6dAG might be incorporated into the cell wall at the tips of growing root hairs, and the fact that 6dAG exposure appears to inhibit root hair elongation implies that it might be incorporated into a polymer that inhibits root hair wall expansion. To begin to address these possibilities, 6dAG-treated, click-labeled seedlings

were stained with Sirofluor, the purified fluorophore from the dye mixture, Aniline Blue, which fluoresces specifically upon binding β-1,3 glucans[24] (Figure 2-9). 6dAG-exposed seedlings show distinct patches of Sirofluor staining in the same subcellular regions that are click-labeled with 6dAG (Figure 2-9A–C). Seedlings with no exposure to 6dAG, but otherwise liquid-incubated, click-reacted, and Sirofluor-stained, showed neither Sirofluor nor 6dAG-labeled fluorescence at analogous sites (Figure 2-9D–F). This suggests that 6dAG both co-localizes with and induces β-1,3 glucan formation at incipient root hair bulges. Sirofluor also stained cells in the division zone of the root tip (Figure 2-9A).

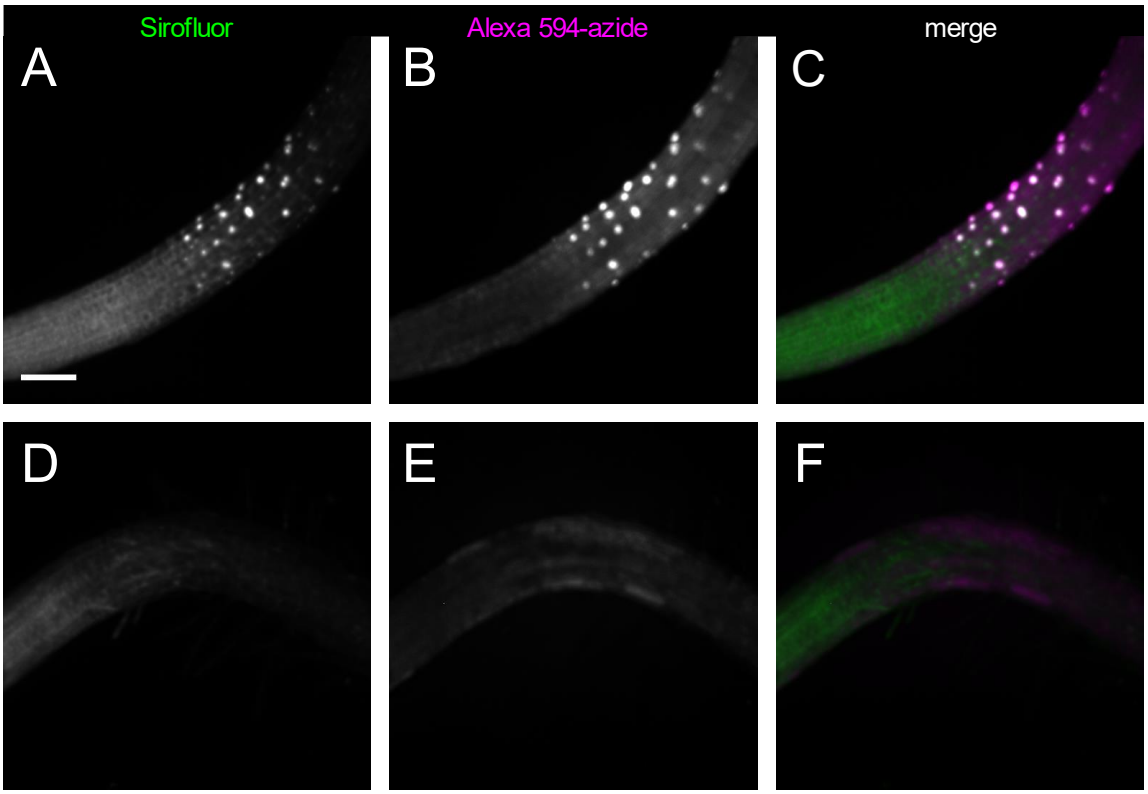

Figure 2-9: 6-deoxy-alkynyl glucose colocalizes with and induces β-1,3-glucan staining at root hair bulges. (A–C) Representative seedling treated with 10 µM 6dAG for 12 h, followed by click-reaction with Alexa 594-azide, then Sirofluor staining. (D–F) Seedling treated with DMSO for 12 h followed by click-reaction with Alexa 594-azide, Sirofluor staining. Alexa 594-azide (A and D) is magenta in (C and F); Sirofluor (B and E) is green in (C and F). Identical brightness and contrast adjustments between treatments were made for each channel. Scale bar = 100 µm**.**

2.4.7 Potential metabolic fates of 6dAG

6dAG was synthesized as a part of a suite of click-compatible chemical reporters for biological polysaccharides. Ideally, a monosaccharide-mimicking chemical reporter should be accepted by sugar "salvage pathways", which are enzymatic steps leading from monosaccharides to NDP-monosaccharides, the activated substrates for glycosyltransferases [25, 26]. In this case, 6dAG is a molecule that is in theory incompatible with the canonical glucose salvage pathway, in that its modification at the C6 position should block phosphorylation by hexokinase, which is the first step in activating salvaged glucose[25]. While other organisms can activate glucose with glucose-1-phosphate phosphodismutase activity[27], no such activity has been found in plants. A search of the MetaCyc database[28] did not reveal any other characterized metabolic steps between glucose and glucose-1-phosphate. However, given the reaction mechanism of phosphoglucomutase, which can transfer an enzyme-linked phosphate group to the C1 position and abstract a C6 phosphate[29], it is possible that 6dAG could act as an alternative substrate for this enzyme, which would then be converted to its respective phosphate, then UDP-esters. Alternatively, the alkynyl group on 6dAG could mimic a relatively hydrophobic aglycone of a small C-glycosyl compound. In this scenario, incorporation could proceed through the action of an enzyme acting on such a compound and transferring the sugar moiety to a polysaccharide acceptor. Despite not having a clear metabolic route to polysaccharide incorporation, 6dAG could be incorporated into a variety of cell wall polymer destinations if it does, in fact, behave as a glucose analog. Callose, a β-1,3 glucan, is a possible molecule into which 6dAG could incorporate. Xyloglucan and cellulose both have β-1,4 linked glucose backbones, but most xyloglucan glucose residues are decorated at C6 with xylose or a xylose-containing oligomer. This position is unavailable for xylose linkages in 6dAG. Cellulose is unlikely to accommodate 6dAG, since the orientation at C6 determines its crystal structure and replacement at this position

of an alkynyl group would have drastic consequences for crystallization[30]. It is also possible that 6dAG is polymerized into a novel glucan analog. Cell wall matrix polysaccharides in eudicots, with the exception of callose[31], are synthesized by glycosyltransferases in the Golgi. Specific glycosyltransferases are uniquely required for tip-growth in plant cells, e.g. *CELLULOSE SYNTHASE-LIKE D* (*CSLD*) family genes show highly-upregulated expression in pollen tubes and root hair tips[32], and *CSLD3* is required both for the normal organization and possibly biosynthesis of a cellulose-like β-1,4 glucan in root hair cell walls[33, 34] and for the initiation of root hair growth[35]. Biochemical activities unique to the emergent root hair tip may predispose this region to incorporate 6dAG here and not in other plant cell walls. Alternatively, a glycosylhydrolase in the apoplast might be able to act in reverse to add 6dAG to existing wall polymers. However, the finding that peracetylated 6dAG is more efficiently incorporated into plant tissues than its non-acetylated precursor (Figure 2-4) does not support this hypothesis, since these data suggest that the entry of 6dAG into the cell is important for its incorporation.

Callose is a known component of nascent cell walls; its deposition timing is essential for cytokinesis and pathogen/wounding responses[36]. Callose is deposited during normal tip growth in pollen tubes[37], and as an abiotic and biotic stress response in root hair tips[33, 38]. 6dAG colocalizes with callose (Figure 2-9), and it may induce callose formation by eliciting callose synthesis as a wounding response due to 6dAG toxicity. In addition, 6dAG could incorporate into the toxin-induced callose in root hairs. If 6dAG is behaving as a glucose analog, it might be incorporated into either the poorly-understood β-1,4 glucan deposited by CSLD3 at root hair tips, or into toxicity-induced callose. Further analysis of 6dAG-labeled seedlings, including cell wall fractionation and enzymatic digestion, will be required to pinpoint the identity of the polymer into which 6dAG is incorporated.

2.4.8 6dAG incorporation differs markedly from FucAl incorporation

The two other click-compatible sugar analogs that have been reported to incorporate into plant cell walls thus far are fucose-alkyne, which is thought to label a pectic polysaccharide[14], and KDO-azide, which incorporates into rhamnogalacturonan-II[17]. 6dAG behaves very differently from fucose-alkyne and KDO-azide: Arabidopsis root epidermal cells incorporate these reporters in as little as 30 min, whereas appreciable 6dAG incorporation occurs only after several hours (Figure 2-8). Whereas the substitution of an alkyne group for the C6 methyl group of fucose is apparently tolerated by fucose salvage pathway enzymes, the more drastic substitution of an alkyne group for a hydroxy group in the case of 6dAG eliminates most of the potential salvage and activation metabolic routes for this compound. Fucose-alkyne is not uniformly distributed after short incorporation periods, but it does eventually become incorporated throughout the cell wall[14], as does KDO-azide[17], whereas 6dAG is preferentially localized to root hair primordia, a specific sub-region of the wall, where it accumulates. These data suggest that pectin is delivered evenly across the growing cell wall, whereas the polymer into which 6dAG is incorporated is apparently targeted specifically to root hair tips (where growth is then arrested).This could be accomplished by a polarized vesicle trafficking pathway or perhaps a root hair-specific glycosyltransferase[34]. The identity of the labeled polymer could be diagnosed in future experiments via exogenous application of glycan hydrolyzing enzymes, such as (1,3)-beta-glucanase.

2.5 Conclusion

6dAG has the potential to probe glycan metabolism in many different biological systems, including plants. Click-chemistry is one of few methods compatible with in vivo imaging of

polysaccharides, compounds that are otherwise difficult to label[39]. The toolbox of click-compatible sugar analogs relevant to plant cell wall chemistry is currently restricted to fucose-alkyne and KDO-azide. Synthesis of 6dAG and the finding that it incorporates into Arabidopsis seedlings in a specific manner add this compound to a short but growing list of chemical reporters available for click-powered glycobiology in plants. Future studies will investigate whether these probes are suitable for probing cell wall dynamics in a wide variety of plant tissues and species.

2.6 Methods

2.6.1. Seedling culture

All click labeled specimens were 4 d-old A. thaliana Col-0 seedlings. 30% (v/v) NaOCl surface-sterilized seeds were imbibed for at least 3 days, then grown vertically for 4 d on MS plates (0.8% agar-agar, MS salts and vitamins used at half the strength as in (Murashige and Skoog, 1962)) at constant light, 22 °C. 6dAG root elongation assays were performed on vertical MS plates to which filter-sterilized 6dAG in DMSO and/or filter-sterilized glucose in H_2O was added during agar cooling.

2.6.2. 6-deoxy-alkynyl glucose click-labeling

Seedlings were click-labeled in a two-step process: (1) incubation with 6dAG, (2) click-reaction with a click-compatible fluorophore. Seedlings were transferred from plates, washed with liquid MS (growth media lacking agar-agar), then incubated in liquid MS (1.8 mL) containing 10 µM 6dAG for 24 h. 6dAG was supplied from a 10 mM stock solution in DMSO. After 24 h incubation at 22 °C, seedlings were washed four times with liquid MS, then transferred

to a click-reaction solution, containing 1 mM $CuSO_4$, 1 mM ascorbic acid, and 1 μM azido-functionalized Alexa fluorophore (Alexa594-azide for most experiments, Alexa488-azide for titration experiment). Ascorbic acid and $CuSO_4$ were introduced from 100 mM stock solutions in H_2O; ascorbic acid stock solutions were made less than 30 min before use. The labeling reaction proceeded in the dark for 1 h at 25 °C, and was quenched by washing four times with liquid MS. Labeled seedlings were stored at 4 °C for less than 48 h before imaging. Seedlings counterstained with Sirofluor were stained for 30 min with 0.01% (w/v) dye solution in H_2O, then washed with H_2O.

2.6.3. Microscopy and image analysis

Root tips of seedlings were imaged with a Zeiss Cell Observer SD spinning disk confocal microscope (488 nm laser excitation, 525/50 emission filter; 561 nm laser excitation, 617/73 emission filter) using either a 63X 1.40 NA oil immersion objective or a 10X 0.3 NA air objective. Z-stacks through the proximal layer of epidermal cells (63X) or half the diameter of the entire root (10X) were collected. Cell wall-associated fluorescence intensity in maximum projections for 63X images was measured using ImageJ, by drawing circular regions of interest at the rootward ends of epidermal cells. Fluorescence intensity for 10X images was calculated by thresholding every maximum projection image above a constant pixel intensity threshold, and then calculating the raw integrated pixel intensity of the remaining image. The threshold was chosen to exclude background, but include globular fluorescent regions at the rootward end of trichoblasts. Root and root hair lengths were measured from images with the aid of ImageJ software. Images of seedlings growing on agar plates were recorded on successive days with a flatbed scanner, from which root lengths were traced and measured. 10X micrographs of root hairs were stitched together with the MosaicJ plugin for ImageJ[40]. Root hair lengths were

measured by tracing hairs; root hair distance along the root axis was measured by finding the point on a traced root axis that was closest to the root hair base, and measuring the distance along the axis from the root tip to that point.

2.6.4. Synthesis of 6-deoxy-alkynyl glucose

2.6.4.1 Synthesis of 6-TBDMS-D-glucose (2)

To an ice-water cooled solution of D-glucose (5.4 g, 30 mmol, 1 equiv) in dry pyridine (50 mL) was added *tert*-butyldimethylsilyl chloride (5.4 g, 36 mmol, 1.2 equiv) portionwise. The ice-water bath was removed after addition, and the reaction mixture was stirred at room temperature overnight. The solution was diluted with EtOAc (250 mL) and washed with diluted HCl and brine. The residue after concentration of the organic layer was purified on flash silica gel chromatography using CH_2Cl_2:MeOH (15:1), giving 6-TBDMS-D-glucose (2) (4.1 g) as a white foam in a yield of 46%. Compound 2 was a mixture of α- and β-anomers, which were inseparable. ^{1}H NMR (MeOH-d4, 360 MHz, ppm): δ 0.08 (s, 6H), 0.91 (s, 9H), 3.09–3.11 (m, 0.45 H), 3.31–3.37 (m, 4H, solvent residue peak included), 3.64–3.69 (t, *J* = 9.0, 9.4 Hz, 0.57 H), 3.74–3.85 (m, 2H), 3.93–3.97 (d, J = 11.1 Hz, 0.50 H), 4.43–4.45 (d, *J* = 7.6 Hz, 0.46 H), 5.08–5.09 (d, *J* = 3.2 Hz, 0.49 H); ^{13}C NMR (MeOH-d_4, 90 MHz, ppm) δ -5.14, -5.02, 19.34, 26.45, 64.13, 64.30, 71.50, 71.56, 73.20, 73.84, 74.91, 76.23, 78.23, 93.92, 98.12, 101.37; HRMS: calculated for $C_{12}H_{26}NaO_6Si^+$ [M+Na^+]: 317.1391; found: 317.1392.

2.6.4.2 Synthesis of 1,2,3,4-tetra-O-methoxymethyl-D-glucose (3)

To an ice-water cooled solution of 6-TBDMS-D-glucose (2) (4.0 g, 13.6 mmol, 1 equiv) in dry DMF (50 mL) was carefully added NaH (3.3 g, 81.5 mmol, 6 equiv, 60% suspended in mineral oil). After 15 min, methoxymethyl chloride (5.2 mL, 68.0 mmol, 5 equiv) in DMF (10 mL) was added dropwise to the solution. The ice-water bath was removed after addition, and the reaction mixture was stirred at room temperature for 2 h. H_2O (100 mL) was slowly added to the reaction mixture to quench the reaction. The resulting clear solution was extracted with EtOAc (50 mL) three times. The combined organic layers were washed thoroughly with water and brine, and dried (anhydr. Na_2SO_4). The residue after concentration was used for the next step without further purification. To a solution of the residue in tetrahydrofuran (50 mL) was added tetra-*n*-butylammonium fluoride (5.3 g, 20.4 mmol, 1.5 equiv). The reaction mixture was stirred at room temperature for 2 h. After completion, the reaction was diluted with EtOAc (200 mL) and washed thoroughly with H_2O and brine. The residue after concentration of the organic layer was purified on flash silica gel chromatography using hexanes:EtOAc (3:1), giving 1,2,3,4-tetra-*O*-methoxymethyl-D-glucose (3) (4.0 g) as a white foam in a yield of 82% over two steps. Compound 3 was a mixture of α- and β-anomer, which were inseparable. ^{1}H NMR ($CDCl_3$, 360 MHz, ppm): δ 2.72–2.76 (m, 1 H), 3.27–3.38 (m, 13 H), 3.52– 3.63 (m, 2 H), 3.76–3.78 (m, 1.8 H), 4.52–4.56 (m, 1.6 H), 4.65– 4.77 (m, 3.2 H), 4.83–4.87 (m, 2.8 H), 4.93–4.95 (m, 1 H); ^{13}C NMR ($CDCl_3$, 90 MHz, ppm) δ 55.66, 56.11, 56.18, 56.30, 56.38, 56.46, 61.59, 71.34, 75.17, 76.36, 76.57, 76.80, 77.16, 77.36, 77.51, 77.61, 77.94, 78.24, 80.91, 93.60, 94.83, 97.10, 97.42, 98.22, 98.41, 98.93; HRMS: calculated for $C_{14}H_{28}NaO_{10}$ + [M+Na^+]: 379.1575; found: 379.1581.

2.6.4.3 Synthesis of 1,2,3,4-tetra-O-methoxymethyl-D-glucose-6-alkyne (4)

To an ice-water cooled solution of compound 3 (4.0 g, 11.2 mmol, 1 equiv) in CH_2Cl_2 (100 mL) was added Dess–Martin periodinane (7.1 g, 16.8 mmol, 1.5 equiv). The reaction mixture was stirred at room temperature for 5 h. After completion, the milky solution was washed thoroughly with saturated $Na_2S_2O_3$ solution and brine. The organic layer was dried (anhydr. Na_2SO_4) and concentrated. The residue was used for the next step without further purification. A solution of diethyl diazomethylphosphonate (2.0 g, 11.2 mmol, 1 equiv) and the residue obtained above in tetrahydrofuran (50 mL) was cooled in an ice-water bath. NaH (1.1 g, 28 mmol, 2.5 equiv, 60% suspended in mineral oil) was added portionwise in an Ar counterflow. The cooling bath was removed after addition. The reaction mixture was stirred for 30 min, and subsequently quenched by careful addition of H_2O (100 mL). The obtained mixture was extracted with EtOAc (50 mL) twice. Combined organic layers were dried (anhydr. Na_2SO_4) and concentrated in vacuo. Purification of the residue by flash silica gel chromatography using hexanes:EtOAc (3:1) 1,2,3,4-tetra-*O*-methoxymethyl-D-glucose-6-alkyne (4) (2.9 g) as a yellow syrup in a yield of 74% over two steps. Compound 4 was a mixture of α- and β-anomers, which were inseparable. ^{1}H NMR ($CDCl_3$, 360 MHz, ppm): δ 2.46–2.49 (m, 1.5 H), 3.35–3.67 (m, 23.5 H), 3.85–3.90 (m, 0.5 H), 4.02–4.06 (m, 1H), 4.38–4.41 (m, 0.5 H), 4.56–5.13 (m, 15 H); ^{13}C NMR ($CDCl_3$, 90 MHz, ppm) δ 55.79, 56.27, 56.37, 56.44, 56.49, 56.57, 56.81, 56.85, 62.34, 66.10, 74.15, 74.58, 78.40, 78.71, 79.69, 80.09, 80.82, 93.61, 93.97, 94.89, 97.31, 97.51, 97.84, 98.39, 98.45; HRMS: calculated for $C_{15}H_{26}NaO_9^+$ [M+Na^+]: 373.1469; found: 374.1467.

2.6.4.4 Synthesis of glucose-6-alkyne (5)

Compound 4 (2.5 g, 7.1 mmol, 1 equiv) was suspended in 0.1% H_2SO_4 (50 mL). The resulting solution was heated at 80 °C overnight. Following neutralization with 1 M $NaHCO_3$, the solution was concentrated to dryness. Purification of the residue by flash silica gel chromatography using CH_3Cl:MeOH (10:1) gave 1.1 g of glucose-6-alkyne (5) (1.1 g) as a white solid in a yield of 89%. Glucose-6-alkyne (5) was an inseparable mixture of α- and β-anomers, with a ratio of 1:0.7 determined by proton NMR. ^{1}H NMR (MeOH d4, 400 MHz, ppm): δ 2.74–2.75 (d, *J* = 1.8 Hz, 1H), 2.82–2.83 (d, *J* = 1.8 Hz, 0.62 H), 3.08–3.12 (t, *J* = 8.4, 8.4 Hz, 0.7 H), 3.23–3.34 (m, 8H), 3.54–3.58 (t, *J* = 9.2, 9.2 Hz, 1H), 3.92–3.94 (d, *J* = 7.6 Hz, 0.7 H), 4.39–4.43 (m, 1.7 H), 5.02–5.03 (d, *J* = 3.6 Hz, 1H); ^{13}C NMR (MeOH-d4, 100 MHz, ppm) δ 62.41, 67.01, 72.14, 72.87, 73.09, 73.76, 73.94, 74.26, 74.52, 75.89, 80.02, 81.06, 92.71, 96.83; HRMS: calculated for $C_7H_9O_5$ [M-H$^+$]: 173.0455; found: 173.0464.

2.6.4.5 Synthesis of glucose-6-alkyne tetraacetate (6) (‘‘6dAG”)

To an ice-water cooled solution of glucose-6-alkyne (5) (174 mg, 1 mmol, 1 equiv) in pyridine (5 mL) was added Ac_2O (942 µL, 10 mmol, 10 equiv), and the reaction was stirred at room temperature overnight. MeOH (1 mL) was added to quench the reaction. The solution was concentrated in vacuo, and the residue was purified by flash silica gel chromatography using hexanes: EtOAc (2:1), giving glucose-6-alkyne tetraacetate (6) (300 mg) as a white solid in a yield of 88%. Glucose-6-alkyne tetraacetate (6) was an inseparable mixture of α- and β-anomers, with a ratio of 1:0.5 determined by proton NMR. ^{1}H NMR ($CDCl_3$, 360 MHz, ppm): δ 2.03–2.20 (m, 19 H), 2.51–2.55 (m, 1.3 H), 4.38–4.40 (m, 0.5 H), 4.65–4.68 (m, 1H), 5.10–5.25 (m, 3.4 H), 5.40–5.46 (m, 1H), 5.72–5.75 (d, *J* = 7.9 Hz, 0.5 H), 6.35–6.36 (d, *J* = 3.6 Hz, 1H); ^{13}C NMR

($CDCl_3$, 90 MHz, ppm) δ 20.52, 20.67, 20.75, 20.85, 20.93, 62.80, 65.42, 69.07, 69.26, 70.09, 70.91, 72.05, 75.63, 75.99, 88.75, 91.41, 168.61, 168.92, 169.29, 169.65, 170.08, 170.19; HRMS: calculated for $C_{15}H_{18}NaO_9$ [M-H^+]: 365.0843; found: 365.0840.

2.7 Acknowledgements

This work was supported as part of The Center for Lignocellulose Structure and Formation, an Energy Frontier Research Center funded by the U.S. Department of Energy, Office of Science, Basic Energy Sciences under Award # DE-SC0001090.

We thank the Office of Collaborative Science (OCS), Microscopy Core, NYU Langone Medical Center for sharing an ImageJ macro that facilitated repeated root hair measurements.

2.8 References

1. Cosgrove, D.J., *Growth of the plant cell wall.* Nat Rev Mol Cell Biol, 2005. **6**(11): p. 850-61.
2. Anderson, C.T., et al., *Real-Time Imaging of Cellulose Reorientation during Cell Wall Expansion in Arabidopsis Roots.* Plant Physiology, 2010. **152**(2): p. 787-796.
3. Fry, S.C., *Primary cell wall metabolism: tracking the careers of wall polymers in living plant cells.* New Phytologist, 2004. **161**(3): p. 641-675.
4. Somerville, C., et al., *Toward a systems approach to understanding plant-cell walls.* Science, 2004. **306**(5705): p. 2206-2211.
5. Chanliaud, E., et al., *Mechanical properties of primary plant cell wall analogues.* Planta, 2002. **215**(6): p. 989-996.
6. Chen, X.Y. and J.Y. Kim, *Callose synthesis in higher plants.* Plant Signal Behav, 2009. **4**(6): p. 489-92.
7. Currier, H.B., *Callose Substance in Plant Cells.* American Journal of Botany, 1957. **44**(6): p. 478-488.
8. Lerouxel, O., et al., *Biosynthesis of plant cell wall polysaccharides - a complex process.* Current Opinion in Plant Biology, 2006. **9**(6): p. 621-630.
9. Worden, N., E. Park, and G. Drakakaki, *Trans-Golgi network: an intersection of trafficking cell wall components.* J Integr Plant Biol, 2012. **54**(11): p. 875-86.
10. Kolb, H.C., M.G. Finn, and K.B. Sharpless, *Click chemistry: Diverse chemical function from a few good reactions.* Angewandte Chemie-International Edition, 2001. **40**(11): p. 2004-2021.

11. Laughlin, S.T. and C.R. Bertozzi, *Imaging the glycome.* Proceedings of the National Academy of Sciences of the United States of America, 2009. **106**(1): p. 12-17.
12. Beatty, K.E., et al., *Fluorescence visualization of newly synthesized proteins in mammalian cells.* Angew Chem Int Ed Engl, 2006. **45**(44): p. 7364-7.
13. Hsu, T.L., et al., *Alkynyl sugar analogs for the labeling and visualization of glycoconjugates in cells.* Proceedings of the National Academy of Sciences of the United States of America, 2007. **104**(8): p. 2614-2619.
14. Anderson, C.T., I.S. Wallace, and C.R. Somerville, *Metabolic click-labeling with a fucose analog reveals pectin delivery, architecture, and dynamics in Arabidopsis cell walls.* Proc Natl Acad Sci U S A, 2012. **109**(4): p. 1329-34.
15. Dolan, L., et al., *Cellular-Organization of the Arabidopsis-Thaliana Root.* Development, 1993. **119**(1): p. 71-84.
16. Vissenberg, K., S.C. Fry, and J.P. Verbelen, *Root hair initiation is coupled to a highly localized increase of xyloglucan endotransglycosylase action in arabidopsis roots.* Plant Physiology, 2001. **127**(3): p. 1125-1135.
17. Dumont, M., et al., *Plant cell wall imaging by metabolic click-mediated labelling of rhamnogalacturonan II using azido 3-deoxy-D-manno-oct-2-ulosonic acid.* Plant J, 2016. **85**(3): p. 437-47.
18. Wang, B., et al., *Synthesis of a suite of click-compatible sugar analogs for probing carbohydrate metabolism.* Carbohydr Res, 2016. **433**: p. 54-62.
19. Müller, S., et al., *An improved one-pot procedure for the synthesis of alkynes from aldehydes.* Synlett, 1996(6): p. 521-522.
20. Roth, G., et al., *Further improvements of the synthesis of alkynes from aldehydes.* Synthesis, 2004(1): p. 59-62.
21. Dasgupta, S. and M. Nitz, *Use of N,O-Dimethylhydroxylamine As an Anomeric Protecting Group in Carbohydrate Synthesis.* Journal of Organic Chemistry, 2011. **76**(6): p. 1918-1921.
22. Nahrwold, M., et al., *"Clicktophycin-52": A Bioactive Cryptophycin-52 Triazole Analogue.* Organic Letters, 2010. **12**(5): p. 1064-1067.
23. Kennedy, D.C., et al., *Cellular Consequences of Copper Complexes Used To Catalyze Bioorthogonal Click Reactions.* Journal of the American Chemical Society, 2011. **133**(44): p. 17993-18001.
24. Stone, B.A., et al., *The Application of Sirofluor, a Chemically Defined Fluorochrome from Aniline Blue for the Histochemical Detection of Callose.* Protoplasma, 1984. **122**(3): p. 191-195.
25. Bar-Peled, M. and M.A. O'Neill, *Plant nucleotide sugar formation, interconversion, and salvage by sugar recycling.* Annu Rev Plant Biol, 2011. **62**: p. 127-55.
26. Feingold, D.S., *Aldo (and Keto) Hexoses and Uronic Acids*, in *Plant Carbohydrates I*, F.A. Loewus, Tanner, W., Editor. 1982, Springer: Berlin, Heidelberg.
27. Leloir, L.F., et al., *The Formation of Glucose Diphosphate by Escherichia-Coli.* Archives of Biochemistry, 1949. **24**(1): p. 65-74.
28. Caspi, R., et al., *The MetaCyc database of metabolic pathways and enzymes and the BioCyc collection of Pathway/Genome Databases.* Nucleic Acids Res, 2014. **42**(Database issue): p. D459-71.
29. Sutherland, E.W., et al., *The Mechanism of the Phosphoglucomutase Reaction.* Journal of Biological Chemistry, 1949. **180**(3): p. 1285-1295.
30. Nelson, M.T. and R.T. O'Connor, *Relation of certain infrared bands to cellulose crystallinity and crystal lattice type. part I. spectra of lattice types I, II, III and of amorphous cellulose.* Journal of Applied Polymer Science, 1964. **8**: p. 1311-1324.

31. Hong, Z.L., A.J. Delauney, and D.P.S. Verma, *A cell plate specific callose synthase and its interaction with phragmoplastin.* Plant Cell, 2001. **13**(4): p. 755-768.
32. Bernal, A.J., et al., *Functional analysis of the cellulose synthase-like genes CSLD1, CSLD2, and CSLD4 in tip-growing Arabidopsis cells.* Plant Physiol, 2008. **148**(3): p. 1238-53.
33. Galway, M.E., et al., *Root hair-specific disruption of cellulose and xyloglucan in AtCSLD3 mutants, and factors affecting the post-rupture resumption of mutant root hair growth.* Planta, 2011. **233**(5): p. 985-999.
34. Park, S., et al., *A role for CSLD3 during cell-wall synthesis in apical plasma membranes of tip-growing root-hair cells.* Nature Cell Biology, 2011. **13**(8): p. 973-U227.
35. Favery, B., et al., *KOJAK encodes a cellulose synthase-like protein required for root hair cell morphogenesis in Arabidopsis.* Genes & Development, 2001. **15**(1): p. 79-89.
36. Thiele, K., et al., *The timely deposition of callose is essential for cytokinesis in Arabidopsis.* Plant Journal, 2009. **58**(1): p. 13-26.
37. Chebli, Y., et al., *The cell wall of the Arabidopsis pollen tube--spatial distribution, recycling, and network formation of polysaccharides.* Plant Physiol, 2012. **160**(4): p. 1940-55.
38. Cooper, K.M., *Callose-Deposit Formation in Radish Root Hairs*, in *Cellulose and Other Natural Polymer Systems*, R.M. Brown, Editor. 1982, Springer: Boston, MA.
39. Sletten, E.M. and C.R. Bertozzi, *Bioorthogonal Chemistry: Fishing for Selectivity in a Sea of Functionality.* Angewandte Chemie-International Edition, 2009. **48**(38): p. 6974-6998.
40. Thevenaz, P. and M. Unser, *User-friendly semiautomated assembly of accurate image mosaics in microscopy.* Microscopy Research and Technique, 2007. **70**(2): p. 135-146.

Chapter 3:

Intra- and extra-cellular orchestration of matrix deposition in growing plant cell walls

3.1 Abstract

Cell expansion is fundamental to plant growth and is controlled by primary cell walls, which are complex microstructures of cellulose and matrix polymers that deform during cell growth. Although both mechanosensing and cortical microtubule (MT) organization have been implicated in the patterned deposition of cellulose, how patterns of matrix deposition are controlled during wall assembly has remained obscure. Here, we used metabolic click labeling with the chemical reporter fucose-alkyne (FucAl) to track new matrix deposition in root epidermal cells of *Arabidopsis thaliana* in a developmental zone where newly deposited matrix adopts a pattern of oblique striations. Using a modified click-reaction that preserved intracellular structures, we observed that these striae coaligned with underlying cortical MTs. Genetic and pharmacological perturbations of actin, MTs, and cellulose synthesis were applied to dissect the cellular control over patterned matrix deposition. Disrupting actin influenced the large-scale homogeneity, but not the overall rate, of FucAl deposition. MT disruptions caused FucAl striae to become less dense and more curved, but did not prevent striae from forming. Disruption of cellulose biosynthesis, however, inhibited FucAl striae formation, instead causing isotropic deposition of matrix. Together, these data indicate that neither actin, cortical microtubules, nor concurrent cellulose biosynthesis is required for the delivery of matrix polysaccharides to the growing cell wall, but rather that all three exert distinct effects on the patterning of that matrix. The finding that cellulose organization can determine matrix patterning has important implications for our understanding of cell wall assembly, architecture, and mechanics.

Permissions for Published Work

Note: Part of Chapter 3 will be included in a report titled “Intra- and extra-cellular orchestration of matrix deposition in growing plant cell walls” to be submitted to *Plant Physiology* with a submission deadline of April 30, 2019.

ASPB permissions:

ASPB grants to authors whose work has been published in Plant Physiology® or The Plant Cell the royalty-free right to reuse images, portions of an article, or full articles in any book, book chapter, or journal article of which the author is the author or editor. Reproductions must bear the full citation, the journal URL (www.plantphysiol.org or www.plantcell.org), and the following notice: “Copyright American Society of Plant Biologists.” ASPB further grants to authors the permission to make digital or hard copies of part or all of a work published in Plant Physiology® or The Plant Cell without fee for personal or classroom use.

3.2 Author Contributions

D.D.M. and C.T.A designed experiments; D.D.M. performed experiments and analyzed results, D.D.M. and C.T.A. wrote the manuscript.

3.3 Introduction

Plants make cell walls to accommodate growth and development. These structures therefore embody large amounts of reduced carbon, captured through photosynthesis, and are a renewable resource. The biochemical composition of cell walls has been analyzed in detail, but the precise structures and conformations of many cell wall components, and how these components interact with each other to build strong, expandable walls, remains unknown. The assembly of primary cell walls that are produced before and during cell expansion involves the production of cellulose at the plasma membrane by large Cellulose Synthesis Complexes (CSCs)[1, 2], as well as the trafficking and exocytosis of matrix polysaccharides from their site of synthesis in the Golgi[3, 4]. However, the temporal order and spatial patterning with which various wall components are delivered to the apoplast and how they assemble there into a functional wall is poorly understood.

Initial assumptions about the connectivity of various cell wall polymers based on *in vitro* binding studies have sometimes been misleading: e.g., xyloglucan was thought to tether cellulose microfibrils together and thus be essential for the mechanical strength of the wall, but the discovery of viable xyloglucan-free mutants called into question this model[5, 6]. Initially distinguished from hemicelluloses by their higher extractability, pectins were later chemically defined as containing galacturonic acid residues with which neutral sugars could alternate or branch. While hemicelluloses were implicated in tethering the load-bearing cellulose componentry, thus forming a part of a load-bearing network, pectins were hypothesized to exist as a distinct coextensive matrix, a passive gel in which the hemicellulose-cellulose network was dispersed[7, 8]. The pectin network was shown to be important for determining certain wall properties, such as pH, porosity, adsorption and collection of biologically important cations, and to serve as a source of signaling molecules such as oligogalacturonides, but the primary

determinant of load-bearing, and thus anisotropic growth, has long been assumed to be the cellulose-hemicellulose network[9].

However, disruptions to pectin can have dramatic effects on cell wall mechanics and cell growth[10]. Mutants with altered pectin molecular weight have elongation phenotypes[11], and disruption of the dimerization of the pectin domain, rhamnogalacturonan-II, has dramatic effects on anisotropic expansion[12, 13]. These findings are in keeping with more recent observations from solid state NMR spectroscopy, which show that pectic residues have very close proximity to cellulosic glucose residues *in muro* [14], and that this is not an artifact of drying[15]. Since these close associations are not recapitulated by *in vitro* binding studies[16], perhaps they are the result of initial physical entanglement with emergent CMFs, or otherwise assembled around cellulose in a concerted way[17].

In this way the timing and order of wall assembly are important, implying active biological regulation of the process. Understanding the rules of cell wall assembly necessitates observing wall synthesis, assembly, and dynamics in a real expanding wall. The advent of fluorescently labeled cellulose synthase complexes (CSCs) revealed that CSCs are not delivered to the plasma membrane in a uniform 2D distribution, but rather are delivered preferentially above sites of cortical microtubules, through interactions via coupling proteins such as CESA INTERACTING PROTEIN1[1, 18]. Due to the spatial separation between synthesis in the Golgi and exocytosis for matrix polysaccharides, combined with the challenges associated with fluorescently labeling polysaccharides *in vivo*, we know much less about the intracellular orchestration of matrix movement from Golgi cisternae to sites of CW polysaccharide deposition, or about their behaviors upon exocytosis and their associations with existing wall components. A recent census of the polysaccharide cargo of a subset of the exocytic vesicles containing SYNTAXIN OF PLANTS61 (SYP61), however, is a major advance[19]. This identified a range of diverse glycans, including all major classes of matrix polysaccharides typical of the primary

wall, in isolated vesicles originating from the trans-Golgi network. Whether these components are all contained in the same vesicles, and thus delivered together, or are contained in sub-sets of SYP61-containing vesicles remains to be seen. Although immuno-EM studies have provided detailed information about the spatial distribution of matrix polysaccharides across cell walls, they label all of a given polysaccharide with equal affinity, providing only a snapshot of total matrix distribution in a given cell type, and the large size of antibodies renders such analysis susceptible to artifacts related to masking by other polymers in the closely-packed wall[4, 20, 21].

One of the most direct methods to address this challenge is to directly observe the polysaccharides themselves by first introducing a chemical reporter that is metabolically incorporated into a subset of matrix polysaccharides, and can then be made visible by ligating the reporter to a fluorophore with a bio-orthogonal click-reaction[22-24]. When this approach is applied in the early differentiation zone of *Arabidopsis* root epidermal cells, newly delivered matrix is sparse enough that discrete delivery events are resolvable from one another with confocal microscopy, but still accumulate rapidly enough to display a patterned arrangement. In this case, this pattern is of discrete striae, where matrix deposition events accumulate into linear forms, which in turn are reminiscent of the underlying cortical microtubule arrangement[25]. These data suggest that the cytoskeleton might function as a determinant of matrix patterning during wall assembly, perhaps by directing the exocytosis of matrix polymers from trafficking vesicles at the cell surface.

In this investigation, we disrupted three potential sources of order that could control this patterning – the actin microfilament network, the cortical microtubule array, and cellulose microfibrils at the most proximal layer of the wall – to determine how plant cells exert control over patterned matrix deposition. While disruption of the two cytoskeletal elements had distinct effects on matrix deposition, cellulose disruption had the largest effect, in keeping with the

hypothesis that there is an initial, tight association between CMFs and delivered matrix polysaccharides in diffusively expanding primary walls.

3.4 Results and Discussion

3.4.1 The actin cytoskeleton influences the homogeneity, but not the overall rate, of FucAl deposition across cell surfaces

The intracellular trafficking of secreted cell wall components, and some of the enzymes that produce them, is critical for the normal assembly and patterning of cell walls [3]. For example, actin microfilaments have been demonstrated to function in the trafficking of cellulose synthase complexes from the Golgi to the plasma membrane [26], and are also required for the even distribution of cellulose synthase complexes across the cell surface, likely via cytoplasmic streaming-driven Golgi motility [27, 28]. We reasoned that analogously, the delivery rates and large-scale distributions of matrix polysaccharides might depend on actin-driven cytoplasmic streaming and/or post-Golgi trafficking. Previously, we found that FucAl was incorporated into the cell walls of epidermal cells in punctate, striated, or diffuse patterns depending on the position of the cells along the developmental axis of the root, and that these patterns were evenly distributed across the cell surface [29]. Here, we tested whether actin microfilaments are necessary for (1) FucAl delivery, and/or (2) the establishment of normal FucAl patterning in Arabidopsis roots. Seedlings were pre-incubated with the actin-depolymerizing drug, latrunculin B (latB) [30], for 30 min, treated with FucAl and latB for an additional 4h, and click-labeled. In control seedlings, 4 h of FucAl incubation resulted in fluorescence in elongation zone cells, and homogenously-distributed punctae in differentiation zone cells (Figure 3-1), in accordance with previous results [29]. In elongation zone cells, the patterns of FucAl delivery after 4 h were

substantially altered in latB-treated cells, with multiple large, round zones of low fluorescence intensity appearing in most cells (Figure 3-1B). In some cases, these regions of low intensity were aligned laterally across multiple cells (Figure 3-1B). The distribution of FucAl labeling across cells in the differentiation zone was also less homogenous than in controls (Figure 3-1C, D), although fluorescence intensity after 4 h of FucAl incubation is low in these cells, possibly due to reduced rates of wall biosynthesis and deposition as cell elongation begins to diminish. Relative intensity distributions of FucAl-associated fluorescence are shown for representative cells in Figure 1E, which demonstrates that the patchiness of FucAl delivery occurs on the order of 5-10 μm in cells treated with latB. There was significant variation in total FucAl-associated intensity per cell within individual seedlings (e.g., Figure 3-1A), so we measured total FucAl-associated intensity per cell across multiple cells per seedling to assess whether any change in FucAl delivery rate, as has been observed in the kinesin mutant *fra1*-5 [31], occurred in the presence of latB. One potential source of variation between cells in the early elongation zone is the presence of two cryptic cell identities; trichoblasts and atrichoblasts have distinct metabolic activities and gene expression at this stage of development[32]. Within-file variation may represent differences in nuclear endoreduplication status, which also begins in this developmental zone[33]. There were no significant changes in average per-cell FucAl-associated intensities between control and latB-treated seedlings ($p > 0.05$, t-test; $n \geq 44$ cells from 5 seedlings per treatment per experiment), meaning that the maximal FucAl-associated fluorescence intensity far exceeded the average intensity in control cells in certain regions of latB-treated cells (see Figure 3-1D), but was much lower in other regions of latB-treated cells than the average intensity in control cells.

Together, the above data indicate that cells can, when actin dynamics are disrupted by latB treatment, deliver sufficient amounts of FucAl-containing matrix polymers to the cell surface, presumably via post-Golgi trafficking pathways. However, an even distribution of matrix polysaccharide delivery across the cell surface on the multi-micron scale appears to depend on

actin-driven movements of Golgi bodies [34], in which matrix polysaccharides are synthesized, and from which they are delivered to the cell surface [35]. This finding is similar to the case for cellulose synthase complexes, which appear in highly clustered regions of Golgi in the cell cortex, and in overlying clusters of plasma-membrane punctae that presumably arise from high local rates of exocytosis after latB treatment [27, 28]. Notably, the differences in labeling intensity were more severe in cells in the elongation zone, where wall synthesis is expected to be maximal, than in differentiation zone cells (Figure 3-1E). It is also possible that latB, which inhibits cell elongation in Arabidopsis [30], causes uneven wall expansion, in which case, the apparent zones of FucAl-associated fluorescence depletion represent zones of greater wall expansion, effectively diluting the fluorescence signal. However, the regions of low FucAl-associated fluorescence intensity do not always extend fully across all cells (Fig. 3-1B). If growth were uneven, those cells would be expected to have bulges or bends, which were not observed.

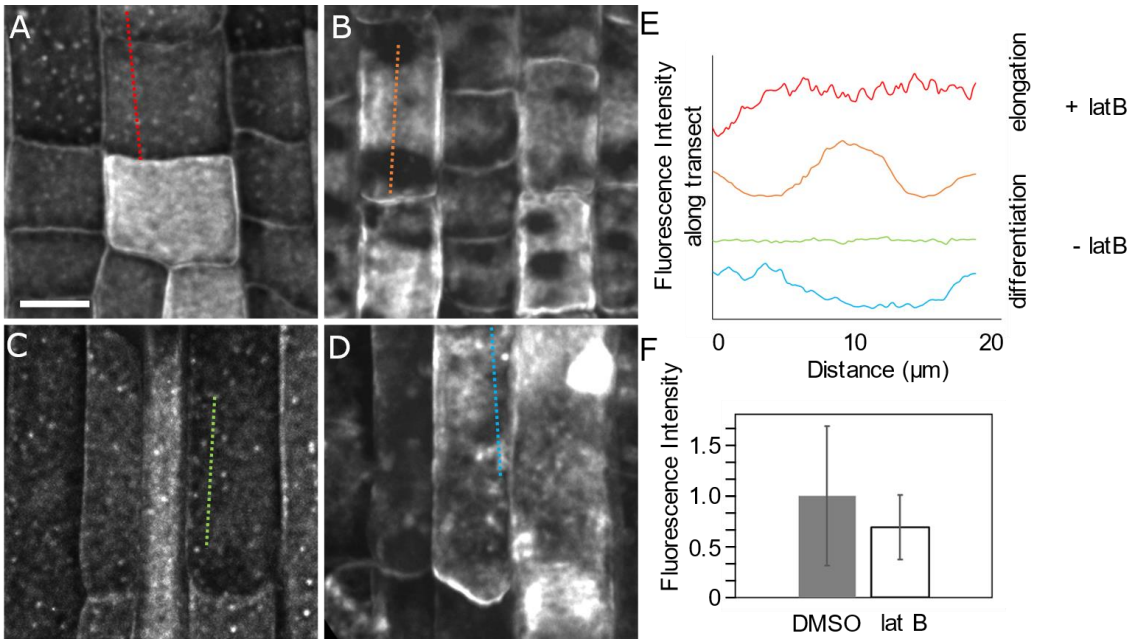

Figure 3-1. Latrunculin B treatment results in uneven matrix deposition. Five-day-old light-grown Arabidopsis seedlings were incubated in 2.5 µM FucAl-containing media for 4 h, then click-labeled with Alexa 488-azide. Epidermal cells in the root elongation zone (A,B) or differentiation zone (C,D), incubated with DMSO (A,C) or 1 µM latrunculin B (latB; B,D) for 30 min before and throughout FucAl incubation. E, Fluorescence intensity differences across traces drawn along cell axes in A-D. Scale bar = 10 µm. F, Average fluorescence intensity per seedling for DMSO or latB-treated seedlings. Error bars = standard deviation. For each treatment, n≥20 seedlings from two independent experiments.

3.4.2 MTs coalign with FucAl striae in root epidermal cells

Actin is required for the long-scale intracellular transport of secreted biomolecules in plant cells, whereas cortical microtubules can guide the localized delivery of vesicles to the cell surface, as in the case of vesicles containing cellulose synthase complexes in diffusely growing cells [27, 28]. In expanding root epidermal cells in the early differentiation zone treated with FucAl for 12 h to allow for more extensive deposition of FucAl-containing polymers, striae of 1-3 µm in width were previously observed [29] that were reminiscent of the organization of cortical

microtubules, which change orientation slowly in root cells [36]. However, the toxicity of Cu-catalyzed click labeling in plants [29] precluded the direct observation of fluorescently labeled microtubules in these cells. Although copper-free click labeling methods have recently been reported for Arabidopsis [22], these methods are not compatible with alkyne-functionalized chemical reporters. Incubating seedlings with 2.5 μM FucAl for 6 h and adding the poly-triazole ligand, 3-[4-([bis[(1-tert-butyl-1H-1,2,3-triazol-4-yl)methyl]amino]methyl)-1H-1,2,3-triazol-1-yl]propanol (BTTP), to the click labeling reaction to reduce the toxicity of the Cu(I) catalyst [37], allowed for click labeling while retaining cell viability in the late elongation zone, as shown by cytoplasmic streaming in cells with FucAl labeling, and by staining with fluorescein diacetate (FDA) but not propidium iodide (Figure 3-2A,B). This ligand was unable to preserve cell viability in the adjacent elongation zone (Figure 3-2C). Performing these experiments in seedlings expressing the microtubule marker GFP-MAP4[38] enabled both the preservation of the intracellular arrangement of microtubules and the detection of FucAl incorporation patterns (Figure 3-3B-F, Figure 3-2). FucAl striae angles were biased in the same direction as the modal microtubule angle (Figure 3-3G), but did not always perfectly match these angles, especially when the total anisotropy of the FucAl incorporation pattern was low (Figure 3-3G, tenth cell).

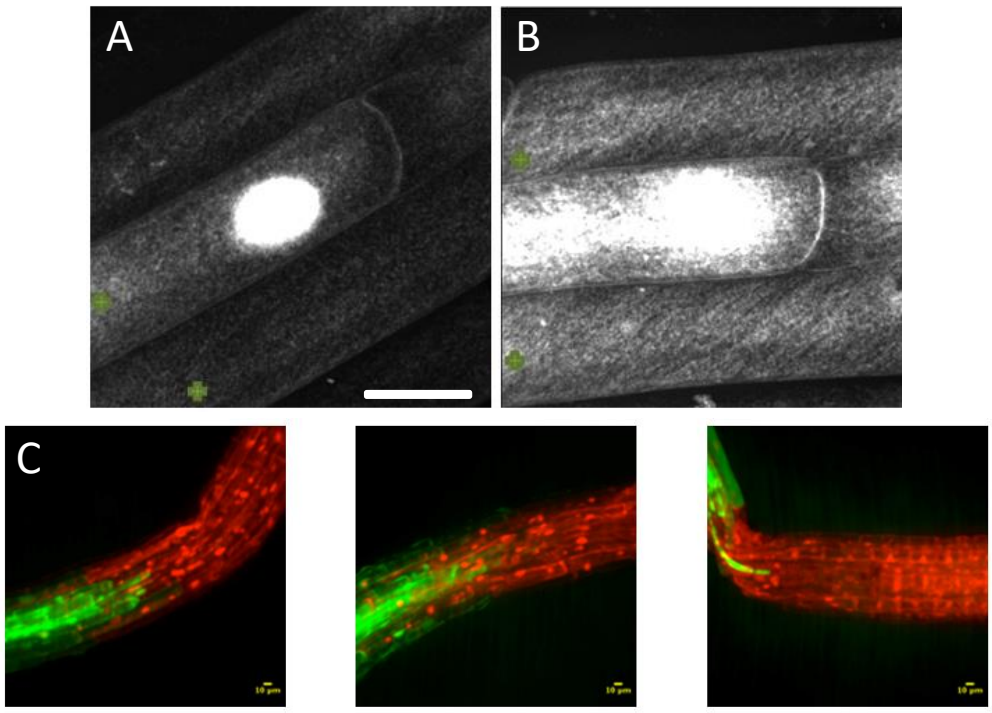

Figure 3-2. The Cu-chelating ligand, BTTP preserves cytoplasmic streaming in some cells after click-labeling. Alexa488-azide fluorescence in root epidermal cells in the early differentiation zone after incubation with 2.5 µM FucAl for 6 h , followed by (A) 10 min or (B) 30 min BTTP-modified click-labeling reaction: 100 µM $CuSO_4$, and 600 µM BTTP, 100 µM ascorbic acid. Green plus-symbols indicate cells that showed active cytoplasmic streaming in the brightfield channel. (C) FDA (green) / PI (red) viability staining patterns for three representative seedlings after the same reaction conditions as in B. The early differentiation zone is oriented to the left in every frame. Scale bars = 10 µm.

These results indicated that microtubules might determine, either directly or indirectly, the directions of the striated patterns of FucAl-containing matrix polymers observed after longer FucAl incubation times in cells in the early differentiation zone of the root. The relatively uncharged BTTP ligand, which when complexed with Cu(I) acts rapidly to catalyze click reactions, has been reported to be effective for copper-catalyzed click labeling of negatively charged molecules [37], of which pectins are an example. By complexing the Cu (I) ions with the triazole alcohol BTTP before subjecting seedlings to the mixture, we were able to maintain cell integrity in the developmental zones of interest. Other developmental zones were still susceptible to copper exposure, including cells in the early elongation zone (Figure 3-2). Why there is

differential sensitivity to the complexed copper in different zones of the root is unclear, but one possibility is that higher polysaccharide turnover during the rapid elongation phase may necessitate a greater rate of endocytosis, exposing the internal cell environment to more of the still-toxic copper complex. Despite these caveats, developing a method that allows for *in vivo* click labeling of alkynyl sugar analogs in plant cells also opens new avenues for further studies of polysaccharide delivery and dynamics in plant cell walls.

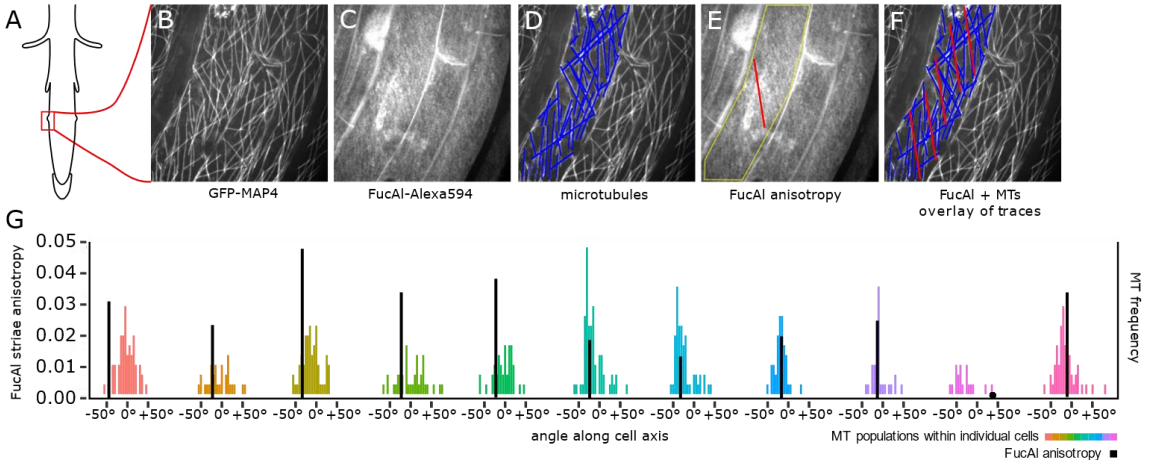

Figure 3-3. Predominant orientations of microtubules and FucAl striae show similar directionalities. Root epidermal cells in the early differentiation zone (A) expressing the microtubule marker GFP-MAP4 (B) were incubated in 2.5 µM FucAl for 6 h, then click-labeled with Alexa 594-azide, 100 µM CuSO4, and 600 µM BTTP (C). Microtubules were traced by hand (D) and the orientation and strength of FucAl labeling anisotropy were scored with FibrilTool (E). G, Distribution of microtubule angles (histograms) in eleven cells where multiple microtubules were visible post click-labeling, plotted along with the angle of anisotropy for the FucAl pattern (black bar), where 0° represents transverse and positive values represent right-handed winding along the root axis. Black bar heights indicate the anisotropy score. Scale bar = 10 µm.

3.4.3 MT disruption decreases the density and linearity of FucAl striae, but does not prevent them from forming

The approximate co-alignment we observed between microtubules and FucAl striae (Figure 3-3) suggests that microtubules might at least partially determine FucAl patterning in the walls of root epidermal cells. However, the lack of complete co-localization between striae and microtubules, and the much closer spacing of striae than microtubules, suggested that other factors might also determine FucAl delivery patterns in these cells. This motivated us to test whether FucAl patterning operationally depends on the cortical MT array, using both pharmacological and genetic perturbations. For the former, seedlings were pre-treated with drugs for 30 min, incubated with FucAl in the presence of drug for 6 h, then click labeled and imaged.

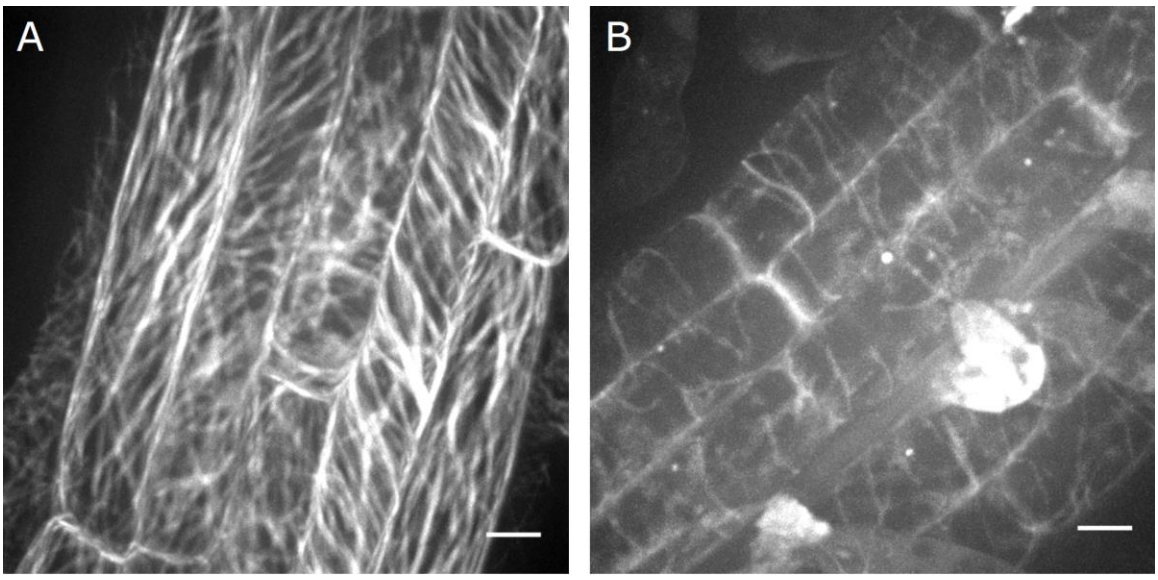

Figure 3-4. Microtubules remain depolymerized after 6 h of oryzalin treatment. Root epidermal cells in the early differentiation zone from seedlings expressing the microtubule marker GFP-MAP4 that were incubated for 6 h in the absence (A) or presence (B) of 1 µM oryzalin, then assayed for cortical MT presence and organization. Strands visible in (B) are not limited to the cell cortex. Scale bar = 10 µm.

A 6 h incubation was chosen because this is near the minimum incubation duration where linear FucAl features emerge, and before seedlings can acclimate to the drug exposure and re-

form normal cortical microtubule arrays (Figure 3-4). Six hours was long enough to observe changes FucAl striae organization as a result of incubation with microtubule-depolymerizing oryzalin, even when applied at a concentration that does not necessarily depolymerize all microtubules (Figure 3-5).

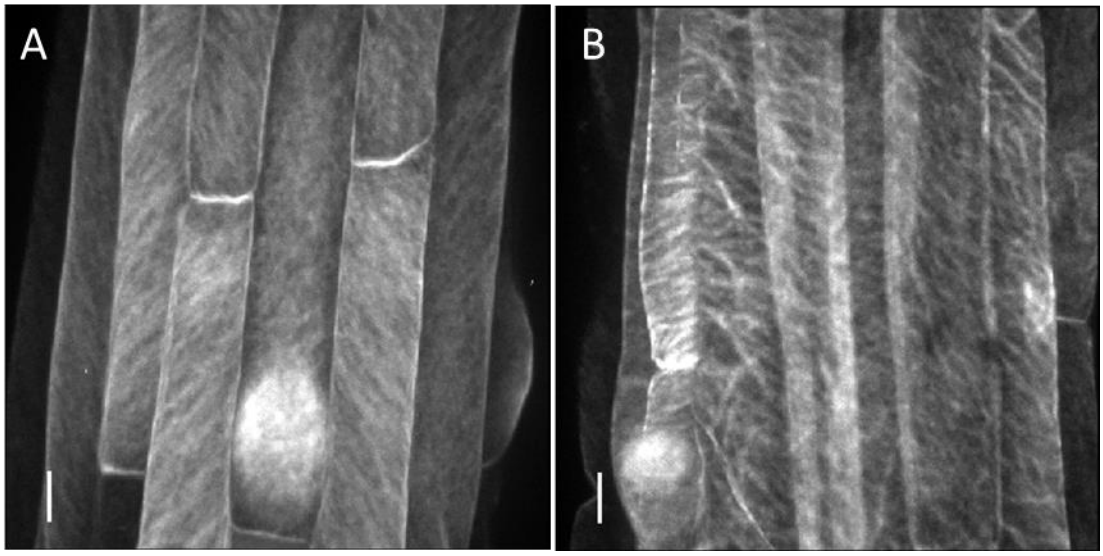

Figure 3-5. Oryzalin treatment disrupts FucAl striae organization. Root epidermal cells in the early differentiation zone from seedlings treated with (A) 0 µM or (B) 560 nM oryzalin; fluorescence is FucAl click-labeled with Alexa488-azide. Scale bars = 10 µm.

For each image set collected, FucAl fluorescence intensity, the proportion of cells with striated patterning, and the predominant strial angle for each cell were quantified (Figure 3-6H-K). Because one mutant of interest was temperature-sensitive, we first examined the effect of the restrictive temperature (29 °C) on matrix delivery and patterning in the corresponding Col wild-type. Although typical FucAl striae, obvious in the 21°C control (Figure 3-6A) were still visible at 29 °C (Figure 3-6B), the intensity of fluorescence (Figure 3-6I) and the number of cells in this zone exhibiting striated patterning (Figure 3-6J) decreased somewhat, although these differences were not statistically significant. Globular, intracellular FucAl-associated fluorescence was often apparent in cells incorporated at 29 °C (Figure 3-6B). This may indicate increased endocytosis of recently deposited matrix at the higher temperature. When present, FucAl striae in Col seedlings

at both temperatures were characteristically oriented obliquely to the cell axis, and were largely linear, parallel, regularly spaced, and of uniform apparent thickness.

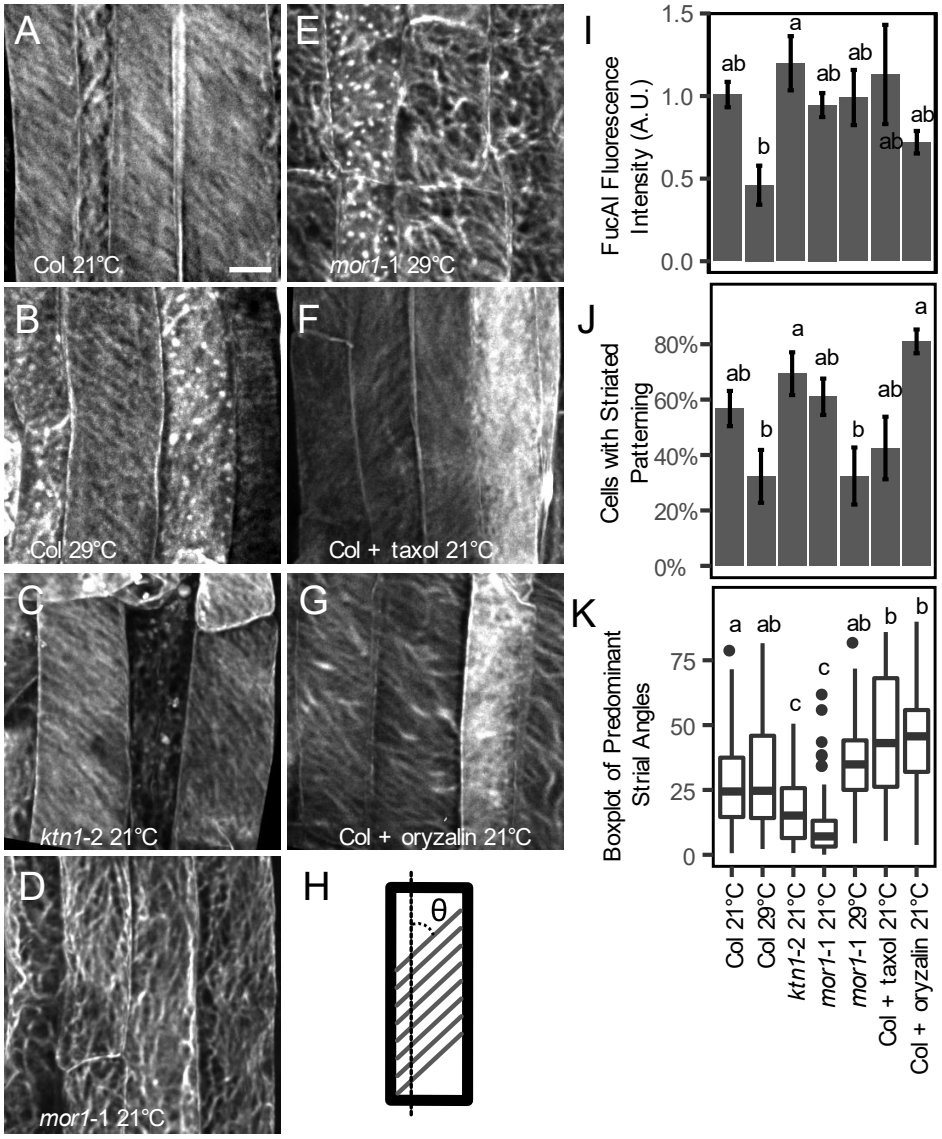

Figure 3-6. Microtubule perturbation disrupts, but does not obliterate, the patterning of newly delivered matrix. A-G, Root epidermal cells in the early differentiation zone incubated with 2.5 µM FucAl for 6 h, then click-labeled with Alexa 488-azide. **A**, Col at 21°C; **B**, Col at 29°C; **C**, *ktn1*-2 at 21°C; **D**, *mor1*-1 at 21°C; **E**, *mor1*-1 at 29°C; **F**, Col at 21°C with 1 µM taxol; **G**, Col at 21°C with 1 µM oryzalin. **H**, Convention for reporting prevailing anisotropy angles relative to longitudinal axis, with a maximal angle of 90° representing transverse, regardless of handedness. **I**, FucAl labeling intensity; **J**, Fraction of cells per seedling with linear, curvilinear, or otherwise striated patterning; K, Box plot of distributions of angles of predominant strial anisotropy. Error bars ± SE; N >= 12 seedlings per treatment from three independent experiments; with at least 5 cells measured per seedling. Scale bar = 10 µm.

FucAl striae in a mutant with an inhibited rearrangement of the cortical MT array, *katanin1-2* [39], still showed obliquely arranged striae; the predominant angles of anisotropy for these striae were significantly more axially-biased (Figure 3-6K). KATANIN1 is a MT-severing protein. Analogously, 1 mM taxol (Figure 3-6F) was applied to test whether stabilizing cortical MTs would disrupt FucAl patterning. Neither genetic nor pharmacological stabilization of cortical MTs appeared to affect FucAl fluorescence intensity or the frequency of cells with striated patterning (Figure 3-6I,J).

FucAl striae in root epidermal cells of the temperature-sensitive mutant *mor1-1,* which displays defects in microtubule length and organization at the restrictive temperature of 29 °C [40], were disorganized (Figure 3D,E) as compared to Col controls. Curiously, we observed abnormal FucAl organization at both the permissive 21 °C and restrictive 29 °C temperatures in *mor1-1* seedlings. FucAl striae in this mutant appeared to be disrupted, adopting wavy, arcing forms with large intervening spaces, and an apparent lack of organized orientation. At the permissive temperature, this resulted in a reduction in the predominant strial angle relative to the long axis of the cell (Figure 3-6K). Additionally, when MTs were depolymerized by treatment with 1 µM oryzalin (Figure 3-4), the morphology of FucAl striae changed markedly (Figure 3-6G): although the prevailing orientation of the striae was still oblique to the cell axis, the striae were now more curved, adopting intersecting arrangements of variable widths and spacings, with the striae themselves also varying in thickness. However, oryzalin treatment did not cause significant reductions in FucAl-associated fluorescence intensity, or the proportion of cells with striated patterning, although the predominant strial angle differed relative to untreated controls (Figure 3-6I-K).

In Col seedlings at 29 °C (Figure 3-6B), YFP-cellulose synthase particle velocities have been reported to be 4.2-fold higher than at 21 °C, but growth rate also increases and cellulose content does not increase at the higher temperature [41]. We did not observe any increase in

FucAl-associated fluorescence, which represents the sum of accumulated matrix polysaccharides over 6 h for a given cell area, in seedlings incubated at 29 °C (Figure 3-6I), although we did observe more intracellular, globular click labeling at 29 °C in both Col and *mor1-1* seedlings (Figure 3-6B, E). Together, these data suggest that matrix delivery rates might remain proportional to cellulose synthesis rates across a range of temperatures; these two rates might be expected to predominantly determine the initial architecture of new wall lamallae.

Both taxol and oryzalin treatments increase the predominant angle of FucAl-associated striae relative to the longitudinal cell axis (Figure 3-6K), suggesting that microtubule dynamics are required to maintain a predominant angle closer to 25°. However, this result might reflect a general growth inhibition in cells treated with taxol or oryzalin, which might slow down the reorientation of wall structures from transverse to longitudinal during cell elongation [42]. The fact that FucAl incorporation occurs at a largely normal rate, albeit with altered patterning, in seedlings treated with oryzalin is distinct from previously published results in which a knockout for a kinesin, FRAGILE FIBER1 (FRA1) showed reduced FucAl incorporation relative to wild type controls ([31], Ch. 4 this work). It is possible that in the absence of FRA1, other motor proteins sequester FucAl-containing vesicles intracellularly, preventing their delivery to the cell surface, but that in the absence of microtubules, redundant exocytic pathways enable the delivery of matrix polymers to the apoplast.

The wavy FucAl incorporation patterns we observe for *mor1-1* seedlings at both 21 °C and 29 °C (Figure 3-6D,E) and for Col seedlings treated with oryzalin (Figure 3-6G) are reminiscent of the trajectories of YFP-cellulose synthase particles at elevated temperatures in *mor1-1* seedlings [41] or in Col seedlings treated with oryzalin [2]. This similarity led us to investigate whether cellulose patterning *per se* affects the patterning of FucAl incorporation in root epidermal cells.

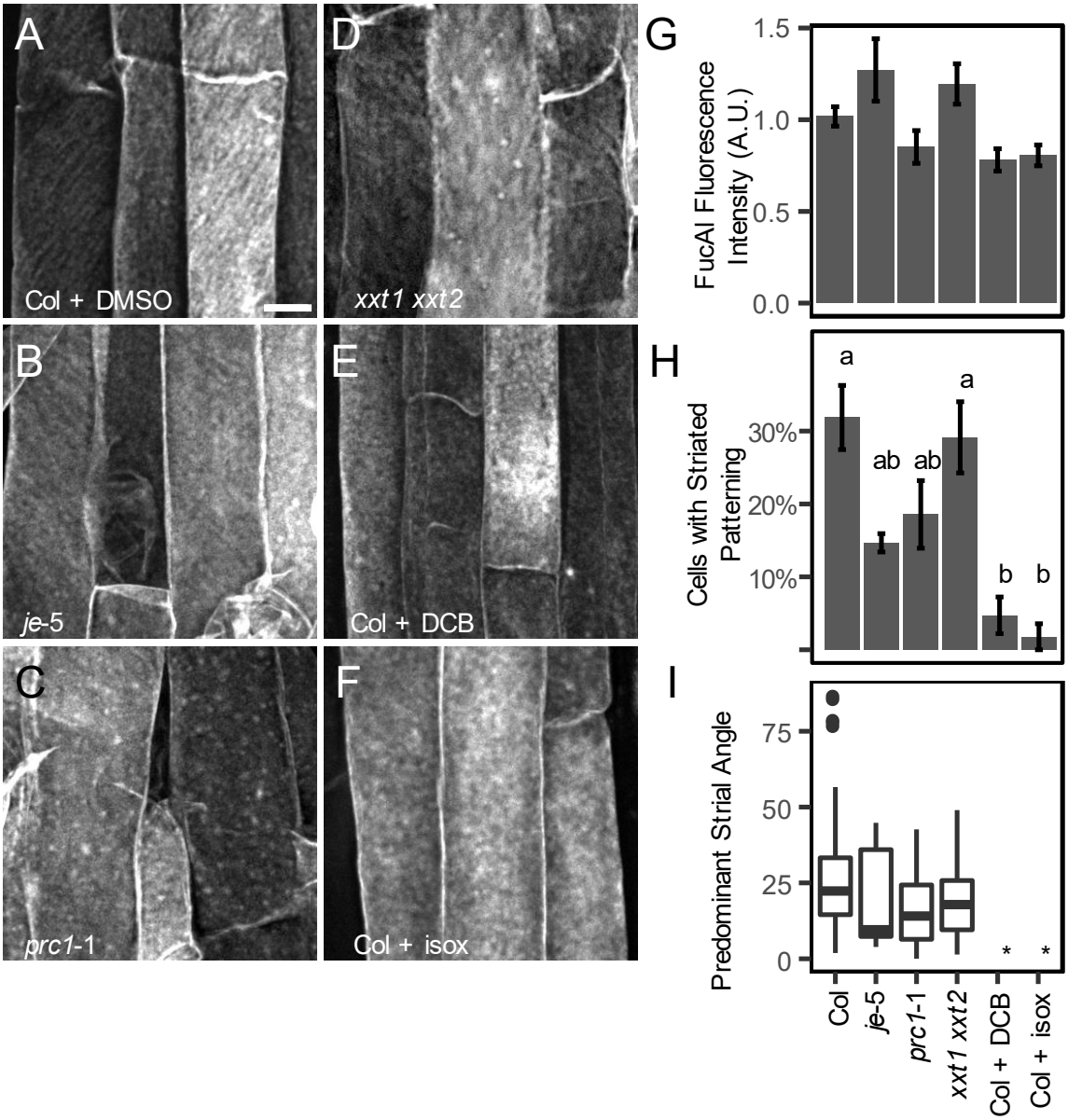

Figure 3-7. The patterning of newly delivered matrix is largely obliterated, although matrix delivery continues, when cellulose biosynthesis is disrupted. A-F, Root epidermal cells in the early differentiation zone incubated with FucAl for 6 h, then click labeled with Alexa 488-azide. A, Col; B, *cesa3*$^{je\text{-}5}$, C, *cesa6*$^{prc1\text{-}1}$; D, *xxt xxt2*, E, Col treated with 1 µM DCB, F, Col treated with 1 µM isoxaben. G, FucAl labeling intensity; H, Fraction of cells per seedling with linear, curvilinear, or otherwise striated patterning; I, Box plot of distributions of cells' angles of predominant strial anisotropy. Asterisks indicate treatments that resulted in too few cells with striated patterning to construct boxplots. Error bars ± SE; N >= 12 seedlings per treatment from three independent experiments; with at least 5 cells measured per seedling. Scale bar = 10 µm**.**

3.4.4 Disruption of cellulose biosynthesis inhibits FucAl striae formation

Patterns of matrix polysaccharide deposition in the cell wall might be determined by their placement during delivery to the apoplast, as governed by intracellular trafficking and cytoskeletal dynamics, but they might also reflect the initiation of nanoscale interactions with cellulose microfibrils in the apoplast. Since we observed FucAl striae despite the absence of microtubules in oryzalin-treated cells (Fig. 3-6G), we hypothesized that the layer of cellulose microfibrils that lies closest to the plasma membrane might be the most proximal cause of FucAl striae formation, serving as a scaffold to which matrix polysaccharides quickly adhere after their exocytosis from post-Golgi trafficking vesicles. To test this possibility, we incubated seedlings exposed to a cellulose biosynthesis inhibitor (CBIs), 2,6-dichlorobenzonitrile (DCB)[43] or isoxaben[44], with FucAl. This treatment should inhibit the synthesis and deposition of new cellulose, but still allow for matrix deposition. Compared to the FucAl striae that were evident in the walls of control seedlings treated with DMSO (Fig. 3-7A), the patterns of FucAl deposition were significantly disrupted in DCB- and isoxaben-treated seedlings (Fig 3-7E,F). These treatments rendered matrix patterning generally diffuse and formless, although uniformly distributed punctae were occasionally observed. This trend was continued, to a lesser degree, in mutants with disrupted CMF organization [11, 45-47]. Three such mutants were tested for effects on FucAl organization. The xyloglucan-deficient mutant *xxt1 xxt2* [5, 6] showed more diffuse, somewhat reticulate FucAl patterning (Fig. 3-7D). In this mutant, CMFs occur in larger bundles in the absence of xyloglucan, but there is also a concomitant destabilizing effect of activated wall integrity sensing on the cortical MT array [11], making it difficult to distinguish the differential contributions of the MT array versus preexisting CMF organization in establishing matrix anisotropy. Seedlings homozygous for the *cesa3*^{je5} [1] or *cesa6*$^{prc1\text{-}1}$ [48] mutations, which are hypomorphic and knock-out alleles of cellulose synthase 3 and 6, respectively, showed fewer

discernible linear FucAl features, and striae in fewer cells than controls (Fig. 3-7B,C,H). However, these phenotypes were variable, and unlike the total ablation of patterning seen after CBI exposure, did not result in a statistically significant decrease in the proportion of cells with striated patterning. When cells with patterning were observed in these mutants, the predominant angle of anisotropy remained oblique with respect to the cell axis, similar to the pattern observed in controls (Figure 3-7I).

The above data indicate that cellulose is necessary for establishing the striated patterns of FucAl-associated fluorescence observed in root epidermal cells in the early differentiation zone. The relative lack of FucAl patterning observed under DCB or isoxaben treatment, both of which prevent cellulose synthesis, might be attributable to the accumulation of one or more uniform, cellulose-free lamellae at the inner surface of the wall. The comparable FucAl-associated fluorescence intensity in control and CBI-treated cells suggests that in the absence of cellulose synthesis, matrix delivery to the apoplast persists. Thus, the internalization of cellulose synthase particles from the plasma membrane under isoxaben treatment might not affect matrix delivery, suggesting that the trafficking pathways for cellulose synthase [49] and matrix polysaccharides [3, 50] might be distinct from one another. Further genetic and pharmacological dissection will be required to fully define how the secretory pathway for matrix polysaccharides relates to the delivery, recycling, and internalization pathways for cellulose synthase[51] and other wall-related proteins.

3.5 Conclusions

Others have recently reported successful *in vivo* click-labeling of plant cell walls with azido-functionalized sugars [22], but FucAl is one of the most fully characterized sugar analogs with respect to cell wall development [29]. FucAl has the disadvantage of being incompatible

with the copper free ring-strained catalyzed cycloaddition that makes azido-sugars visible [52], but the toxicity of the copper (I) catalyst can be attenuated with the use of polydenatate ligands [37]. Our finding that the use of BTTP as a ligand allowed for the retention of some cell viability and preserved intact microtubules opens up new potential avenues for studying the trafficking and dynamics of wall polysaccharides by metabolic labeling.

We found that the intensity of both microtubule and actin networks is important for establishing normal matrix patterns, but at distinct spatial scales. Disruption of the actin network resulted in patchy FucAl incorporation across larger areas of the cell surface, whereas perturbing MTs resulted in striae that were less linear, potentially reflecting changes in the patterning of cellulose synthesis that occur after MT disruption [41]. The existing organization of cellulose microfibrils in the wall appears to be more important for directing matrix deposition patterns than intracellular determinants. Cellulose biosynthesis inhibition effectively removed all matrix anisotropy, and mutants with altered cellulose organization had dramatically altered matrix patterning (Figure 4). In our experiments, cortical MTs persisted after 6.5 h treatment with CBIs, so in the case of isoxaben and DCB treatment, the relative contributions of intra- and extra-cellular factors to the establishment of matrix patterning by could be distinguished from one another, with the latter contributing more dominantly to patterning.

In summary, our experiments to track the patterning of newly delivered matrix suggest that cellulose microfibrils impose anisotropy onto matrix components. This is in agreement with the models of wall architecture that are emerging from solid-state NMR experiments [53] that have detected nm-scale interactions between pectic polysaccharides and cellulose microfibrils, and have even distinguished mobile from immobile matrix elements, where immobile elements are most closely associated with cellulose microfibrils. Since FucAl is hypothesized to be a chemical reporter for fucose-containing galactan sidechains of rhamnogalacturonan-I [29], and rhamnogalacturonan-I has been proposed to interact with cellulose [15, 54], FucAl-containing

polysaccharides might in effect be “painting” newly synthesized CMFs, that is, adhering to nascent microfibrils, rather than adopting self-organized configurations or directly translating microtubule organization into the apoplast. How matrix polysaccharides in turn might influence cellulose microfibril organization [11], bundling, and dynamics in the wall will be an interesting topic for further study. We anticipate that this method could also be useful for interrogating the current question of whether the pectin network or the cellulose microfibril network initially determines the direction of cell expansion, by differentially labeling new pectin in cells that are about to undergo anisotropic expansion.

3.6 Methods

3.6.1 Seedling culture

Arabidopsis thaliana seeds of the Columbia-0 (Col) ecotype or mutant genotypes were surface-sterilized with 30% household bleach + 0.1% sodium dodecylsulfate for 20 min, washed four times with sterile distilled water, and stratified in 0.15 % agar gel for ≥3 days at 4 °C. Seeds were sown on vertical media plates (2.2 g/L Murashige and Skoog salts, Caisson Labs, 0.6 g/L MES, pH 5.6, 1% w/v sucrose, 0.8% agar) media and grown in 24 h light at 21°C for 5 days.

3.6.2 Chemical reporter incorporation

Seedlings were rinsed with MS liquid media (2.2 g/L Murashige and Skoog salts, 0.6 g/L 2-(*N*-morpholino)ethanesulfonic acid (MES), pH 5.6) and then immersed in MS liquid media with FucAl (peracetylated, 2.5 µM, from a 25 mM stock solution in DMSO stored at -80°C in O-ring tubes to prevent water contamination, Life Technologies) in constant light at 21°C. For experiments where a pharmacological inhibitor was used, seedlings were pre-incubated for 30 min in MS liquid media including the inhibitor (latrunculin B, EMD Millipore; paclitaxel, Sigma; oryzalin, Chem Service; 2,6-dichlorobenzonitrile, Chem Service; isoxaben, Chem Service) at its final concentration diluted from a 100X stock solution in DMSO prior to being transferred to MS liquid media including both the inhibitor and 2.5 µM FucAl. Seedlings were removed from incubation liquid and washed four times with MS liquid media to remove excess FucAl.

3.6.3 Click-labeling

FucAl-containing components of root epidermal cell walls were tagged by covalently ligating Alexa 488 or Alexa 594 fluorophores to them with a copper-catalyzed click-reaction as in [29]. Seedlings were incubated in half-strength MS liquid containing 1 mM $CuSO_4$, 1 mM ascorbic acid, and 1 µM Alexa 488-azide (from a 1 mM stock solution in DMSO, Life Technologies) for 1 h in darkness. The reaction was quenched by washing four times with MS liquid. To preserve microtubule organization during labeling, seedlings expressing GFP-MAP4 [55] were incubated in a modified click reaction mixture containing 100 µM copper sulfate and 600 µM BTTP (purchased from the Chemical Biology Core Facility, Albert Einstein College of Medicine, Bronx, NY) [37] in place of 1 mM copper sulfate, and the reaction was carried out for 30 min. To avoid overlap with GFP fluorescence, 1 µM Alexa 594-azide was used instead of Alexa 488-azide. Click-labeled seedlings were stored at 4°C for a maximum of 12 h before imaging, with the exception of GFP-MAP4 expressing seedlings, which were imaged immediately after the labeling reaction and subsequent washes. Viability staining was performed with sequential staining with fluorescein diacetate (5µg / mL. 30 sec) and propidium iodide (6 µg / mL), but with a longer (5 min) propidium iodide incubation, following the method of [56].

3.6.4 Imaging and image analysis

Cells in the early elongation zone and early differentiation zone of seedling roots were located by identifying root hair bulges as the boundary between these zones. Root epidermal cells in these zones were imaged with a Zeiss Cell Observer SD spinning disk confocal microscope (488 nm laser excitation, 525/50 emission filter; 561 nm laser excitation, 617/73 emission filter) using a 63X 1.4 NA oil immersion objective or a 100X 1.4 NA oil immersion objective. Z-stacks

through outer periclinal walls of the outermost layer of cells were collected. AutoQuant X2 software (Oxford Instruments) was used to perform blind 3D deconvolution on the collected stacks.

Cell wall-associated fluorescence intensity and anisotropy were measured in maximum projections assembled using ImageJ software, by drawing polygonal regions of interest within, but not including, boundaries formed by underlying cross-walls. In some cases, multiple z-projections had to be assembled to avoid cases where inner periclinal walls contributed to the fluorescence observed in maximum z-projection. Fluorescence intensity was measured as mean gray value on a per-cell basis, and then averaged on a per-seedling basis. Fluorescence patterning anisotropy was measured with the plugin, "FibrilTool', which quantifies the predominant orientation and degree of alignment of fibrillar textures [57]. Figures were prepared and ANOVA was performed with the use of the ggplot2 and agricolae packages for the statistical programming language, R [58].

3.7 Acknowledgements

Thanks to Ram Dixit for sharing *katanin1-2* seeds, Peng Wu for providing advice on the use of the BTTP ligand, and members of the Anderson Lab for helpful discussions and comments on the manuscript. This work was supported as part of The Center for Lignocellulose Structure and Formation, an Energy Frontier Research Center funded by the U.S. Department of Energy, Office of Science, Basic Energy Sciences under Award # DE-SC0001090.

3.8 References

1. Gutierrez, R., et al., *Arabidopsis cortical microtubules position cellulose synthase delivery to the plasma membrane and interact with cellulose synthase trafficking compartments.* Nat Cell Biol, 2009. **11**(7): p. 797-806.
2. Paredez, A.R., C.R. Somerville, and D.W. Ehrhardt, *Visualization of cellulose synthase demonstrates functional association with microtubules.* Science, 2006. **312**(5779): p. 1491-5.
3. Kim, S.J. and F. Brandizzi, *The plant secretory pathway for the trafficking of cell wall polysaccharides and glycoproteins.* Glycobiology, 2016. **26**(9): p. 940-949.
4. Moore, P.J. and L.A. Staehelin, *Immunogold Localization of the Cell-Wall-Matrix Polysaccharides Rhamnogalacturonan-I and Xyloglucan during Cell Expansion and Cytokinesis in Trifolium-Pratense L - Implication for Secretory Pathways.* Planta, 1988. **174**(4): p. 433-445.
5. Cavalier, D.M., et al., *Disrupting two Arabidopsis thaliana xylosyltransferase genes results in plants deficient in xyloglucan, a major primary cell wall component.* Plant Cell, 2008. **20**(6): p. 1519-37.
6. Park, Y.B. and D.J. Cosgrove, *Xyloglucan and its interactions with other components of the growing cell wall.* Plant Cell Physiol, 2015. **56**(2): p. 180-94.
7. Ridley, B.L., M.A. O'Neill, and D.A. Mohnen, *Pectins: structure, biosynthesis, and oligogalacturonide-related signaling.* Phytochemistry, 2001. **57**(6): p. 929-967.
8. Atmodjo, M.A., Z. Hao, and D. Mohnen, *Evolving views of pectin biosynthesis.* Annu Rev Plant Biol, 2013. **64**: p. 747-79.
9. Bidhendi, A.J. and A. Geitmann, *Relating the mechanics of the primary plant cell wall to morphogenesis.* J Exp Bot, 2016. **67**(2): p. 449-61.
10. Braybrook, S.A. and A. Peaucelle, *Mechano-Chemical Aspects of Organ Formation in Arabidopsis thaliana: The Relationship between Auxin and Pectin.* Plos One, 2013. **8**(3).
11. Xiao, C., et al., *Xyloglucan Deficiency Disrupts Microtubule Stability and Cellulose Biosynthesis in Arabidopsis, Altering Cell Growth and Morphogenesis.* Plant Physiol, 2016. **170**(1): p. 234-49.
12. O'Neill, M.A., et al., *Requirement of borate cross-linking of cell wall rhamnogalacturonan II for Arabidopsis growth.* Science, 2001. **294**(5543): p. 846-849.
13. Ryden, P., et al., *Tensile properties of Arabidopsis cell walls depend on both a xyloglucan cross-linked microfibrillar network and rhamnogalacturonan II-borate complexes.* Plant Physiology, 2003. **132**(2): p. 1033-1040.
14. Dick-Perez, M., et al., *Structure and Interactions of Plant Cell-Wall Polysaccharides by Two- and Three-Dimensional Magic-Angle-Spinning Solid-State NMR.* Biochemistry, 2011. **50**(6): p. 989-1000.
15. Wang, T., et al., *Cellulose-Pectin Spatial Contacts Are Inherent to Never-Dried Arabidopsis Primary Cell Walls: Evidence from Solid-State Nuclear Magnetic Resonance.* Plant Physiol, 2015. **168**(3): p. 871-84.
16. Lopez-Sanchez, P., et al., *Cellulose-pectin composite hydrogels: Intermolecular interactions and material properties depend on order of assembly.* Carbohydrate Polymers, 2017. **162**: p. 71-81.
17. Tan, L., et al., *An Arabidopsis cell wall proteoglycan consists of pectin and arabinoxylan covalently linked to an arabinogalactan protein.* Plant Cell, 2013. **25**(1): p. 270-87.

18. Li, S.D., et al., *Cellulose synthase interactive protein 1 (CSI1) links microtubules and cellulose synthase complexes.* Proceedings of the National Academy of Sciences of the United States of America, 2012. **109**(1): p. 185-190.
19. Wilkop, T., et al., *A hybrid approach enabling large scale glycome analysis of post-Golgi vesicles reveals a transport route for polysaccharides.* Plant Cell, 2019.
20. Lee, K.J.D., S.E. Marcus, and J.P. Knox, *Cell Wall Biology: Perspectives from Cell Wall Imaging.* Molecular Plant, 2011. **4**(2): p. 212-219.
21. Marcus, S.E., et al., *Pectic homogalacturonan masks abundant sets of xyloglucan epitopes in plant cell walls.* Bmc Plant Biology, 2008. **8**.
22. Hoogenboom, J., et al., *Direct imaging of glycans in Arabidopsis roots via click labeling of metabolically incorporated azido-monosaccharides.* BMC Plant Biol, 2016. **16**(1): p. 220.
23. Dumont, M., et al., *Plant cell wall imaging by metabolic click-mediated labelling of rhamnogalacturonan II using azido 3-deoxy-D-manno-oct-2-ulosonic acid.* Plant J, 2016. **85**(3): p. 437-47.
24. McClosky, D.D., et al., *The click-compatible sugar 6-deoxy-alkynyl glucose metabolically incorporates into Arabidopsis root hair tips and arrests their growth.* Phytochemistry, 2016. **123**: p. 16-24.
25. Anderson, C.T., I.S. Wallace, and C.R. Somerville, *Metabolic click-labeling with a fucose analog reveals pectin delivery, architecture, and dynamics in Arabidopsis cell walls.* Proc Natl Acad Sci U S A, 2012. **109**(4): p. 1329-34.
26. Sampathkumar, A., et al., *Patterning and life-time of plasma membrane localized cellulose synthase is dependent on actin organization in Arabidopsis interphase cells.* Plant Physiology, 2013.
27. Gutierrez, R., et al., *Arabidopsis cortical microtubules position cellulose synthase delivery to the plasma membrane and interact with cellulose synthase trafficking compartments.* Nature Cell Biology, 2009. **11**(7): p. 797-806.
28. Crowell, E.F., et al., *Pausing of Golgi bodies on microtubules regulates secretion of cellulose synthase complexes in Arabidopsis.* Plant Cell, 2009. **21**(4): p. 1141-54.
29. Anderson, C.T., I.S. Wallace, and C.R. Somerville, *Metabolic click-labeling with a fucose analog reveals pectin delivery, architecture, and dynamics in Arabidopsis cell walls.* Proceedings of the National Academy of Sciences of the United States of America, 2012. **109**(4): p. 1329-34.
30. Baluska, F., et al., *Latrunculin B-induced plant dwarfism: Plant cell elongation is F-actin-dependent.* Developmental Biology, 2001. **231**(1): p. 113-24.
31. Zhu, C., et al., *The fragile Fiber1 kinesin contributes to cortical microtubule-mediated trafficking of cell wall components.* Plant Physiol, 2015. **167**(3): p. 780-92.
32. Scheres, B., P. Benfey, and L. Dolan, *Root development.* Arabidopsis Book, 2002. **1**: p. e0101.
33. Bhosale, R., et al., *A Spatiotemporal DNA Endoploidy Map of the Arabidopsis Root Reveals Roles for the Endocycle in Root Development and Stress Adaptation.* Plant Cell, 2018. **30**(10): p. 2330-2351.
34. Boevink, P., et al., *Stacks on tracks: the plant Golgi apparatus traffics on an actin/ER network.* Plant J, 1998. **15**(3): p. 441-7.
35. Wang, H., et al., *A Distinct Pathway for Polar Exocytosis in Plant Cell Wall Formation.* Plant Physiol, 2016. **172**(2): p. 1003-1018.
36. Sugimoto, K., R.E. Williamson, and G.O. Wasteneys, *New techniques enable comparative analysis of microtubule orientation, wall texture, and growth rate in intact roots of Arabidopsis.* Plant Physiol, 2000. **124**(4): p. 1493-506.

37. Wang, W., et al., *Sulfated ligands for the copper(I)-catalyzed azide-alkyne cycloaddition.* Chemistry, an Asian journal, 2011. **6**(10): p. 2796-802.
38. Marc, J., et al., *A GFP-MAP4 reporter gene for visualizing cortical microtubule rearrangements in living epidermal cells.* Plant Cell, 1998. **10**(11): p. 1927-40.
39. Burk, D.H., et al., *A katanin-like protein regulates normal cell wall biosynthesis and cell elongation.* Plant Cell, 2001. **13**(4): p. 807-27.
40. Whittington, A.T., et al., *MOR1 is essential for organizing cortical microtubules in plants.* Nature, 2001. **411**(6837): p. 610-3.
41. Fujita, M., et al., *Cortical microtubules optimize cell-wall crystallinity to drive unidirectional growth in Arabidopsis.* Plant Journal, 2011. **66**(6): p. 915-28.
42. Green, P.B., *Multinet growth in the cell wall of Nitella.* J Biophys Biochem Cytol, 1960. **7**: p. 289-96.
43. DeBolt, S., et al., *Nonmotile cellulose synthase subunits repeatedly accumulate within localized regions at the plasma membrane in Arabidopsis hypocotyl cells following 2,6-dichlorobenzonitrile treatment.* Plant Physiol, 2007. **145**(2): p. 334-8.
44. Heim, D.R., et al., *Isoxaben Inhibits the Synthesis of Acid Insoluble Cell Wall Materials In Arabidopsis thaliana.* Plant Physiol, 1990. **93**(2): p. 695-700.
45. Rui, Y. and C.T. Anderson, *Functional Analysis of Cellulose and Xyloglucan in the Walls of Stomatal Guard Cells of Arabidopsis.* Plant Physiology, 2016. **170**(3): p. 1398-1419.
46. Miart, F., et al., *Spatio-temporal analysis of cellulose synthesis during cell plate formation in Arabidopsis.* Plant Journal, 2014. **77**(1): p. 71-84.
47. Anderson, C.T., et al., *Real-Time Imaging of Cellulose Reorientation during Cell Wall Expansion in Arabidopsis Roots.* Plant Physiology, 2010. **152**(2): p. 787-796.
48. MacKinnon, I.M., et al., *Cell-wall structure and anisotropy in procuste, a cellulose synthase mutant of Arabidopsis thaliana.* Planta, 2006. **224**(2): p. 438-48.
49. Bashline, L., S. Li, and Y. Gu, *The trafficking of the cellulose synthase complex in higher plants.* Ann Bot, 2014. **114**(6): p. 1059-67.
50. Gendre, D., et al., *Trans-Golgi network localized ECHIDNA/Ypt interacting protein complex is required for the secretion of cell wall polysaccharides in Arabidopsis.* Plant Cell, 2013. **25**(7): p. 2633-46.
51. Polko, J.K. and J.J. Kieber, *The Regulation of Cellulose Biosynthesis in Plants.* Plant Cell, 2019. **31**(2): p. 282-296.
52. Baskin, J.M., et al., *Copper-free click chemistry for dynamic in vivo imaging.* Proceedings of the National Academy of Sciences of the United States of America, 2007. **104**(43): p. 16793-7.
53. Wang, T. and M. Hong, *Solid-state NMR investigations of cellulose structure and interactions with matrix polysaccharides in plant primary cell walls.* J Exp Bot, 2016. **67**(2): p. 503-14.
54. Zykwinska, A., J.F. Thibault, and M.C. Ralet, *Organization of pectic arabinan and galactan side chains in association with cellulose microfibrils in primary cell walls and related models envisaged.* Journal of experimental botany, 2007. **58**(7): p. 1795-802.
55. Marc, J., et al., *A GFP-MAP4 reporter gene for visualizing cortical microtubule rearrangements in living epidermal cells.* The Plant cell, 1998. **10**(11): p. 1927-40.
56. Jones, K.H. and J.A. Senft, *An Improved Method to Determine Cell Viability by Simultaneous Staining with Fluorescein Diacetate Propidium Iodide.* Journal of Histochemistry & Cytochemistry, 1985. **33**(1): p. 77-79.
57. Boudaoud, A., et al., *FibrilTool, an ImageJ plug-in to quantify fibrillar structures in raw microscopy images.* Nat Protoc, 2014. **9**(2): p. 457-63.

58. Wickham, H., *ggplot2: Elegant Graphics for Data Analysis*. Ggplot2: Elegant Graphics for Data Analysis, 2009: p. 1-212.

Chapter 4:

Metabolic labeling reveals a role for a developmentally-regulated kinesin in supporting rapid plant cell wall expansion

4.1 Abstract

Plants express a diversity of kinesins, molecular motors that can transport organellar and vesicular cargo within a cell along microtubules. While many plant kinesin genes have roles specific to mitosis and cytokinesis, one, *FRAGILE FIBER1*, encodes a kinesin that is active during interphase. A mutation at this locus, *fra1-1*, had phenotypes that suggested a role for this gene in cell wall synthesis. Earlier workers attributed these phenotypes to defects in cellulose organization. However, using a metabolic labeling approach to assess these phenotypes more directly, and in a *bona fide* knockout mutant, *fra1-5*, we found that while cellulose organization was unaltered, the bulk exocytosis rate of wall material was much reduced. A series of mutants in an importin-like gene, *IMB4*, which has been shown to regulate *FRA1* activity, also show a reduction in click-labeled cell wall matrix delivery. Together, these results point to at least a limited, though developmentally regulated, role for kinesins in supporting the bulk vesicular export of cell wall material, particularly in developmental zones of rapid cell elongation.

Permissions for Published Work

Chapter 4 includes figures and data from two publications:

Chuanmei Zhu, Anindya Ganguly, Tobias I. Baskin, Daniel D. McClosky, Charles T. Anderson, Cliff Foster, Kristoffer A. Meunier, Ruth Okamoto, Howard Berg, and Ram Dixit. (2015) The Fragile Fiber1 kinesin contributes to cortical microtubule-mediated trafficking of cell wall components. Plant Physiology, Vol. 167: 780-792, doi: https://doi.org/10.1104/pp.114.251462

ASPB permissions:

ASPB grants to authors whose work has been published in Plant Physiology® or The Plant Cell the royalty-free right to reuse images, portions of an article, or full articles in any book, book chapter, or journal article of which the author is the author or editor. Reproductions must bear the full citation, the journal URL (www.plantphysiol.org or www.plantcell.org), and the following notice: "Copyright American Society of Plant Biologists." ASPB further grants to authors the permission to make digital or hard copies of part or all of a work published in Plant Physiology® or The Plant Cell without fee for personal or classroom use.

Anindya Ganguly, Logan DeMott, Chaunmei Zhu, Daniel D. McClosky, Charles T. Anderson, Ram Dixit. (2018) Importin-β directly regulates the motor activity and turnover of a kinesin-4. Developmental Cell, Vol. 44: 642-651, doi: https://doi.org/10.1016/j.devcel.2018.01.027

4.2 Author Contributions

For the chapter as presented, R.D., C.Z., A.G., C.T.A., and D.D.M. devised experiments, D.D.M. carried out experiments for Figures 4-1, Figure 4-2, and Figure 4-3., and D.D.M. and C.T.A. wrote the accompanying text and analyzed data. However, please see individual published reports for full author contributions of all the work presented in each report. The initial isolation and characterization of *fra1*-5 was carried out by C.Z. and R.D.; of *imb4* mutant series, A.G. and R.D.

4.3 Introduction

With the exception of cellulose microfibrils, cell wall polysaccharides are synthesized intracellularly, and then must be trafficked to the apoplast via vesicles[1, 2]. Much of our knowledge of matrix polysaccharide delivery and synthesis derives from immuno-electron microscopy investigations. These studies detected distinct matrix polysaccharide epitopes between the various cisternae of the Golgi, as well as the trans-Golgi network (TGN), suggesting biosynthetic specialization of each compartment[3-5]. However, the detection of matrix polysaccharide in the TGN may not represent its biosynthesis here, but rather its internalization from the wall, as the TGN in plants also functions as an early endosome. Regardless, matrix polysaccharide residing in these compartments must then be delivered in vesicles to the expanding cell wall, though this final process is poorly understood.

Vesicle transport in plants can be carried out via kinesins, motor proteins that move along microtubules[6]. Since they lack dyneins, plants must carry out much of their microtubule-guided transport with kinesins, of which they have many[7]. Plant kinesins have been implicated in a number of intracellular processes, including generalized unidirectional transport of cargo (including organelles), cytokinesis, and signal transduction, in addition to wall synthesis. Though varied in function as a class, individual kinesins appear to be highly specialized, with distinct functions for each kinesin subfamily. AtKinesin-13A, for example, appears to be involved in maintenance of interphase Golgi morphology in specialized cell types, such as Arabidopsis trichomes and cotton fibers[8, 9]. Other plant kinesins have well-characterized roles during mitosis[10]. Some notable mitosis-active kinesins include POKs (Phragmoplast Orienting Kinesins), at least one of which (POK1) plays an important role in retaining the positional information of the transient pre-prophase band of microtubules and actin microfilaments[11, 12]. Near the start of cytokinesis, the kinesins AtNACK1 and AtNACK2 (*Arabidopsis thaliana*

NPK1-activating kinesin1 and 2) participate in a MAPK-signaling cascade that is essential for the lateral expansion of the phragmoplast, and thus the complete extension of the newly-forming wall across the width of the mother cell[13, 14]. During cytokinesis, another kinesin, AtPAKRP2 (*Arabidopsis thaliana* phragmoplast-associated kinesin-related protein 2), is specialized for the transport of bodies from the Golgi to the incipient cell plate along phragmoplast microtubules[15].

One kinesin, Fragile Fiber1, however, is active during interphase, particularly in rapidly-expanding cells[16]. This marks it for particular interest for a role in the transport of cell wall material during diffuse wall expansion. Its encoding gene was first identified in a screen of ethyl methanesulfonate-induced Arabidopsis mutants for defective fiber mechanical strength. The identified mutant, *fra1-1* was reported to have altered cellulose organization in its fiber cells, despite having unaltered cortical microtubules[17]. This finding was intriguing, since it suggested that the gene-product of *FRA1* might have a linking role between the cortical MT array and CMF organization. The orthologous gene in rice (*Oryza sativa*), *bc12* also had defective fiber cell cellulose organization, accompanied by a brittle-stem phenotype, though this gene also has transcription factor activity[18]. The encoded protein in Arabidopsis was discovered to be a bona-fide kinesin *in vitro*, moving rapidly along microtubules in (+)-end directed fashion, and maintaining an unusually long run-length, exceeding 3 μm on average and 10 μm in extreme cases[19, 20]. Together, these findings point to a role for FRA1 in translating the organization of the cortical MT array to the organization of cellulose microfibrils, perhaps by ferrying vesicles containing cellulose synthase complexes in an ordered way along MTs.

Careful examination of an additional allele at this locus, *fra1-5*, presented some problems for this interpretation[16, 21]. Since *fra1-1* was predicted to encode nearly a full transcript based on the location of the EMS-induced lesion, further work on this gene was carried out with *fra1-5*, a T-DNA insertional mutation that resulted in unambiguous knock-out of transcription.

Consistent with the role of FRA1 in regulating cellulose orientation, *fra1-5* has mechanically weaker inflorescence stems with decreased growth anisotropy. However, cellulose microfibril orientation in both pith and interfascicular fiber cells of inflorescence stems, revealed by SEM, is not distinct from those of the wildtype. In fiber cell walls, regions can be found in either genotype that could reasonably be described as "disorganized" or "organized" depending on the sub-cellular region sampled. This observation casts some doubt on the previous characterization of cellulose orientation in *fra1-1* as disorganized. *fra1-5*, does, however, display phenotypes consistent with an overall reduction in wall secretion. Stem growth velocity is nearly halved, and wall thickness in protoxylem, fiber, and pith cells are all reduced similarly. It was speculated that the kinesin has a role in determining the rate of wall component secretion, rather than a role in establishing the organized deposition of cellulose[16].

Kinesins are energy-intensive motors, and therefore plant cells have a large incentive to keep them turned off when not in use[22]. An interphase-expressed kinesin such as FRA1 presents a particularly high regulatory priority. A yeast two-hybrid assay showed that FRA1 interacted with an importin-β protein, IMB4. Further investigations have shown that this interaction occurs *in vivo*, where IMB4 appears to play a dual role in regulating FRA1 through binding to it[23]. FRA1 bound to IMB4 is sequestered from proteasome-mediated degradation while also being prevented from binding to MTs. Accordingly, the T-DNA insertional mutants *imb4-1* and *imb4-2*, both likely loss-of-function alleles, have defective cell elongation phenotypes. The *imb4* mutants show defects in growth that exceed those found in *fra1*, and are not restricted to cell elongation, however, with abnormal cell division planes and much-delayed emergence of primary inflorescence stems. A double mutant, *imb4-1 fra1-5*, has quantitative changes in growth and developmental defects that matches *imb4-1*, affirming that these genes are epistatic, with proteins acting in the same pathway[23].

To test the hypothesis that the IMB4-FRA1 system is involved in setting the rate of overall wall polysaccharide secretion rate, rather than establishing the patterning of matrix deposition, we used FucAl as a chemical reporter for newly-synthesized pectin to examine rates of pectin delivery in these mutants.

4.4 Results and Discussion

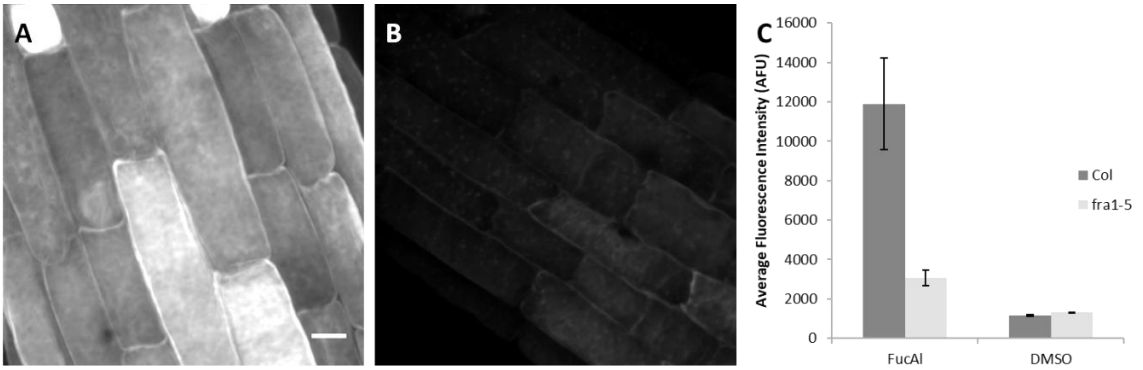

Figure 4-1: Metabolic labeling of pectin with 2 h FucAl is reduced in *fra1-5* root epidermal cells. (A) FucAl-associated fluorescence is evident in *Col-0* root elongation zone epidermal cells. (B) *fra1-5* seedlings show reduced wall-associated fluorescence. (C) Averages of cell wall-associated fluorescence (mean fluorescence intensity values were calculated for ≥ 6 cells per seedling; bars represent average values for 9 seedlings per treatment; error bars = SEM).

To test whether the *fra1-5* mutation results in defects in the export of cell wall matrix components, seedlings were exposed to a click chemistry-compatible fucose analog, fucose-alkyne (FucAl), which is incorporated into pectic rhamnogalacturonan-I[24]. Seedlings were grown vertically for 4 d, under 24 h light, on agar plates. The extent and pattern of FucAl incorporation into root elongation zone epidermal cell walls over 2 h was visualized after copper-catalyzed labeling of FucAl with Alexa 488-azide using spinning disk confocal microscopy. A shorter incubation time was chosen for quantifying FucAl related fluorescence than in (Ch. 3, this work), because cells that end their incubation period in the elongation zone incorporate FucAl into their walls more quickly than cells that end their incubation period in the differentiation zone [24]. Cell walls from *fra1-5* plants showed reduced FucAl incorporation relative to Col-0 controls (Figure 4-1), however, the pattern of fluorescence was still diffuse overall within any particular cell. The nearly 4-fold reduction in fluorescence may indicate a level of reduced wall synthesis about twice as severe as the two-fold reduction in wall diameter (in inflorescence stem

tissues[16]), and the reduction in overall axial elongation otherwise seen in *fra1-5*.[16, 21] This may indicate a special role for FRA1 in cells undergoing the initiation of a rapid elongation, such as root epidermal cells. However, other interpretations are also possible. Altered wall architecture in *fra1-5*, though not consistently detected in this allele, may have altered the uptake kinetics of the FucAl chemical reporter.

We next examined the role of a putative regulator of FRA1, IMB4, in the export of cell wall matrix. Seedlings were labeled as before, but with a longer incubation time (4 h) with the FucAl chemical reporter. This was done to accomplish even labeling in cells that, at the conclusion of the incubation period, are present in the differentiation zone, since preliminary experiments showed much-reduced labeling in *imb4* mutants, falling below the limit of detection at 2 h. Surprisingly, *imb4* mutants showed brighter FucAl-associated fluorescence in the differentiation zone than in the elongation zone (Figure 4-2), which is the opposite of the pattern typical for FucAl labeling, where elongation zone cells typically incorporate the reporter into their walls at rates only surpassed by root hairs[24]. However, this pattern is consistent with the generalized form of the developmental gradient in which *IMB4* is hypothesized to exist [25], wherein *IMB4* expression is highest in tissues where cells are rapidly elongating, decreasing with distance from this point. While this was demonstrated in etiolated hypocotyls in [25], the pattern should still hold in roots, where cell elongation is also rapid. In *imb4* mutants, the IMB4-FRA1 machinery, thought to accomplish augmented vesicle secretion in zones of highest elongation and cell wall matrix flux, is rendered inactive, perhaps uniquely inhibiting the export of bulk cell wall material in those zones. It is also possible that *imb4* mutants were differentially sensitive to the transfer to liquid media, or to the chemical reporter itself, and that this differential sensitivity resulted in lower flux through the relevant monosaccharide salvage pathway in the darker developmental zones.

We lack direct measurements of the kinematics of epidermal cells as they mature along a developmental gradient from the quiescent center to the differentiation zone. While these measurements are generally well-characterized for Arabidopsis root tips growing vertically along solid media[26], during the course of FucAl exposure in these experiments the roots were submerged in liquid media, which was not oxygenated via bubbling or other means. This could result in much slower growth than was observed, for example by [26]. It should be added that cell fluorescence in these experiments is indicative of matrix delivery throughout the lifetime of FucAl exposure. That is, metabolism and cell wall polymer dynamics in earlier zones may contribute to the patterns observed at the end of the incubation period.

This experiment also included a complementation line expressing FRA1-3GFP (3 tandem GFP) to demonstrate the ability of the construct to functionally complement the *fra1-5* mutation. The double mutant, *fra1-5 imb4-1*showed a matrix delivery phenotype that was essentially indistinguishable from *imb4-1,* consistent with an epistatic relationship between these genes, which are hypothesized to act in the same pathway.

4.5 Conclusion

Metabolic labeling experiments with FucAl applied to the mutant *fra1-5* and a series of mutations in its putative interactor, *imb4*, support a role for the FRA1-IMB4 system in supporting the overall secretion of wall polysaccharide, particularly in zones of highest cell wall metabolic flux. However, this interpretation should be made with some caution, as at least part of the reduction in fluorescent matrix could be attributed to slower axial organ expansion, rather than specifically a reduction in polysaccharide deposition. These two processes, in fact, may feedback on one another; it is conceivable that altered wall mechanics may result from altered polysaccharide deposition rates, for example. These results also point to IMB4 as a potentially

important upstream regulator of matrix polysaccharide trafficking, particularly in developmental contexts like hypocotyl elongation and primary root establishment, where precisely-timed rapid cell expansion is vital for seedling establishment.

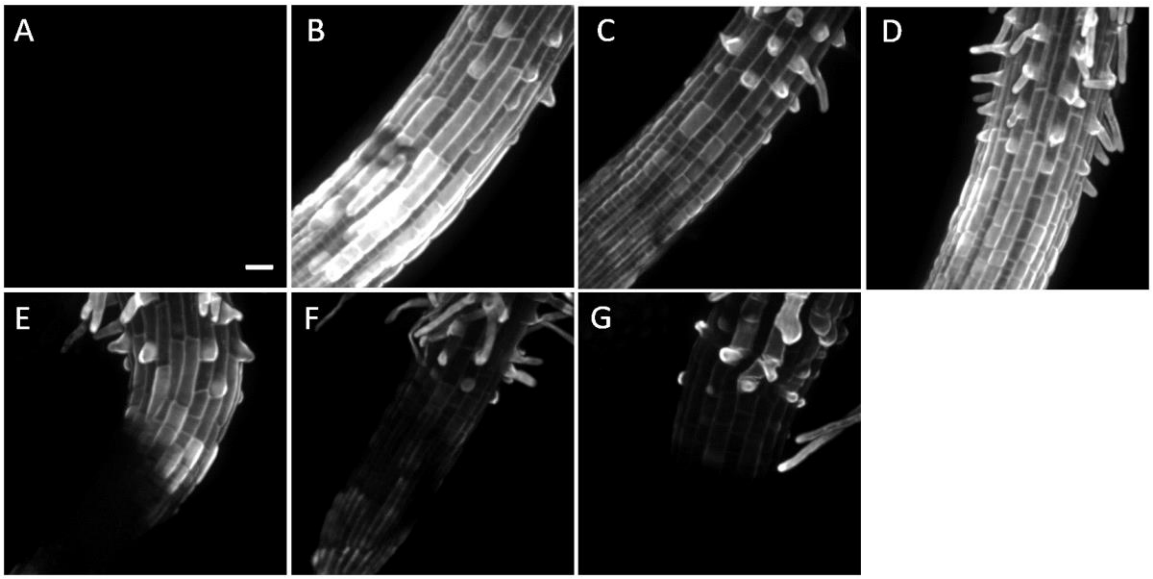

Figure 4-2: Metabolic labeling with 4 h FucAl across a series of mutants in the putative FRA1-IMB4 pathway reveals defects in pectin secretion – representative images. (A) An equivalent volume of the solvent dimethyl sulfoxide (DMSO) is used as a negative control. (B) Col-0, (C) *fra1-5*, (D) *fra1-5* / FRA1-3GFP complementation line, (E) *imb4-1*, (F) *imb4-2*, (G) *imb4-1 fra1-5*. Scale bar = 10 μm. All images depicted with the same brightness and contrast settings. Representative images from three replicate experiments..

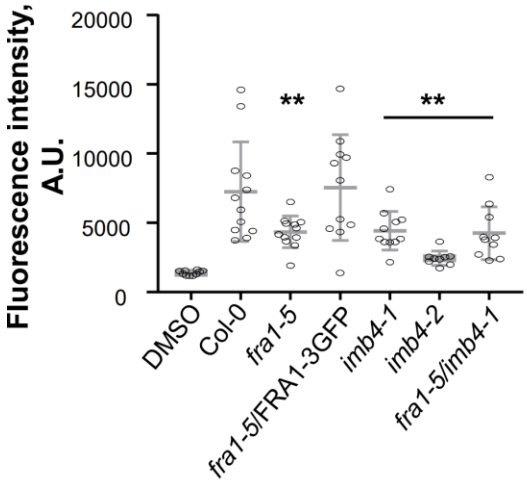

Figure 4-3: Metabolic labeling with 4 h FucAl across a series of mutants in the putative FRA1-IMB4 pathway reveals defects in pectin secretion – quantification. Quantification of FucAl fluorescence. Values are means ± S.E.M. (n > 6 cells per seedling 9-10 seedlings per treatment, pooled from three experiments). Double asterisks indicate significant differences as determined by Student's t test, $p < 0.001$.

4.6 Methods

4.5.1. Seedling culture

Arabidopsis *Col-0*, *fra1-5*, *imb4-1*, *imb4-2*, *imb4-1 fra1-5* seeds were surface-sterilized in 30% bleach + 0.01% SDS (w/v) for 20 min, washed 4 times with sterile MilliQ water, suspended in sterile 0.15% agar (w/v), and stored in the dark at 4°C for 2-7 days before being grown vertically for 4 d under 24 h light on square Petri plates containing MS medium (2.2 g/L Murashige and Skoog salts (Caisson Laboratories), 0.6 g/L MES (2-N-morpholino-ethanesulfonic acid; Research Organics), 1% (w/v) sucrose, 0.8% (w/v) agar-agar (Research Organics), pH 5.6). For *imb4* mutant series (and accompanying controls, including *fra1-5* and *fra1-5* complementation line), plants were analyzed after 5 d of vertical growth to ensure a vertically-growing primary root was always evident.

4.5.2 Metabolic labeling

Seedlings were transferred to MS liquid media containing either 5 μM fucose-alkyne (FucAl, Life Technologies) dissolved in DMSO or an equal volume of DMSO alone. After 2 h of incubation at 22°C, seedlings were washed 4x with MS liquid. FucAl-containing pectic polysaccharides were then labeled with a reaction mixture containing 1 μM Alexa 488-azide (Life Technologies), 1 mM $CuSO_4$, and freshly prepared 1 mM ascorbic acid dissolved in MS liquid with rocking in the dark at room temperature for 1 h, followed by washing 4x with MS liquid. For imb4 mutant series (and accompanying controls, including *fra1-5* and *fra1-5* complementation line), incubation time in FucAl was increased to 4 h.

4.5.3. Microscopy and image analysis

The root elongation zones of labeled seedlings were imaged with a Zeiss Cell Observer SD spinning disk confocal microscope (488 nm laser excitation, 525/25 emission filter) using a 63X 1.40 NA oil immersion objective. Z-stacks deep enough to image entire epidermal cells were collected. Cell wall-associated fluorescence intensity in maximum projections of Z-stacks was measured using ImageJ, by calculating mean pixel intensity values for individual cells. For lower magnification images showing multiple developmental zones, a 20X 0.50 NA air objective lens was used, with z-stacks taken every 500 µm, rather than every 200 µm.

4.7 Acknowledgements

This work was supported as part of The Center for Lignocellulose Structure and Formation, an Energy Frontier Research Center funded by the U.S. Department of Energy, Office of Science, Basic Energy Sciences under Award # DE-SC0001090. *Fra1-5, fra1-5* / FRA1-3GFP, *fra1-5 imb4-1*, *imb4-1*, *imb4-2* seeds were supplied by Ram Dixit and Anindya Ganguly (Washington University of St. Louis).

4.8 References

1. Worden, N., E. Park, and G. Drakakaki, *Trans-Golgi network: an intersection of trafficking cell wall components.* J Integr Plant Biol, 2012. **54**(11): p. 875-86.
2. Sinclair, R., M.R. Rosquete, and G. Drakakaki, *Post-Golgi Trafficking and Transport of Cell Wall Components.* Frontiers in Plant Science, 2018. **9**.
3. Moore, P.J. and L.A. Staehelin, *Immunogold Localization of the Cell-Wall-Matrix Polysaccharides Rhamnogalacturonan-I and Xyloglucan during Cell Expansion and Cytokinesis in Trifolium-Pratense L - Implication for Secretory Pathways.* Planta, 1988. **174**(4): p. 433-445.
4. Zhang, G.F. and L.A. Staehelin, *Functional Compartmentation of the Golgi-Apparatus of Plant-Cells - Immunocytochemical Analysis of High-Pressure Frozen-Substituted and Freeze-Substituted Sycamore Maple Suspension-Culture Cells.* Plant Physiology, 1992. **99**(3): p. 1070-1083.
5. Moore, P.J., et al., *Immunogold Localization of Xyloglucan and Rhamnogalacturonan-I in the Cell-Walls of Suspension-Cultured Sycamore Cells.* Plant Physiology, 1986. **82**(3): p. 787-794.
6. Brandizzi, F. and G.O. Wasteneys, *Cytoskeleton-dependent endomembrane organization in plant cells: an emerging role for microtubules.* Plant Journal, 2013. **75**(2): p. 339-349.
7. Lee, Y.R.J. and B. Liu, *Cytoskeletal motors in arabidopsis. Sixty-one kinesins and seventeen myosins.* Plant Physiology, 2004. **136**(4): p. 3877-3883.
8. Mucha, E., et al., *RIP3 and AtKinesin-13A-A novel interaction linking Rho proteins of plants to microtubules.* European Journal of Cell Biology, 2010. **89**(12): p. 906-916.
9. Oda, Y. and H. Fukuda, *Initiation of Cell Wall Pattern by a Rho- and Microtubule-Driven Symmetry Breaking.* Science, 2012. **337**(6100): p. 1333-1336.
10. Vanstraelen, M., D. Inze, and D. Geelen, *Mitosis-specific kinesins in Arabidopsis.* Trends in Plant Science, 2006. **11**(4): p. 167-175.
11. Muller, S., S.C. Han, and L.G. Smith, *Two kinesins are involved in the spatial control of cytokinesis in Arabidopsis thaliana.* Current Biology, 2006. **16**(9): p. 888-894.
12. Lipka, E., et al., *The Phragmoplast-Orienting Kinesin-12 Class Proteins Translate the Positional Information of the Preprophase Band to Establish the Cortical Division Zone in Arabidopsis thaliana.* Plant Cell, 2014. **26**(6): p. 2617-2632.
13. Nishihama, R., et al., *Expansion of the cell plate in plant cytokinesis requires a kinesin-like protein/MAPKKK complex.* Cell, 2002. **109**(1): p. 87-99.
14. Tanaka, H., et al., *The AtNACK1/HINKEL and STUD/TETRASPORE/AtNACK2 genes, which encode functionally redundant kinesins, are essential for cytokinesis in Arabidopsis.* Genes to Cells, 2004. **9**(12): p. 1199-1211.
15. Lee, Y.R.J., H.M. Giang, and B. Liu, *A novel plant kinesin-related protein specifically associates with the phragmoplast organelles.* Plant Cell, 2001. **13**(11): p. 2427-2439.
16. Zhu, C., et al., *The fragile Fiber1 kinesin contributes to cortical microtubule-mediated trafficking of cell wall components.* Plant Physiol, 2015. **167**(3): p. 780-92.
17. Zhong, R., et al., *A kinesin-like protein is essential for oriented deposition of cellulose microfibrils and cell wall strength.* Plant Cell, 2002. **14**(12): p. 3101-17.
18. Li, J.A., et al., *Mutation of Rice BC12/GDD1, Which Encodes a Kinesin-Like Protein That Binds to a GA Biosynthesis Gene Promoter, Leads to Dwarfism with Impaired Cell Elongation.* Plant Cell, 2011. **23**(2): p. 628-640.

19. Zhu, C. and R. Dixit, *Single molecule analysis of the Arabidopsis FRA1 kinesin shows that it is a functional motor protein with unusually high processivity.* Mol Plant, 2011. **4**(5): p. 879-85.
20. Zhu, C. and R. Dixit, *In Vitro and In Vivo Single-Molecule Imaging Experiments Provide Mechanistic Insight into the Role of the Arabidopsis FRA1 Kinesin in Cell Wall Assembly.* Molecular Biology of the Cell, 2011. **22**.
21. Kong, Z.S., et al., *Kinesin-4 Functions in Vesicular Transport on Cortical Microtubules and Regulates Cell Wall Mechanics during Cell Elongation in Plants.* Molecular Plant, 2015. **8**(7): p. 1011-1023.
22. Ganguly, A. and R. Dixit, *Mechanisms for regulation of plant kinesins.* Current Opinion in Plant Biology, 2013. **16**(6): p. 704-709.
23. Ganguly, A., et al., *Importin-beta Directly Regulates the Motor Activity and Turnover of a Kinesin-4.* Dev Cell, 2018. **44**(5): p. 642-651 e5.
24. Anderson, C.T., I.S. Wallace, and C.R. Somerville, *Metabolic click-labeling with a fucose analog reveals pectin delivery, architecture, and dynamics in Arabidopsis cell walls.* Proc Natl Acad Sci U S A, 2012. **109**(4): p. 1329-34.
25. Ganguly, A., et al., *Importin-beta Directly Regulates the Motor Activity and Turnover of a Kinesin-4.* Developmental Cell, 2018. **44**(5): p. 642-+.
26. Beemster, G.T. and T.I. Baskin, *Analysis of cell division and elongation underlying the developmental acceleration of root growth in Arabidopsis thaliana.* Plant Physiol, 1998. **116**(4): p. 1515-26.

Chapter 5:

Summary and Future Work

5.1 Summary and Connections Between Chapters

In this dissertation I have described our efforts to expand the toolbox of available click sugars to fluorescently label other cell wall matrix polysaccharides, during which we discovered a putative glucose analog (6dAG) that differentially labels a distinct tip-growth-associated polysaccharide. This labeling may indicate, for example, the presence of a specialized glucan, however, it may also indicate wound-induced callose. In either case, this chemical reporter's distribution differs markedly from other click-compatible sugars[1-3], which do not show cell-type specific labeling patterns. This also suggests that the alkynyl moiety is not merely entering primary metabolism at many, non-specific junctures, but is reporting on the presence of a specific scavenging and biosynthetic pathway in a specific cell type. Perhaps with click-compatible probes with greater cell-permeation, such as the promising 'click-on' coumarin-based-azides[4], we will be able to use 6dAG to visualize sites of callose synthesis and recycling at the cell plate during cytokinesis. This role for callose synthase activity is supported, for example, in the characterization of mutants with reduced expression of *GSL8* (*Glucan Synthase-Like8*)[5], a suspected callose synthase gene. Even the dynamics of wound-induced callose production[6] in tip-growing cells could be explored.

While demonstrating the utility of BTTP to preserve plant cell viability during the CuAAC ligation reaction, we discovered a hint that the cortical microtubule array may play an important role in establishing matrix polysaccharide anisotropy. However, following this lead, we discovered that this role is probably indirect and mediated through the cortical microtubule array's influence on cellulose microfibril orientation (Ch. 3). This finding affirms the importance

of cellulose-matrix intermolecular interactions, and more specifically cellulose-pectin contacts, if FucAl is a *bona fide* RG-I reporter. These interactions appear to be strong enough to be the primary directors of the arrangement and organization of pectic polysaccharides, at least in the case of root epidermal cells.

It is important to note in this interpretation that we have assumed that growth kinematics are slow enough in aqueous culture, that over the course of FucAl exposure, cells in the early differentiation zone have only progressed to that point from one of the preceding elongation zones. If this cohort of cells were actually, for instance, initially present in the division zone, where cortical microtubule and CMF arrangements are more isotropic, permitting some isotropic swelling (effecting a widening of the root circumference), then their relative contributions to matrix polysaccharide organization becomes less clear.

This CMF-centric model of the determination of matrix anisotropy is somewhat in conflict with the model that was developed in Chapter 4, where a kinesin, FRA1, emerged as an potentially important player in facilitating bulk transport of matrix polysaccharide to the growing wall – but one that requires cortical microtubules for its motion. If the cortical microtubule cytoskeleton only indirectly influences the anisotropy of matrix deposition, it is surprising that total removal of FRA1 effects such a reduction in matrix delivery. Since kinesins move along MTs, we would expect MT depolymerization to perhaps phenocopy *fra1-5* in FucAl labeling. Instead, as shown in Chapter 3, FucAl delivery is merely spatially disrupted, and on a fine-scale, and most pertinently not reduced in amount. This disagreement may point to an alternative interpretation where FRA1 plays a less direct role in matrix polysaccharide delivery than hypothesized in Chapter 4.. Alternatively, the loss of FRA1 may in fact change the organization of the cortical microtubule array in such a way that matrix polysaccharide delivery is slowed to the point of dramatic reduction. These possibilities could be partially resolved by imaging cortical MTs in *fra1-5*, for example.

5.2 Future Work

There are multiple routes for future work in metabolic labeling of plant cell walls. The advent of super-resolution imaging of click-sugar distribution is particularly attractive[7]. By moving beyond traditionally diffraction-limited localization, we could visualize, for instance, distinct exocytic events, as the improvement in spatial resolution approaches the size of exocytic vesicles, which have diameters in the range of 50 nm, depending cell type, developmental context, and vesicle identity[8-10]. This prompts the possibility of simultaneously imaging cellulose synthase complex and matrix polymer trafficking. Are matrix polysaccharides delivered alongside cellulose synthase complexes, or are they kept initially separate? How does the bolus of newly-delivered matrix spread or otherwise move once it is deposited in the wall? The combination of *in vivo* labeling techniques and could potentially answer these questions and more, shedding light on the timing and order-of-operations for cell wall assembly.

As the above questions illustrate, higher-resolution imaging of cell wall polymers would be a much more powerful tool if coupled to an *in vivo*-compatible ligation system that was more reliably compatible with cell viability, without having to flood the study system with copper ions, or rely on relatively bulky cyclooctyne probes. To make further progress on this front, we should remember Huisigen rearrangements, of which the CuAAC reaction referred to in this dissertation is just a subset, is itself a subset of many potential bio-orthogonal click reactions. The Sonogashira coupling reaction, between terminal alkynes and iodo-groups, is particularly attractive, and has already been demonstrated in a bacterial system[11]. Iodo-modified sugar analogs, for instance, might be better tolerated by sugar salvage pathways. Alternatively, an iodo-modified fluorescent probe could be used as a copper-free ligation alternative to imaging alkynyl residues, permitting the use of the well-characterized FucAl reporter, or even 6dAG, in *in vivo*-compatible experiments[11].

Finally, determining with greater certainty the identity of the FucAl-containing polymer(s?) remains a major goal, and would aid in the interpretation of future metabolic labeling experiments greatly. To this end, FucAl click labeling was carried out in some preliminary experiments in *gals1 gals2 gals3*, a recently-characterized triple knockout mutant in all three members of the Arabidopsis *(1,4)-beta-Galactan Synthase (GalS)* gene family. This insertional mutant, though it apparently completely lacks this enzymatic activity, results in plants with only subtle growth phenotypes[12]. Immunodot blot assays probing for galactans with LM5, an antibody with specificity for (1,4)-beta-galactan, showed no presence of this glycan in cell wall extracts prepared from this mutant[12]. If the alkynyl moiety were really being added as part of a fucose residue to RG-I galactan, then presumably removal of extended galactan chains from RG-I would result in the loss of FucAl labeling. Additionally, at least one of these enzymes, GALS1, has been shown to be bifunctional, capable of catalyzing both the transfer of galactose and the transfer of arabinose from their respective nucleotide-sugars to both growing and terminating galactan chains[13]. This demonstration of substrate tolerance made GALS1 a particularly attractive candidate for the gycosyltransferase responsible for incorporating FucAl into the Arabidopsis cell wall. However, our preliminary experiments with this triple knockout mutant revealed FucAl associated fluorescence of the same intensity as observed in wildtype. Furthermore, we examined FucAl labeling in *fkgp*-3, an insertional Arabidopsis mutant that does not produce the bifunctional fucose-scavenging enzyme, L-Fucose Kinase/ GDP-L-Fucose Pyrophosphorylase[14]. These activities are thought to be essential for fucose scavenging and recycling[15]. However, even in this mutant our preliminary click-labeling attempts have shown intensity and patterning of labeling that are only somewhat altered (in some experiments, a 34% reduction in labeling intensity[16]), not obliterated. These surprising results suggest that restricting the range of our hypothesized destinations for FucAl to biomolecules that normally contain fucose was perhaps naïve, and raises the possibility that FucAl is chemically reporting on

the location of some other natively scavenged sugar. Based on the dramatic reduction of both FucAl label patterning and intensity after cellulose biosynthesis is disrupted (Ch. 3), perhaps a more rational search for the FucAl-containing glycan would focus on polysaccharides that closely interact with cellulose.

5.3 References

1. Hoogenboom, J., et al., *Direct imaging of glycans in Arabidopsis roots via click labeling of metabolically incorporated azido-monosaccharides.* BMC Plant Biol, 2016. **16**(1): p. 220.
2. Dumont, M., et al., *Plant cell wall imaging by metabolic click-mediated labelling of rhamnogalacturonan II using azido 3-deoxy-D-manno-oct-2-ulosonic acid.* Plant J, 2016. **85**(3): p. 437-47.
3. Anderson, C.T., I.S. Wallace, and C.R. Somerville, *Metabolic click-labeling with a fucose analog reveals pectin delivery, architecture, and dynamics in Arabidopsis cell walls.* Proc Natl Acad Sci U S A, 2012. **109**(4): p. 1329-34.
4. Rong, L., et al., *A coumarin derivative as a fluorogenic glycoproteomic probe for biological imaging.* Chemical Communications, 2014. **50**(6): p. 667-669.
5. Chen, X.Y., et al., *The Arabidopsis callose synthase gene GSL8 is required for cytokinesis and cell patterning.* Plant Physiol, 2009. **150**(1): p. 105-13.
6. Cooper, K.M., *Callose-Deposit Formation in Radish Root Hairs*, in *Cellulose and Other Natural Polymer Systems*, R.M. Brown, Editor. 1982, Springer: Boston, MA.
7. Zhuang, X., *Nano-imaging with Storm.* Nat Photonics, 2009. **3**(7): p. 365-367.
8. Ketelaar, T., et al., *Rates of exocytosis and endocytosis in Arabidopsis root hairs and pollen tubes.* J Microsc, 2008. **231**(2): p. 265-73.
9. Wilkop, T., et al., *A hybrid approach enabling large scale glycome analysis of post-Golgi vesicles reveals a transport route for polysaccharides.* Plant Cell, 2019.
10. Sinclair, R., M.R. Rosquete, and G. Drakakaki, *Post-Golgi Trafficking and Transport of Cell Wall Components.* Frontiers in Plant Science, 2018. **9**.
11. Li, N., et al., *Copper-free Sonogashira cross-coupling for functionalization of alkyne-encoded proteins in aqueous medium and in bacterial cells.* J Am Chem Soc, 2011. **133**(39): p. 15316-9.
12. Ebert, B., et al., *The Three Members of the Arabidopsis Glycosyltransferase Family 92 are Functional beta-1,4-Galactan Synthases.* Plant Cell Physiol, 2018. **59**(12): p. 2624-2636.
13. Laursen, T., et al., *Bifunctional glycosyltransferases catalyze both extension and termination of pectic galactan oligosaccharides.* Plant J, 2018. **94**(2): p. 340-351.
14. Villalobos, J.A., B.R. Yi, and I.S. Wallace, *2-Fluoro-L-Fucose Is a Metabolically Incorporated Inhibitor of Plant Cell Wall Polysaccharide Fucosylation.* PLoS One, 2015. **10**(9): p. e0139091.

15. Kotake, T., et al., *A bifunctional enzyme with L-fucokinase and GDP-L-fucose pyrophosphorylase activities salvages free L-fucose in Arabidopsis.* J Biol Chem, 2008. **283**(13): p. 8125-35.
16. Price, E. *Investigation of cell wall uptake, trafficking, and organization in Arabidopsis thaliana using a metabolically incorporated click reporter.* B.S. Thesis, Schreyer Honors College, Pennsylvania State University, PA, 2018.

VITA

Daniel D. McClosky

EDUCATION

Aug 2011 – Present	PhD candidate, Plant Biology Graduate Program, The Pennsylvania State University
Aug 2006 – May 2011	BS (Chemistry), Michigan State University
Aug 2006 – May 2010	BS (Plant Biology, Biochemistry), Michigan State University

PUBLICATIONS

5. Ganguly, A., DeMott, L., **McClosky, D. D.**, Anderson, C. T., Dixit, R. 2018. Importin-β directly regulates the motor activity and turnover of a kinesin-4. *Developmental Cell* 44(5): 642-651.
4. Wang, B., **McClosky, D. D.**, Anderson, C. T., Chen, G. Synthesis of a suite of click-compatible sugar analogs for probing carbohydrate metabolism. 2016. *Carbohydrate Research* 433: 54-62.
3. **McClosky, D. D.**, Wang, B., Chen, G., Anderson, C. T. 2016. The click-compatible sugar 6-deoxy-alkynyl glucose metabolically incorporates into Arabidopsis root hair tips and arrests their growth. *Phytochemistry* 123: 16-24.
2. Zhu, C., Ganguly, A., Baskin, T. I., **McClosky, D. D.** Anderson, C. T., Foster, C., Meunier, K. A., Okamoto, R., Berg, H., Dixit, R. 2015. The Fragile Fiber1 kinesin contributes to cortical microtubule-mediated trafficking of plant cell wall components. *Plant Physiology* 167: 780-792.
1. Durrett, T. P., **McClosky, D. D.**, Tumaney, A. W., Elzinga, D. A., Ohlrogge, J., Pollard, M. 2010 A distinct DGAT with sn-3 acetyltransferase activity that synthesizes unusual, reduced-viscosity oils in Euonymus alatus transgenic seeds. Durrett, T. P., **McClosky, D. D.**, Tumaney, A. W., Elzinga, D. A., Ohlrogge, J., Pollard, M. *PNAS* 107(20): 9464-9469.

CONFERENCE AND SEMINAR PRESENTATIONS

1. The 2014 Midwest Plant Cell Dynamics Meeting, Madison, WI, USA: June 4-6, 2014.